

ON THE DERIVATION OF THE DESCRIBING FUNCTION FOR
HYSTERETIC NONLINEAR ELEMENTS

A Thesis

Presented to

the Faculty of Graduate Studies and Research

The University of Manitoba

In Partial Fulfillment

of the Requirements for the Degree

Master of Science in Electrical Engineering

by

Chanan Achsaf

Winnipeg, October, 1965



ABSTRACT

In the last few years there has been a tremendous increase in focus towards nonlinear control systems, and the number of methods suggested to deal with these problems is rapidly increasing.

One of the most common methods, to be found in almost any modern textbook dealing with control systems, is the describing function method.

Some of the suggested techniques dealing with nonlinear elements incorporating hysteretic phenomena (i.e. double valued nonlinearities) are herein reviewed; and an attempt is made to extend the analytical techniques to physical elements (magnetic cores).

A set of measurements is then made to determine deviations between the measured describing function of such elements and the calculated one. It is found that the analytical techniques do not, in some cases, yield satisfactory results, and therefore, it might be better to obtain for symmetric multi-valued polynomial nonlinearities (such as hysteresis loops for magnetic materials) special results for special cases, since a general analysis appears hopelessly unwieldy.

An attempt to verify these conclusions is made by means of an analog computer study. A number of practical applications for the type of elements being studied is then pointed out.

ACKNOWLEDGEMENT

The author wishes to express his sincere thanks and appreciation to the following for their help in the preparation of this thesis:

R. A. Johnson, Associate Professor, Department of Electrical Engineering, the University of Manitoba, for his perpetual encouragement and helpful advice which contributed immensely to this thesis.

The Arnold Engineering Company, Marengo, Illinois, U.S.A., for their valuable assistance by supplying the cores used in the experiments, and the technical data pertaining to the cores.

E. R. Zaidman for her valuable assistance in editing this thesis.

The National Research Council of Canada, under whose grant the author carried out this investigation.

TABLE OF CONTENTS

	<u>Page</u>
Abstract	i
Acknowledgement.	ii
List of Figures.	vii
List of Graphs	x
List of Tables	xiii
List of Photographs.	xiv
Chapter I. INTRODUCTION	I
Chapter II. TECHNIQUES CONCERNING THE DERIVATION OF THE DESCRIBING FUNCTION FOR DOUBLE VALUED NONLINEARITIES.	5
II. 1 Sources of hysteresis in control systems.	5
II. 2 Derivation of describing function for hysteresis type nonlinearity, using a piece wise linear approximation.	9
II. 3 Additional methods available for deter- mining the describing function of double valued nonlinearities.	15
II. 3.1 Polynomial curve fitting method	15
II. 3.2 Graphic method.	16
II. 3.3 Block diagram method.	17
II. 4 Validity of previously stated methods. .	20

Chapter III.	THEORIES CONCERNING THE BEHAVIOUR OF MAGNETIC MATERIALS.	23
III. 1	The magnetization curve.	23
III. 2	The shape of the hysteresis loop when the applied field is of low magnitude.	26
III. 3	Residual induction	28
III. 4	The coercive force under the foregoing assumptions.	29
III. 5	Approximation for small signal input .	30
III. 6	Experimental tests of Rayleigh's assumptions.	31
III. 7	The relation between coercive force, residual induction and the applied field.	31
III. 8	The influence of working frequency on the shape of the hysteresis loop . . .	34
III. 9	Proposed relation between frequency and coercive force	35
III. 10	Summary.	38
Chapter IV.	EXTENSION OF DESCRIBING FUNCTION TECHNIQUES TO MORE GENERALIZED FORMS OF HYSTERESIS NONLINEARITY.	40

IV. 1	Piece wise linear model in which the width of the loop is linearly proportional to the input signal.	40
IV. 2	Piece wise linear model in which the width of the loop is a nonlinear function of the input signal.	52
Chapter V.	EXPERIMENTAL DERIVATION OF THE DESCRIBING FUNCTION FOR NONLINEAR MAGNETIC CORES . .	58
V. 1	The nature of the chosen cores	58
V. 2	Set-up of the cores for testing.	64
V. 3	Tests that may be performed.	66
V. 4	Describing function measurements under sinusoidal applied voltage to cores. . .	73
V. 4.1	Tests on 3T4178-P1	73
V. 4.2	Tests on 4T4168-D2	81
V. 5	Source impedance influence on the derivations of the describing function ,	85
V. 5.1	Tests on 3T4178-P1	88
V. 5.2	Tests on 4T4178-S4	97
V. 5.3	Tests on 4T4168-D2	97
V. 6	Analog computer verification of the results.	103
Chapter VI.	CONCLUSIONS.	113
REFERENCES.	117

Page

Appendix A. TECHNICAL DATA FOR THE TESTED CORES. . .	124
Appendix B. NUMERICAL DATA FOR GRAPHS.	125

LIST OF FIGURES

	<u>Page</u>
Fig. 2.1 Basic components of a simple control system	5
Fig. 2.2 Most encountered forms of hysteresis loops in control systems.	7
Fig. 2.3 Piece wise linear model for hysteresis non- linearity	9
Fig. 2.4 Piece wise linear model for hysteresis when saturation is present	12
Fig. 2.5 Describing function (saturation occurs) . .	14
Fig. 2.6 Describing function (saturation does not occur).	14
Fig. 2.7 Resolving multivalued nonlinear elements into single valued nonlinear elements . . .	18
Fig. 3.1 Three sections of the magnetization curve .	24
Fig. 3.2 Relation between magnetization curve and hysteresis loops for 4-79 Permalloy	25
Fig. 3.3 Variation of permeability with the applied field	26
Fig. 3.4 Residual induction, using the Rayleigh approximation	28
Fig. 3.5 Proposed shape of the hysteresis loop for low inputs according to Rayleigh.	29
Fig. 3.6 Relation between B_r and H_c for small signal inputs.	30

	<u>Page</u>
Fig. 3.7 Parameters used to estimate loop area . . .	37
Fig. 4.1 The variation of the width of the hysteresis loop with amplitude	40
Fig. 4.2 Piece wise linear approximation for hysteresis loop	49
Fig. 4.3 Analog computer set-up for simulating general forms of hysteresis nonlinearity. .	56
Fig. 5.1 Variation of Deltamax hysteresis loop with peak magnetizing force.	59
Fig. 5.2 D.C. and A.C. permeability curves of Deltamax.	60
Fig. 5.3 Variation of 4-79 Mo Permalloy hysteresis loop with peak magnetizing force.	62
Fig. 5.4 D.C. and A.C. permeability curves of 4-79 Mo Permalloy.	63
Fig. 5.5 Experimental set-up for derivation of the describing function for the cores	64
Fig. 5.6 Magnetic hysteresis loop.	66
Fig. 5.7 Hysteresis loop obtained under constant current drive	66
Fig. 5.8 Loop distortion with sinusoidal applied voltage	67
Fig. 5.9 Loop distortion with sinusoidal applied current	67

Fig. 5.10 Phase shift between input voltage and out- put voltage	80
Fig. 5.11 Behaviour of hysteresis loops near the origin.	84
Fig. 5.12 Simulated control system.	107
Fig. 5.13 The requirements for low amplitude limit cycle	112
Fig. 6.1 Mechanical hysteresis for a steel spring. .	114
Fig. 6.2 Hysteresis loop for dielectric materials. .	115

LIST OF GRAPHS

	<u>Page</u>
Graph 3.1 Coercive force vs. magnetizing force for various materials.	33
Graph 4.1 Describing function for non-saturating model.	44
Graph 4.2 Describing function for saturating model .	45
Graph 4.3 Critical loci for the piece wise linear model.	46
Graph 4.4 Describing function for second model (no saturation).	50
Graph 4.5 Describing function for second model, (saturation exists).	51
Graph 4.6 Approximated relation between b and A. . .	55
Graph 4.7 Describing function for nonlinear relation between b and A.	56
Graph 5.1 Describing function for 4-79 Mo Permalloy.	75
Graph 5.2 H_m/H_c vs. input amplitude for 4-79 Mo Permalloy.	76
Graph 5.3 Variation of saturation amplitude, and maximum value of the describing function with frequency for Supermalloy	77
Graph 5.4 Critical loci for 3T4178-P1.	82
Graph 5.5 Describing function for Deltamax	83
Graph 5.6 Critical locus for Deltamax.	86

Page

Graph 5.7	Describing function for Permalloy core (source impedance = 600 ohms).	89 .
Graph 5.8	Normalized curves for Permalloy.	90
Graph 5.9	Input impedance variations for Permalloy core	92
Graph 5.10	Effects of source impedance on the describ- ing function for Permalloy core.	94
Graph 5.11	Parameter variations for Permalloy core. .	95
Graph 5.12	Critical loci for Permalloy (source impedance = 600 ohms).	96
Graph 5.13	Describing function for Supermalloy core (source impedance = 600 ohms).	98
Graph 5.14	Normalized describing function for Supermalloy.	99
Graph 5.15	Critical loci for Supermalloy core	100
Graph 5.16	Describing function for Deltamax core (source impedance = 600 ohms).	101
Graph 5.17	Normalized describing function for Deltamax	102
Graph 5.18	Input impedance variations for Deltamax core	104
Graph 5.19	Comparison between two sets of describing functions.	105

Page

Graph 5.20 Critical loci for Deltamax core. 106

Graph 5.21 Prediction of limit cycle for Permalloy
core. 108

Graph 5.22 Prediction of limit cycle for Deltamax core 109

LIST OF TABLES

	<u>Page</u>
Table 3.1 Value of constants in relation H_m/H_c . . .	32 .
Table 5.1 Frequency and amplitude of limit cycle for Permalloy core	110
Table 5.2 Frequency and amplitude of limit cycle for Deltamax core.	111
Table B-1 Numerical data for graph 5.1	125
Table B-2 Numerical data for graph 5.5	127
Table B-3 Numerical data for graph 5.7	129
Table B-4 Numerical data for graph 5.13.	131
Table B-5 Numerical data for graph 5.16.	133

LIST OF PHOTOGRAPHS

	<u>Page</u>
Photo #1 Instrument set-up for testing cores	65
Photo #2 D. C. bias effect on the cores.	65
Photo #3 4T4178-S4 installed for testing	68
Photo #4 4T4168-D2 installed for testing	68
Photo #5 Dynamic hysteresis loops for Supermalloy.	70
Photo #6 Dynamic hysteresis loops for Deltamax	70
Photo #7 Input current and voltage to Deltamax	70
Photo #8 Input voltage and input current for Deltamax (600 ohms in series).	71
Photo #9 Input voltage and input current for Deltamax (no resis. in series).	71
Photo #10 Output voltage and input current for Permalloy	71
Photo #11 Input voltage and input current for Permalloy for 30 c/s.	72
Photo #12 Input voltage and input current for Permalloy for 40 c/s.	72
Photo #13 Current through Permalloy core and flux	72
Photo #14 Analog computer set-up.	79
Photo #15 Limit cycle with Deltamax core (current and input voltage).	79
Photo #16 Limit cycle with Deltamax core (current and output voltage)	79

CHAPTER I
INTRODUCTION

The describing function method of analyzing nonlinear systems is based on three assumptions:

- (i) There is only one nonlinear element in the system.
- (ii) The output of the nonlinear element depends only on the present value and past history of the input. No time-varying characteristics are included in the nonlinear elements.
- (iii) If the input of the nonlinear element is a sinusoidal signal, only the fundamental component of the output is considered.

Independent developments of essentially the same methods were made by R. J. Kochenburger (1) in the U.S.A., by L. C. Goldfarb (2) in the U.S.S.R., by A. Tustin (3) in Great Britain, by W. Oppelt (4) in Germany, and by J. R. Dutilh (5) in France. E. C. Johnson (6) applied the sinusoidal method of analysis to study the free play of backlash in servomechanisms.

The describing function method has been given in many standard textbooks (7, 8 and 9), and need not be given in detail here.

In this thesis we are concerned only with the application of the Fourier describing function method to systems with hysteresis type nonlinearities, and especially to those incorporating the magnetic or dielectric hysteresis phenomena.

When dealing with physical nonlinear elements, the degree of success from a practical point of view is usually determined by the nature of the assumptions that are made in the attempt to obtain a tractable answer. However, workable solutions can be obtained within certain classes of the problem.

For example, when the nonlinear characteristic is single valued, the input -- output relationship can be expressed analytically in the following ways:

- (i) as piece wise linear
- (ii) as a polynomial
- (iii) as a transcendental function.

To obtain the describing function for such nonlinear elements, one needs to evaluate an integral which determines the fundamental coefficient of a Fourier series. The derivation of certain describing functions derived from the piecewise expression is well known.

Those derived from the polynomial expressions are in the forms of gamma functions (8). When the nonlinearity is expressed by a transcendental function, say, a segment of a sine wave for the case of saturation, the corresponding describing function formula is in terms of Bessel functions (8).

There are some disadvantages in the analytical technique mentioned above:

(i) Many times it is necessary to assume unrealistic approximations when the actual nonlinearity is neither piecewise linear, an exact polynomial, nor, a transcendental function.

(ii) In using certain mathematical formulae, one is apt to lose sight of the physical picture involved in the nonlinearity.

However, these disadvantages are comparatively less serious in the case of single valued nonlinearities than the difficulties encountered in the case of double valued (or multiple-valued) nonlinearities such as hysteresis loops and backlashes.

In addition, complexity also arises in the nature of the applied signal. If, for example, a sufficiently large driving signal is applied, the character of the steady state solution usually becomes a strong function of the initial condition. Thus it becomes difficult to predict the resultant operation accurately. This is particularly true when the nonlinearity is also multivalued, e.g., the B-H characteristic of magnetic material.

As mentioned previously, the purpose of this thesis is to review some of the most common techniques which are used to derive the describing function for double valued nonlinearities and to point out the deviations in actual results while dealing with physical elements, as compared to theoretical results which were obtained under the assumptions mentioned later.

Chapter II outlines some of the techniques used to evaluate the describing function for double valued nonlinearities, and points out some considerations that should be taken into account while dealing with physical nonlinear elements.

Chapter III presents the theory of magnetic materials in order to evaluate the approximations which were used to represent hysteresis loops.

Chapter IV discusses some attempts which were made to evaluate the describing function for nonlinear elements in more complete form.

Chapter V investigates the actual behaviour of hysteresis type elements (magnetic cores) by a series of experiments. An attempt to verify the results thus obtained is made through the use of an analog computer study.

Chapter VI presents practical applications and conclusions of this work.

CHAPTER II

TECHNIQUES CONCERNING THE DERIVATION OF THE DESCRIBING FUNCTION FOR DOUBLE VALUED NONLINEARITIES

This chapter presents some of the techniques which are used while dealing with multi-valued nonlinearities. An evaluation of these methods in view of experimental results is made later.

II.1 Sources of Hysteresis in Control Systems

Consider a simple electromechanical servo control system as shown in Fig. 2.1.

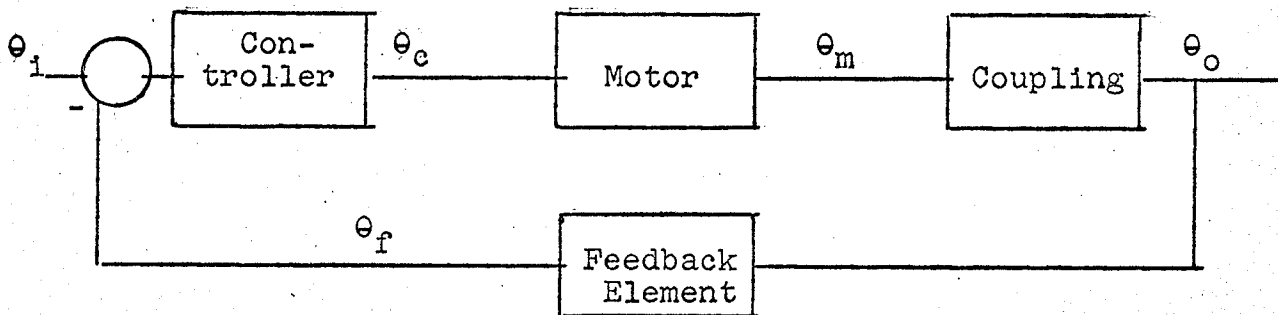


Fig. 2.1; Basic components of a simple control system.

The basic components of this system are:

- (i) the error sensing unit
- (ii) the controller amplifier unit
- (iii) the motor
- (iv) the output coupling unit.

One or more of these units generally has a hysteresis-type nonlinearity, whose source could be:

- (i) Backlash in the output coupling unit.
- (ii) The controller in a contactor system which incorporates a contactor, e.g., a bipolarized (electromagnetic) relay, possessing hysteresis.
- (iii) Field controlled electromagnetic devices such as amplidyne generators in the controller unit, field controlled motors, magnetic amplifiers or any other type of saturable reactor transducer, dielectric amplifier, etc.

That hysteresis might arise from sources (ii) or (iii) is evident. Backlash in the output coupling produces an hereditary effect when the load has negligible inertia and damping, equal to or greater than critical (3).

The functional characteristics arising from such a nonlinearity in different cases are illustrated in Figs. 2.2(a) through 2.2(f).

Performance of the system shown in Fig. 2.1 is difficult to analyze when more than one form of hysteresis occurs simultaneously. Analysis of individual effects of these nonlinearities has, however, been made.

The frequency response approach, in which the nonlinearity is replaced by its describing function, has been found most convenient for stability analysis of nonlinear systems.

The describing functions for double valued nonlinear elements whose characteristics are observed in Figs. 2.2(a), 2.2(b) and 2.2(f) have been discussed in published literature, (10, 11 and 12).

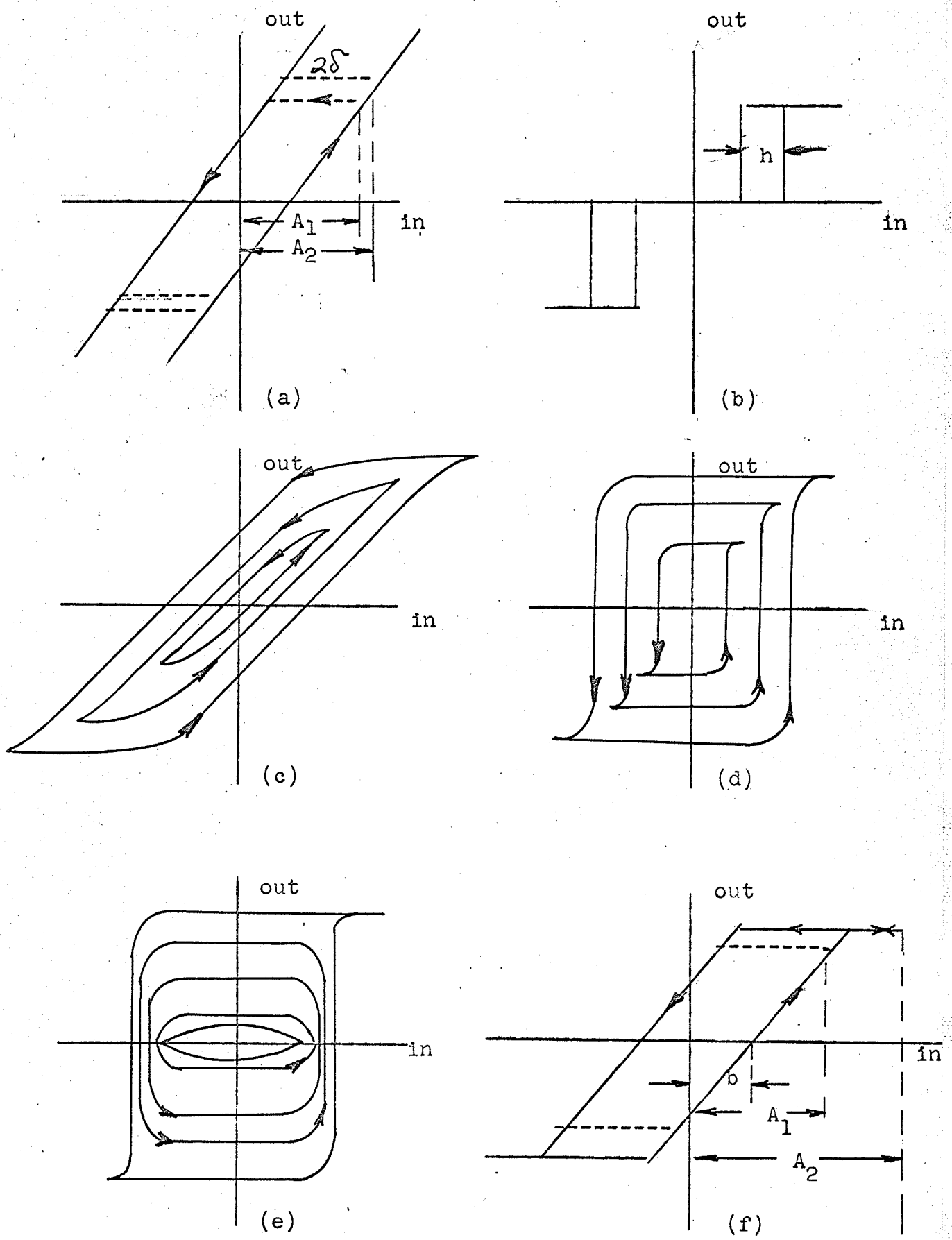


Fig. 2.2: Most encountered forms of hysteresis loops in control systems

Although these functions differ in detailed properties, a common feature is the predominance of nonlinear effects at comparatively small signal amplitudes, where a reduction in the magnitude of transfer gain is produced, together with a lagging phase shift. Both effects increase as the signal amplitude approaches the hysteresis width.

The phase lags cause the system's stability to be impaired at small signal levels, producing sustained oscillations of essentially small amplitude in an otherwise stable system.

In order to derive the describing function for the nonlinear characteristics shown in Fig. 2.2(c) through Fig. 2.2(e), it is required that the hysteresis characteristics would be expressible by convenient mathematical relationships. The forms of Figs. 2.2(c) through 2.2(e) require quite a complicated mathematical relationship (14) to describe them. A simplification, to be found in most of the books dealing with this subject (8, 9, 10 and 11), is obtained by assuming a hysteresis curve shown in Fig. 2.2(f).

The analysis of this approximation, which corresponds to the shape of the hysteresis loop presented in Fig. 2.2(f) is introduced first, due to the fact that this model might be improved upon in order to represent behaviour of hysteresis loops of the types shown in Figs. 2.2(c), 2.2(d) and 2.2(e).

II.2 Derivation of Describing Function for Hysteresis Type Nonlinearity, Using a Piece Wise Linear Approximation

A piece wise linear approximation for a hysteresis loop is shown in Fig. 2.3. The relation between the input and the output, V_{out} , is shown in Fig. 2.3

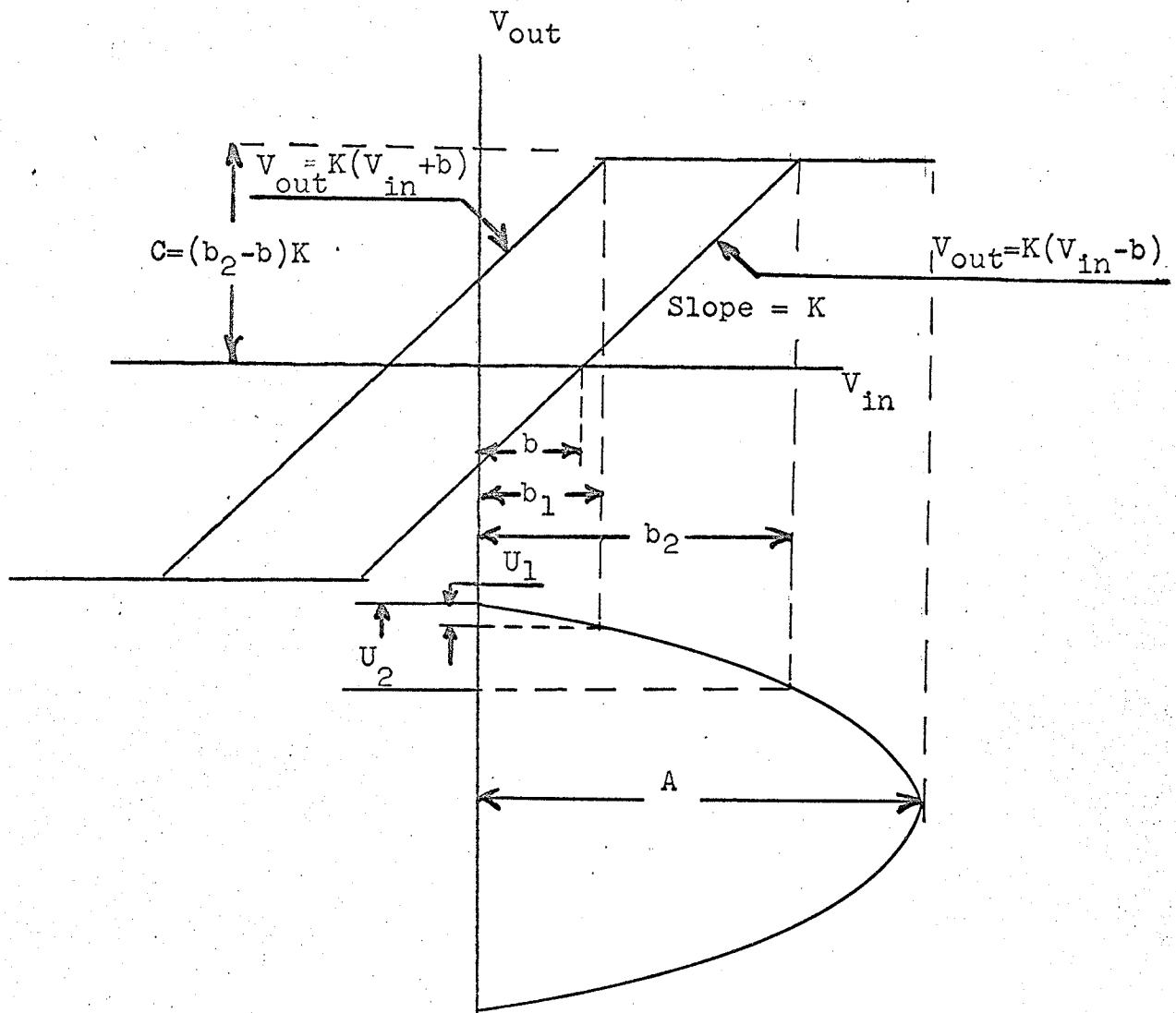


Fig. 2.3: Piece wise linear model for hysteresis nonlinearity.

The equivalent gain: "Keq" of such a nonlinear component might be given in cartesian co-ordinates by: $\overline{Keq} = G(A) + jB(A)$ where $G(A)$ and $B(A)$ are the normalized Fourier coefficients and may be given by:

$$G(A) = \frac{1}{\pi A} \int_0^{2\pi} f(A \sin \theta) \sin \theta d\theta, \text{ in phase component} \quad (2.1)$$

$$B(A) = \frac{1}{\pi A} \int_0^{2\pi} f(A \sin \theta) \cos \theta d\theta, \text{ quadrature component} \quad (2.2)$$

In our own case, if we put $X=A \sin U$ and write the integral as a sum of integrals arising from each segment, we get:

$$\begin{aligned} G(A) &= \frac{1}{\pi A} \int_0^{2\pi} f(A \sin U) \sin U dU = \\ &\quad \frac{1}{\pi A} \int_0^{U_2} K(A \sin U - b) \sin U dU + \\ &\quad + \frac{1}{\pi A} \int_{U_2}^{\pi-U_1} K(A-b) \sin U dU + \\ &\quad + \frac{1}{\pi A} \int_{\pi-U_1}^{\pi+U_2} K(A \sin U + b) \sin U dU + \\ &\quad + \frac{1}{\pi A} \int_{\pi+U_2}^{2\pi-U_1} K(A-b) \sin U dU + \\ &\quad + \frac{1}{\pi A} \int_{2\pi-U_1}^{2\pi} K(A \sin U - b) \sin U dU. \end{aligned} \quad (2.3)$$

Because of symmetry conditions in the shape of the wave form going out of the nonlinear element ($f(U) = -f(-U)$), we can integrate only over a half-period. Thus, we get:

$$\begin{aligned}
 G(A) = & \frac{2}{\pi A} \int_0^{U_2} K(A \sin U - b) \sin U \, dU + \\
 & + \frac{2}{\pi A} \int_{U_2}^{\pi - U_1} K(A - b) \sin U \, dU + \\
 & + \frac{2}{\pi A} \int_{\pi - U_1}^{\pi} K(A \sin U + b) \sin U \, dU.
 \end{aligned} \tag{2.4}$$

This can be worked out into:

$$\begin{aligned}
 G(A) = & \frac{K}{\pi} \left[(U_1 + U_2) + \frac{1}{2}(\sin 2U_1 - \sin 2U_2) + \frac{2b}{A} (\cos U_2 - \cos U_1) + \right. \\
 & \left. + \frac{2C}{KA} (\cos U_2 + \cos U_1) \right].
 \end{aligned} \tag{2.5}$$

Referring to Fig. 2.3 one can see that $U_1 = \arcsin \frac{b_1}{A}$,

$U_2 = \arcsin \frac{b_2}{A}$, $C = (b_2 - b) K = (A \sin U_2 - b)K$, $b_2 = A \sin U_2$

and $b = \frac{1}{2}(b_2 - b_1) = \frac{1}{2}(A \sin U_2 - A \sin U_1)$.

Substituting into (2.5) we get:

$$G(A) = \frac{K}{\pi} \left[U_1 + U_2 + \frac{1}{2} \sin 2U_1 + \frac{1}{2} \sin 2U_2 \right], \tag{2.6}$$

we can similarly derive the expression for $B(A)$

$$\begin{aligned}
 B(A) = & \frac{2}{\pi A} \int_0^{U_2} K(A \sin U - b) \cos U \, dU + \\
 & + \frac{2}{\pi A} \int_{U_2}^{\pi - U_1} C \cos U \, dU + \\
 & + \frac{2}{\pi A} \int_{\pi - U_1}^{\pi} K(A \sin U + b) \cos U \, dU.
 \end{aligned} \tag{2.7}$$

Thus, after carrying out the same procedure as before, we get

$$B(A) = \frac{-K}{\pi} (\sin^2 U_2 - \sin^2 U_1). \quad (2.8)$$

The above expressions for $G(A)$ and $B(A)$ were derived under the assumption of saturation conditions. If, however, saturation is not present, then we have the condition as shown in Fig. 2.4.

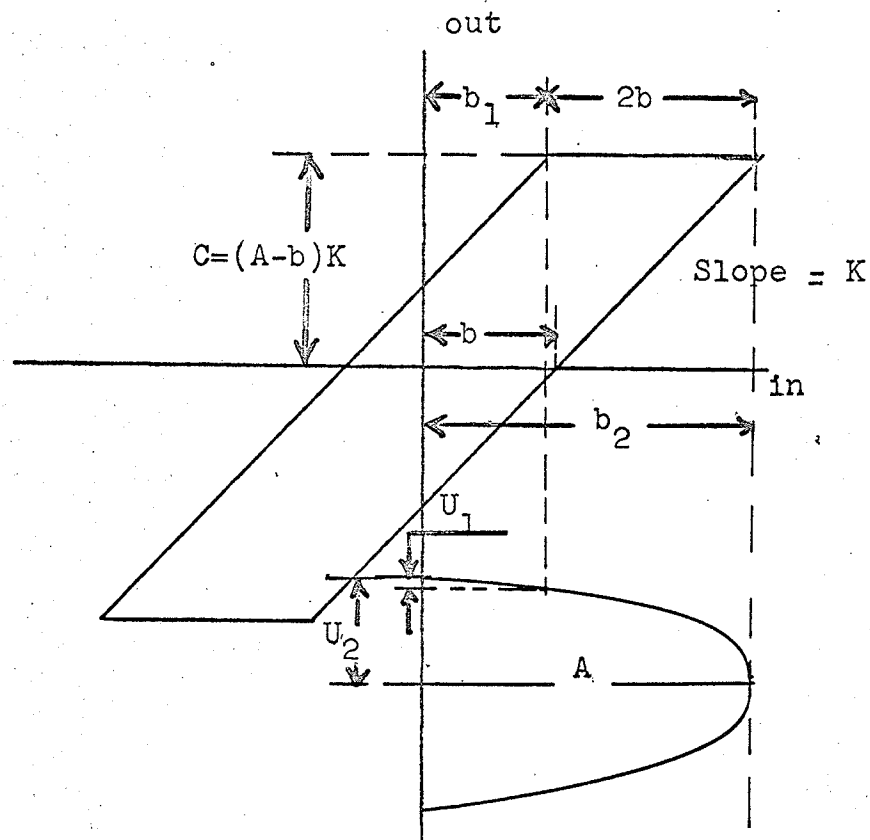


Fig. 2.4: Piece wise linear model for hysteresis when saturation is not present.

Thus U_2 becomes equal to $\frac{\pi}{2}$,

U_1 becomes equal to $\arcsin \frac{A-2b}{A}$,

and

C becomes equal to $(A-b)K$.

Let us substitute these conditions into the equations of $B(A)$ and $G(A)$ which were derived before.

The form of $G(A)$ when saturation is present is given by:

$$G(A)_{\text{sat.}} = \frac{K}{\pi} (U_1 + U_2 + \frac{1}{2} \sin 2U_1 + \frac{1}{2} \sin 2U_2).$$

Substituting the new relations yields:

$$G(A)_{\text{no sat.}} = \frac{K}{\pi} (U_1 + \frac{\pi}{2} + \frac{1}{2} \sin 2U_1). \quad (2.9)$$

The form of $B(A)$ when saturation is present is given

by:

$$B(A)_{\text{sat.}} = \frac{-K}{\pi} (\sin^2 U_2 - \sin^2 U_1)$$

Substituting the new relations yields:

$$B(A)_{\text{no sat.}} = \frac{-K}{\pi} (1 - \sin^2 U_1) = \frac{-K}{\pi} \cos^2 U_1. \quad (2.10)$$

Using the relations

$$\sin U_1 = \frac{A-2b}{A} = \left(1 - \frac{2b}{A}\right), \quad (2.11)$$

$$\cos^2 U_1 = 1 - \sin^2 U_1 = \left(\frac{4b}{A} - \frac{4b^2}{A^2}\right) = \frac{4b}{A} \left(1 - \frac{b}{A}\right). \quad (2.12)$$

And substituting (2.12) into (2.10) we get:

$$B(A)_{\text{no sat.}} = \frac{-4Kb}{\pi A} \left(1 - \frac{b}{A}\right) \quad (2.13)$$

The equivalent gain in its absolute value is given by:

$$|K_{\text{eq}}| = \left[G(A)^2 + B(A)^2 \right]^{\frac{1}{2}} \quad (2.14)$$

And the phase shift of the nonlinear element is given by:

$$\text{tg } \varphi(A) = \frac{B(A)}{G(A)} \quad \text{or}$$

$$\varphi(A) = \text{arc tg } \frac{B(A)}{G(A)}. \quad (2.15)$$

It should be noted, that throughout the entire derivation, the width of the hysteresis loop (b) was assumed constant, and that the formulae are not valid for $A < b$, since then the output is actually zero.

The equivalent gain and phase for both cases is shown in Figs. 2.5 and 2.6.

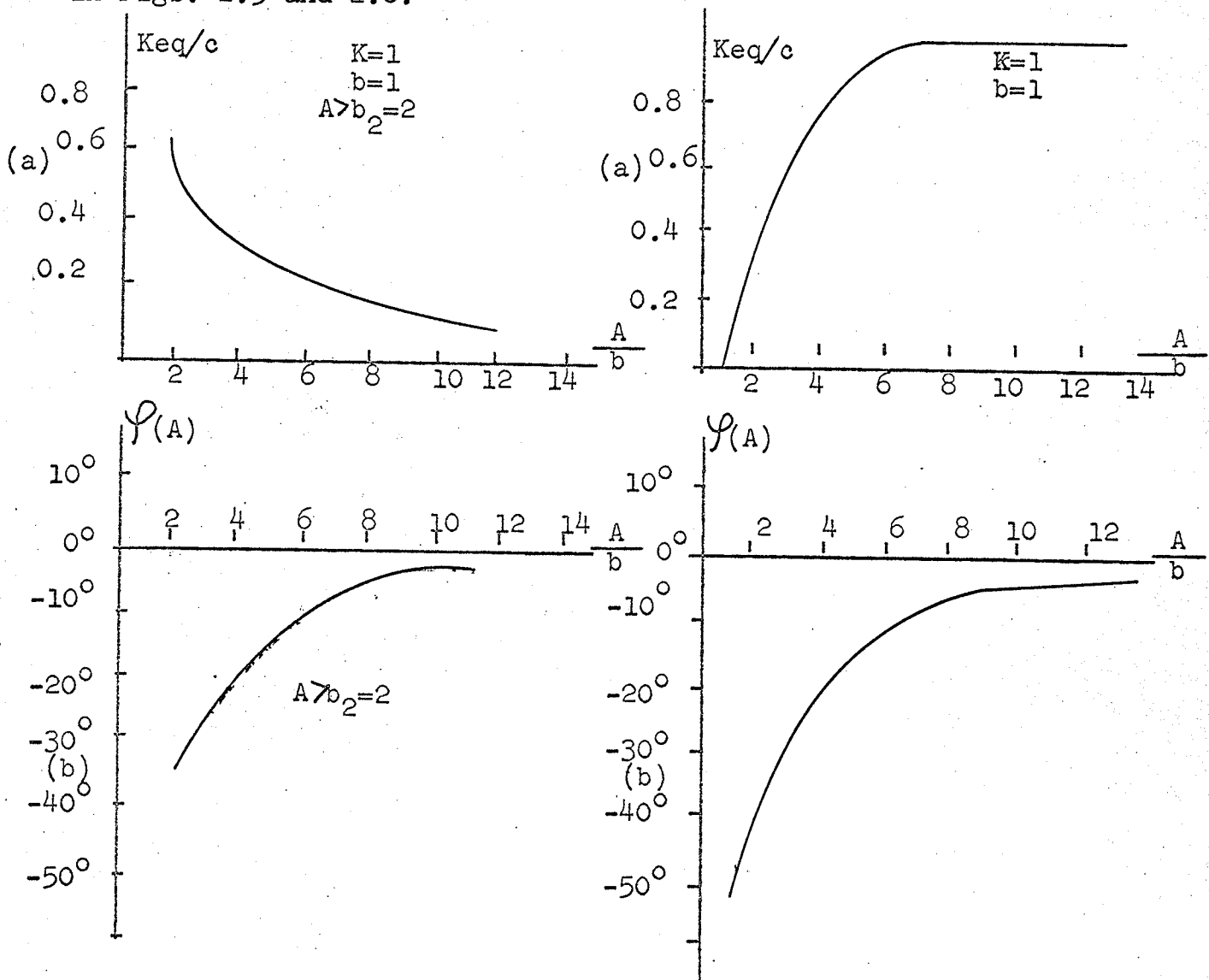


Fig. 2.5: Describing function when saturation occurs, (a) magnitude - (b) phase.

Fig. 2.6: Describing function when saturation does not occur, (a) magnitude - (b) phase shift.

II.3 Additional Methods Available for Determining The Describing Function of Double Valued Nonlinearities

In this section, less common methods for deriving the describing function for hysteresis type nonlinearity will be mentioned briefly.

II.3.1 Polynomial Curve Fitting Method

This method was proposed by C. Lakshmi-Bai in 1960 (15). According to this method, a simple transformation is advanced for correlating the characteristic of a nonlinear element with the harmonic content in its frequency response to sinusoidal inputs. By a process of curve fitting, the characteristic is represented by a polynomial. The frequency response to sinusoidal inputs is represented as a Fourier series. The polynomial and the Fourier series are related by means of the simple transformation:

$$X = \sin \theta \quad -1 \leq X \leq +1. \quad (2.16)$$

The nonlinear characteristic is represented as a polynomial in X (and therefore in $\sin \theta$) by virtue of equation (2.16), and by using simple trigonometric identities, it is possible to calculate the harmonic content in the response of the nonlinear element. This method is limited only to sinusoidal inputs.

Although this technique yields better results in comparison to other techniques, it is obvious that it is useless when the width of the hysteresis loop is a function of the input signal.

II.3.2 Graphic Method

This method was proposed by Y. H. Ku and C. F. Chen in 1962 (16) for evaluating the describing function of hysteresis type nonlinearities. According to this method, a circle with radius A is constructed to represent sinusoidal input $A \sin \theta$, where $\theta = \omega t$. Then, output contour C with area A_1 and output contour C' with area B_1 are constructed. To simplify, the amplitude of the sinusoidal input signal is taken as unity. The area of the input unit circle then becomes π .

Also, the output contour C has its area given by

$$A_1 = \int_0^{2\pi} f(\theta) \sin \theta \, d\theta, \quad (2.17)$$

where $f(\theta)$ denotes the output as a function of $\theta = \omega t$. The ratio of the area A_1 to the area of the unit circle is given by:

$$a_1 = \frac{A_1}{\pi} = \frac{1}{\pi} \int_0^{2\pi} f(\theta) \sin \theta \, d\theta. \quad (2.18)$$

Thus, A_1 is the Fourier coefficient for the fundamental sine component of the output wave $f(\theta)$. Similarly, the output contour C' has its area given by:

$$B_1 = \int_0^{2\pi} f(\theta) \cos \theta \, d\theta. \quad (2.19)$$

The ratio of the area B_1 to the area of the unit circle is given by:

$$b_1 = \frac{B_1}{\pi} = \frac{1}{\pi} \int_0^{2\pi} f(\theta) \cos \theta \, d\theta. \quad (2.20)$$

Thus, b_1 is the Fourier coefficient for the fundamental cosine component of the output wave $f(\theta)$.

The amplitude of the fundamental component of the output wave is given by

$$c_1' = \sqrt{(a_1^2 + b_1^2)}, \quad (2.21)$$

and the phase shift is given by

$$\phi_1 = \text{tg}^{-1} \frac{(b_1)}{(a_1)}. \quad (2.22)$$

As with the previous method, so this one too cannot be used when the width of the hysteresis loop is a function of the input signal.

II.3.3 Block Diagram Method

The following method, presented by A. K. Mahalanobis (18) and A. K. Nath is based on the fact that generally it is possible to specify any double valued nonlinearity by three or four different entities. These are:

- (i) the amount of hysteresis width,
- (ii) the number of piece wise linear segments along with their slopes, and,
- (iii) the saturation level.

In addition, there may also be a dead-band width, as in the case of three position relays.

For a double valued nonlinear element which might be specified in terms of the four entities stated above, it is

possible to represent the double valued nonlinearity by a combination of elements, as shown in Fig. 2.7.

The first element is a dead-band type nonlinearity with the same width as found in the original nonlinearity and the slope of the segments is unity.

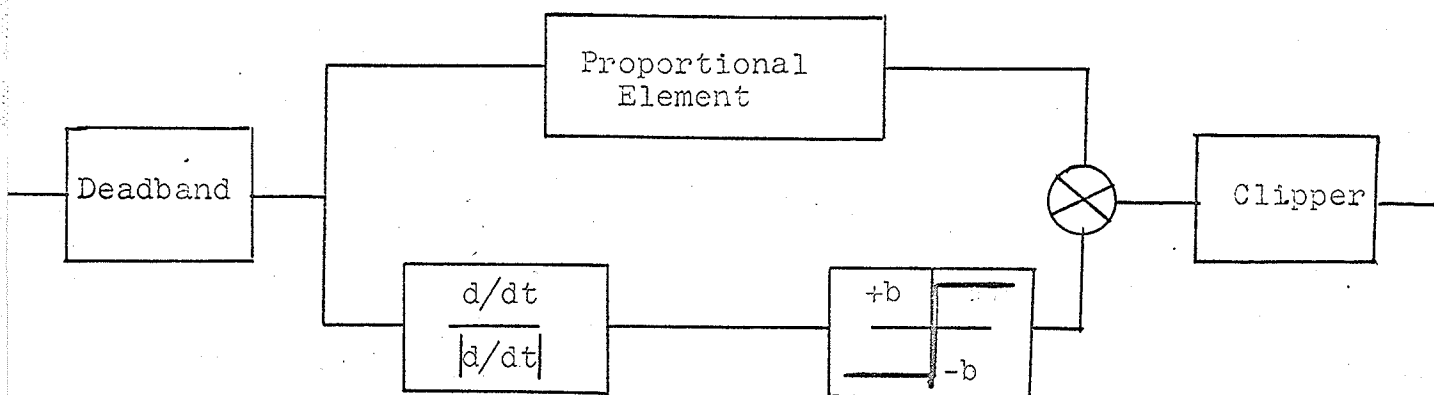


Fig. 2.7: Resolving multi-valued nonlinear elements into single valued nonlinear elements.

Following this element are two branches - the upper being a simple proportional element with a constant of proportionality equal to one, while the lower branch gives an output of \pm (half the hysteresis width), the sign being determined by that of the input derivative. Following these elements is another element of the limiter type with slope and limiting level equal to that of the actual nonlinearity. The dead-band and the limiting effect might be eliminated, depending on the actual type of double valued nonlinearity under discussion.

The result is that a double valued nonlinearity, $N(i)$, is resolved into two simple nonlinearities.

$$N(i) = N_1(i) + N_2 \left(\frac{di/dt}{|di/dt|} \right) \quad (2.23)$$

Where both N_1 and N_2 represent a single valued nonlinearity to which the conventional method of deriving the describing function is applicable, what is now needed is knowledge of the equivalent gains of two or three single valued nonlinearities and of the rules of computing the effective gain of these in series or in parallel. The former are available from the literature, and as to the latter, it can be proved that the effective equivalent gain of two nonlinearities with individual gains N_1 and N_2 in the minimum R.M.S. sense is:

$$N_s = N_1 N_2 \quad (2.24)$$

when they are in cascade, and

$$N_p = N_1 + N_2 \quad (2.25)$$

when they are in parallel.

This method is invaluable in simulating double valued nonlinearities, and also in compensating hysteresis effects in control systems by simulating with the proposed block diagram a positive hysteresis which would cancel the effects of the usual one by connecting it into the system (19).

It is readily seen that for cases in which the width of the hysteresis loops depend upon the input amplitude, this technique has no advantage over the one proposed in Sec. II.2.

II.4 Validity of Previously Stated Methods

All the techniques discussed thus far might yield relatively reasonable results when applied to certain types of systems incorporating double valued nonlinearities.

However, a clear distinction must be made as to which double valued nonlinear elements the results derived under the preceding techniques might be applied.

It is a common practice in most of the available texts to mention the phenomena of hysteresis and backlash and to apply the same describing function to any nonlinear element incorporating either of these phenomena.

The word hysteresis is derived from the Greek meaning "to lag behind" (20). Therefore, any element which would cause the output to lag behind the input might actually be classified as a hysteretic element.

There are, however, some basic differences among all these types of nonlinearities which do not allow us to apply indiscriminately the results which were obtained under previous assumptions.

Comparison of a backlash characteristic (Fig. 2.2(a)) with either one of the hysteresis characteristics shown in Fig. 2.2(c) through Fig. 2.2(e) shows that the fundamental difference between the two types of characteristics is in the dependence of the x and y intercepts upon the magnitude of the input signal and in the presence of saturation effects.

While the methods discussed thus far might cope with backlash characteristics or with a combined effect of backlash and saturation or any type of double valued nonlinearity having a constant width; only the first method (Sec. II.2) and to some extent the fourth method (Sec. II.3.3) might partially be put to deal with a hysteresis type nonlinearity in which the width of the hysteresis loop is a function of the input signal.

Due to the complexity involved in the mathematical description of this phenomena, very few attempts were made to represent the mathematical model needed for the evaluation of the describing function for this type of nonlinearity. Only three attempts in this direction have actually been made, the first by L. M. Vallese (21 and 22) who studied the effects of a hysteresis nonlinearity on the operation of a second order servomechanism by applying the method of Kryloff and Bogoliouboff to make an approximate time domain analysis of the system.

Additional work done by A. K. Mahalanobis (23) as well as C. B. Neal and D. B. Bunn (24) assumed a linear relationship between the width of the hysteresis loop and the input signal.

These publications referred to magnetic hysteresis as being the most important and the most encountered type of hysteresis in control systems. Needless to say, there are also other elements involved in the operation of control

systems that might present the same type of phenomena, i.e., dielectric capacitors and mechanical transducers.

However, by analyzing the behaviour of the magnetic elements, one can extend the results to different types of elements, due to similarities in the nature of the involved phenomena.

Before presenting or evaluating the aforementioned publications, it is necessary to review some of the properties of magnetic materials in connection with the theory of hysteresis loops.

CHAPTER III
THEORIES CONCERNING THE BEHAVIOUR OF
MAGNETIC MATERIALS

This chapter presents some theories regarding the behaviour of magnetic materials, to the extent which they are needed for the purposes of our discussion.

III.1 The Magnetization Curve

A typical magnetization curve, showing the relation between B the induction and H the field strength, in a specimen initially unmagnetized, is shown in Fig. 3.1.

In the first region, the curve starts from the origin with finite slope $\frac{dB}{dH} = \mu_0$ and rises so that it is concave upward, usually following the Rayleigh relation (25).

$$\mu = \mu_0 + \gamma H \quad (3.1)$$

where μ is the normal permeability in the field H, $\gamma = \frac{d\mu}{dH}$ and has a constant value and μ_0 is the initial permeability. Also,

$$B = \mu H = \mu_0 H + \gamma H^2. \quad (3.2)$$

The initial portion of the curve is said to be reversible, that is, the magnetization curve is approximately retraced when the magnetizing field is diminished; thereby not giving rise to a hysteresis loop.

In the reversible region, we have $\frac{dB}{dH} \approx \mu_r$ where $\mu_r = \mu$ reversible region.

In the second portion of the curve, $\frac{dB}{dH}$ might be one hundred times larger than μ_r . This portion is not reversible,

i.e., when the field is diminished, we would no longer retrace the original curve.

Above the knee, or in the third portion, we use the formula given by Fröelich and Kennelly -- $\frac{1}{\mu} = a+bH$, where a and b are constants, depending upon the material at hand (26 and 27).

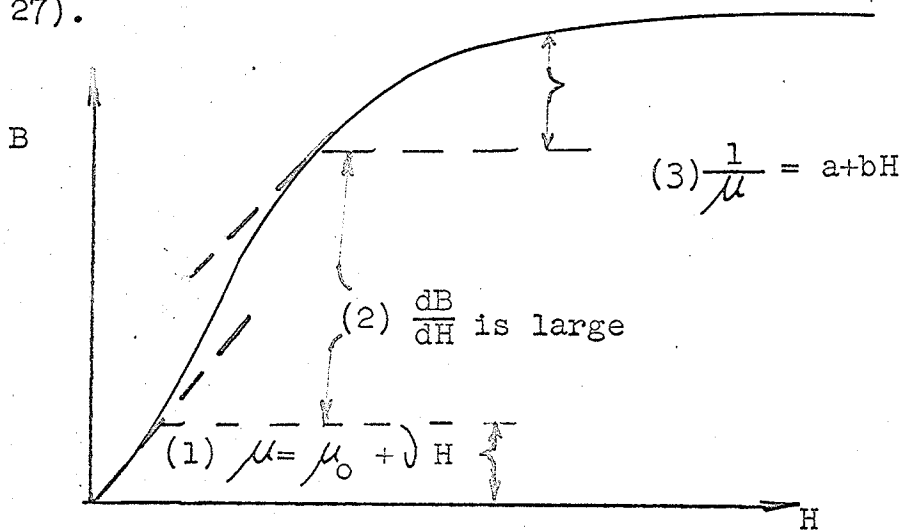


Fig. 3.1: Three sections of the magnetization curve.

The correspondence between these three regions of the magnetization curve and the hysteresis loop is shown in Fig. 3.2. The process which occurs during the magnetization of the specimen may be classified as irreversible or reversible, according to whether or not the energy dissipated in heat is a relatively large or small fraction of the potential energy. Considering these classifications, the three main parts of the magnetization curve may be identified with the processes as follows:

- (1) reversible boundary displacement,
- (2) irreversible boundary displacement, and,
- (3) reversible rotation.

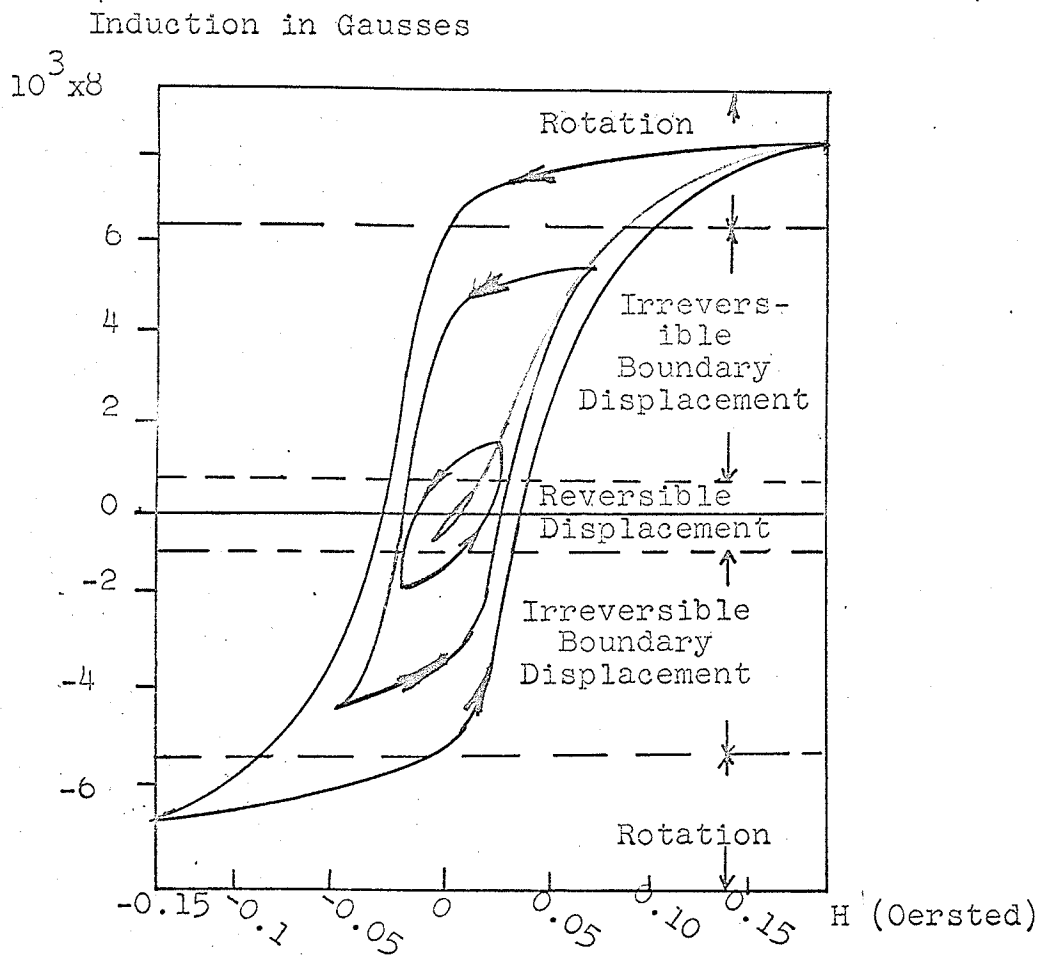


Fig. 3.2: Relation between magnetization curve and hysteresis loops for 4-79 Permalloy.

III.2 The Shape of the Hysteresis Loop When the Applied Field is of Low Magnitude

An experimental formula for the initial portion of the magnetization curve was given by Lord Rayleigh, and was previously presented in section III.1.

From (3.1) we can see that by this formula $\mu = \mu_0$ when H becomes zero. A typical relation between μ and H is shown in Fig. 3.3.

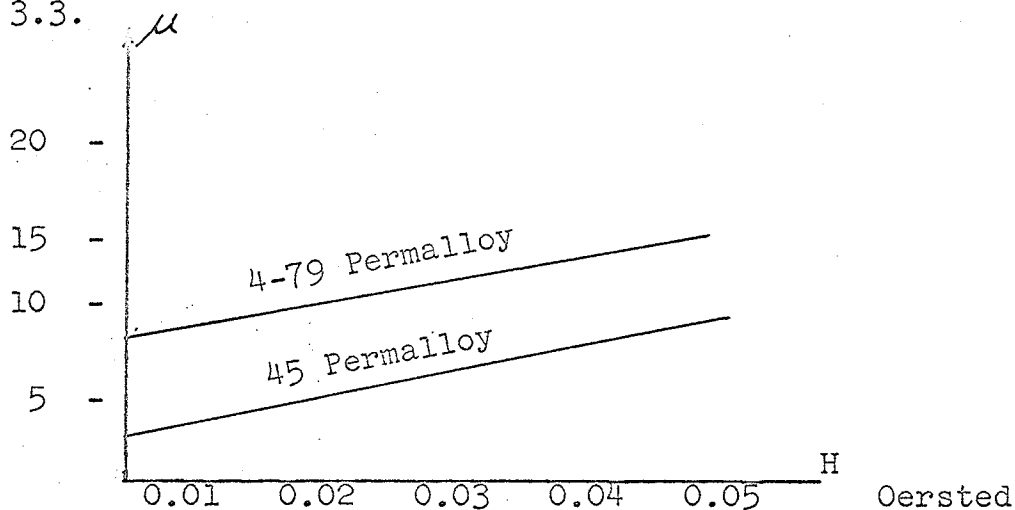


Fig. 3.3: Variation of permeability with the applied field.

One of the questions to be answered when deriving the describing function is: what are the shapes of hysteresis loops for low excitations, and how do they shrink when the field is diminished?

Rayleigh proposed a model which quite agrees with experiments done later by Ellwood (28).

According to Rayleigh, the hysteresis loops for low excitation are in the shape of parabolic segments. This parabola can be represented by a straight line with positive correction for the upper branch and negative correction for the lower one. The corrective terms must be equal to zero at $H = \pm H_m$, where H_m is the maximum amplitude of the applied field. Also, the initial slope of the parabolic curves as they leave the tips should be μ -- the same as the initial slope of the magnetization curve. Under these assumptions, it follows that

$$B = \mu^* H + K(H_m^2 - H^2), \quad (3.3)$$

where $\mu^* = \mu_0 + \gamma H_m$, and K is a proportionality constant. In order to evaluate K , we take the derivative of B with respect to H ,

$$\frac{\partial B}{\partial H} = \mu^* - 2KH, \quad (3.4)$$

For $H = H_m$, we require that the slope of the upper branch will be

$$\mu^* - 2KH_m = \mu_0. \quad (3.5)$$

Therefore,

$$K = \frac{\mu^* - \mu_0}{2H_m},$$

and the general equation would be:

$$B = \mu^* H \pm \frac{\mu^* - \mu_0}{2H_m} (H_m^2 - H^2). \quad (3.6)$$

$$\text{Recall } \mu^* = \frac{B_m}{H_m} = \mu_0 + \gamma H_m,$$

and by substituting it into (3.6), we get

$$B = (\mu_0 + \gamma H_m) H \pm \left\{ \frac{\gamma}{2} \right\} (H_m^2 - H^2). \quad (3.7)$$

The slope of the lower branch is

$$\frac{dB}{dH} = \mu_0 + \nu_{H_m} + \nu_H,$$

and it is easily seen that for $H=H_m$ this slope would be equal to

$$\mu_0 + \nu_{H_m} + \nu_{H_m} = \mu_0 + 2\nu_{H_m}. \quad (3,8)$$

III.3 Residual Induction

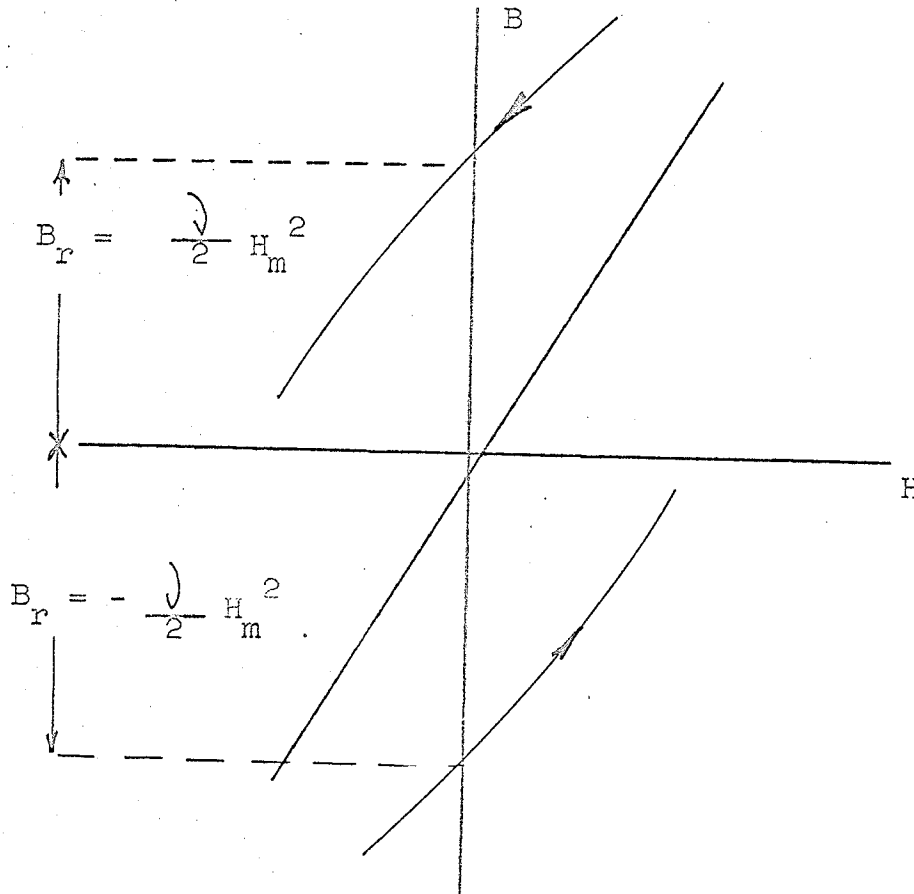
Under the foregoing assumptions:

$$B = (\mu_0 + \nu_{H_m}) H - \left(\frac{\nu}{2}\right) (H_m^2 - H^2).$$

Setting $H=0$ into the above expression, we get

$$B_r = \pm \frac{\nu}{2} H_m^2. \quad (3.9)$$

This is shown in Fig. 3.4.



g. 3.4: Residual induction using the Rayleigh approximation.

Fig. 3.5 illustrates all relations derived thus far.

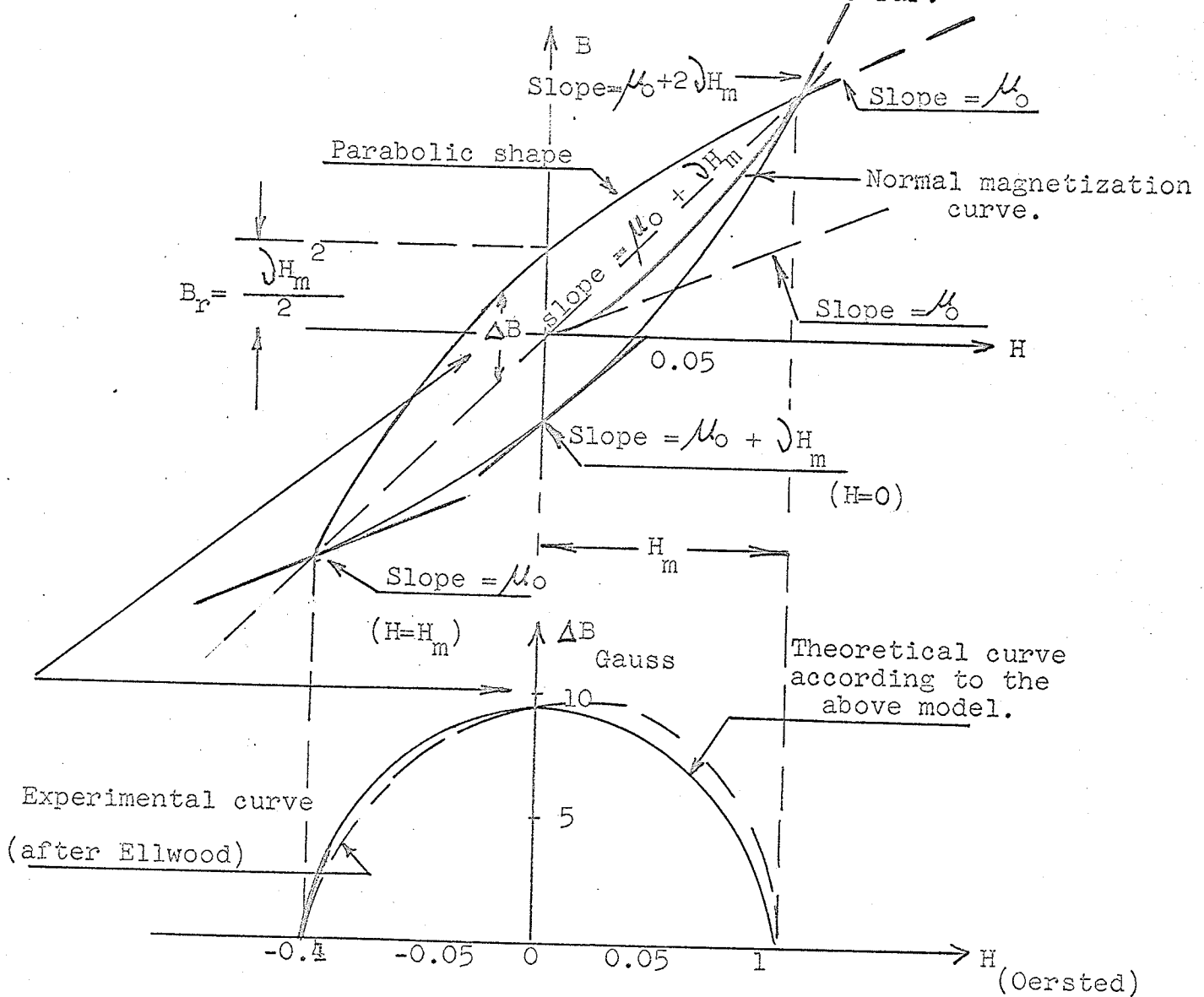


Fig. 3.5: Proposed shape of the hysteresis loop for low inputs according to Rayleigh.

III.4 The Coercive Force Under the Foregoing Assumptions

Setting $B=0$ in the general equation, we get for the

lower branch (see equation 3.7):

$$(\mu_0 + \delta H_m) H_c - \frac{\delta}{2} (H_m^2 - H_c^2) = 0.$$

$$\frac{\delta}{2} H_c^2 + (\mu_0 + \delta H_m) H_c - \frac{\delta}{2} H_m^2 = 0$$

$$H_c = -\frac{1}{\mathcal{J}} (\mu_0 + \mathcal{J}H_m) + \sqrt{\left(\frac{1}{\mathcal{J}}\right)^2 (\mu_0 + \mathcal{J}H_m)^2 + H_m^2}$$

If we recall: $\mu_0 + \mathcal{J}H_m = \mu^*$,

we get:

$$H_c = \sqrt{\frac{\mu^{*2}}{\mathcal{J}^2} + H_m^2} - \frac{\mu^*}{\mathcal{J}} \quad (3.10)$$

Note: When H_m is zero, so is H_c .

III.5 Approximation for Small Signal Input

For very small loops, i.e. for a very low H_m , we might also use the following approximation:

If $H_m \ll \frac{\mu^*}{\mathcal{J}}$, the loop becomes very narrow, then the relation between H_c and B_r is given by the slope of the axis μ^* , that is $H_c = \frac{B_r}{\mu^*} = \frac{\mathcal{J}H_m^2}{2\mu^*}$. (3.11)

The reason for this approximation is shown in Fig. 3.6.

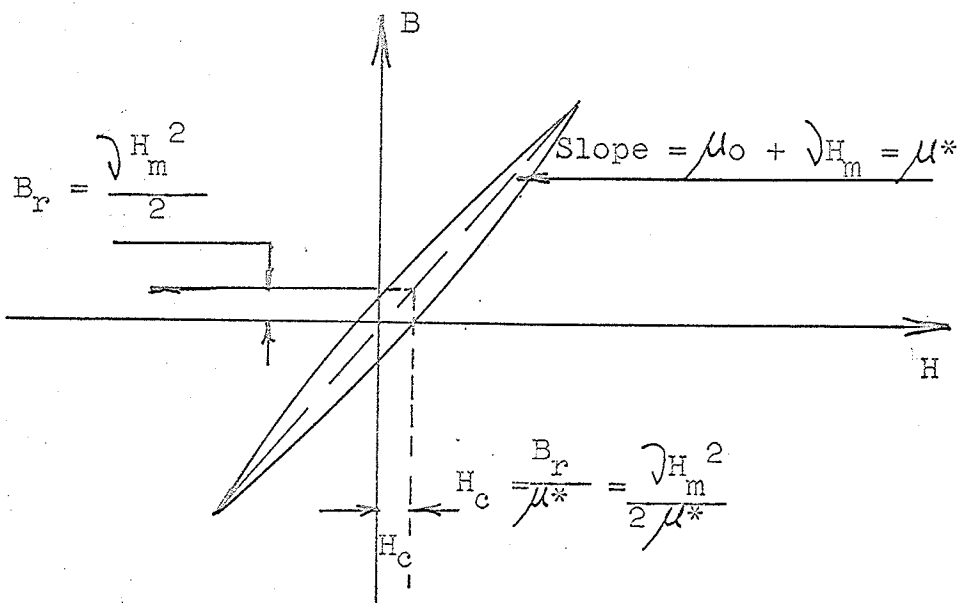


Fig. 3.6: Relation between B_r and H_c for small signal input.

III.6 Experimental Tests of Rayleigh's Assumptions

Since Rayleigh's experiments, the most careful measurements on the size and shape of hysteresis loops and also on the μ and H curves were done by Ellwood (28). The shape of the loops thus obtained were somewhat different, but within the limits of experimental errors. Comparison between Ellwood's results and Rayleigh's results are shown in Fig. 3.5, p. 29.

III.7 The Relation Between Coercive Force, Residual Induction and The Applied Field

From the theory presented thus far, we can conclude that in weak fields, the coercive force and residual induction are proportional to the square of the maximum field strength H_m^2 . (See Sec. III.3, p.28)

However, in strong fields, they approach limiting values which are called "The Coercivity" and "The Retentivity". An exhaustive set of experiments done by Sanford and Cheney (29 and 30) illustrates that the curves showing the relation between H_c (the coercive force) and H_m ; and B_r (the remnant induction) and H_m are similar to the normal magnetization curve.

The major difference between the above mentioned curves and the normal magnetization curve is that they start from the origin with an initial slope equal to zero, while the magnetization curve starts with slope equal to μ_0 .

While for low values of H_m we use the theory presented by Rayleigh, Sanford and Cheney found that the upper portion of these curves might be represented quite adequately by the following analytical expressions, which closely resemble the expression first proposed by Frölich and Kennelly for the upper portion of the normal magnetization curve:

$$H_m/H_c = a_1 + b_1 H_m \quad (3.12)$$

$$H_m/B_r = a_2 + b_2 H_m \quad (3.13)$$

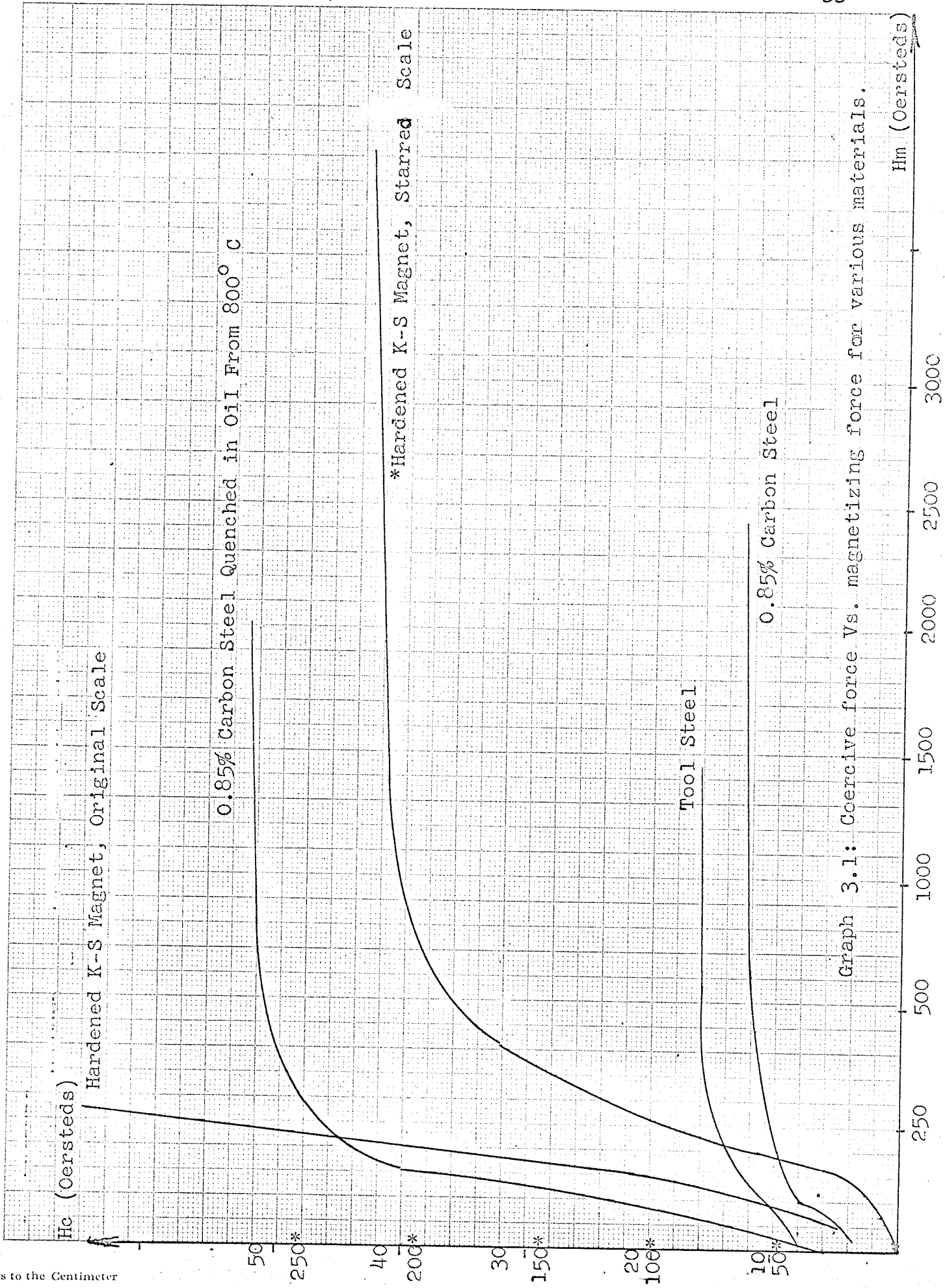
where a_1 and a_2 are constants, b_1^{-1} is the coercivity and b_2^{-1} the retentivity.

Typical values of a_1 and of the coercivity $H_c \infty = \frac{1}{b_1}$ for some materials are shown in Table 3.1.

<u>Material</u>	<u>a_1</u>	<u>$1/b_1 = H_c \infty$</u>	<u>H_m for $H_c = 0.95 H_c \infty$</u>
4-79 Mo Permalloy	0.3	0.037	0.2
Iron	0.25	0.73	3.7
Mild Steel	0.26	4.1	23
Honda Steel	0.4	220	1750

Table 3.1 Value of constants in relation $H_m/H_c = a_1 + b_1 H_m$, and calculated field required for H_c to be 0.95 of its limiting value.

Typical graphs showing the coercive force for some materials are plotted in Graph 3.1, p.33.



Graph 3.1: Coercive force Vs. magnetizing force for various materials.

III.8 The Influence of Working Frequency on The Shape of The Hysteresis Loop

So far, no attempt has been made to take frequency into account when deriving the describing function for nonlinear magnetic or dielectric elements.

It is a well known fact that losses in such materials increase rapidly with frequency, and also that said losses are proportional to the area traced by the B-H (or D-E where D is electric displacement, and E is the field strength) characteristics of such materials. This fact suggests a relation between the frequency of the applied signal and the width of the hysteresis loop (which, of course, is proportional to the area of the loop).

Although there are many experimental formulae relating losses in the core to frequency (27 and 30), no expression relating the width of the loop to the frequency is available.

If we assume operation in a constant or very narrow band of frequencies, it is legitimate to assume that the loop shape would not be appreciably changed with frequency, thus eliminating this factor from our calculations.

However, while trying to predict a limit cycle in a control system, one must take into account the fact that instability might occur for more than one frequency, or for quite a wide band of frequencies, depending upon the system's gain.

The experimental results which are shown later clearly prove that frequency must be accounted for. Most texts concerned with the describing function do not discuss frequency dependent nonlinearities. Nevertheless, sometimes, by transformation of the frequency dependent nonlinearity into a frequency independent nonlinearity and linear storage element, one can derive the describing function in the conventional manner.

The first step in using such a method is to determine how the nonlinear element behaves through frequency changes, and this, of course, brings us back to the problem mentioned before.

III.9 Proposed Relation Between Frequency and Coercive Force

The following derivations were not checked experimentally due to the complexity involved in such measurements, and their purpose is to present the problem rather than solve it.

It is well known that losses in magnetic materials are mainly due to two factors:

(1) Iron losses were given experimentally by Steinmetz as $W_h = K_h f B_m^n$ watts, where K_h is the characteristic constant of the core, f is the frequency, B_m maximum induction and n the experimental factor which varies between 1.5 and 2.

(2) Eddy current losses are given experimentally by $P_e = K_e f^2 B_m^2$ watts. K_e is another characteristic constant.

The total losses due to both factors would therefore be:

$$W_t = W_h + P_e = K_h f B_m^n + K_e f^2 B_m^2. \quad (3.14)$$

This value should be proportional to the area of the hysteresis loop. The area of the loop may be found by evaluating the integral $S = \int B dH$. (3.15)

Usually, graphical methods are used to evaluate this integral; however, an approximate mathematical formula might be derived (32 and 33) by harmonic analysis.

For example, the hysteresis loop can be represented by the following parametric equations:

$$B = B_m \sin wt \quad (3.16)$$

$$H = H_1 \sin wt + H_1' \cos wt + H_3 \sin 3wt + H_3' \cos 3wt + H_5 \sin 5wt + H_5' \cos 5wt \dots \quad (3.17)$$

The absence of even harmonics follows from the stipulation that the bottom half of the loop be symmetrical to the top half reversed. Differentiation of (3.17) and substitution of it along with (3.16) into (3.15) yields:

$$S = wB_m H_1 \int \sin wt \cos wt dt - wB_m H_1' \int \sin^2 wt dt + 3wB_m H_3 \int \sin wt \cos 3wt dt - 3wB_m H_3' \int \sin wt \cdot \sin 3wt dt + \dots$$

Integration from $t = 0$ to $t = T$ (where $T = \frac{2\pi}{w}$) all terms

but the second produces zero and we are left with

$$S = wB_m H_1' \int_0^T \sin^2 wt dt = \pi B_m H_1' \quad (3.18)$$

By combining trigonometrical identities, the value of H_1' might be given as $H_1' = 1/6 (H_0 + \sqrt{3} H_{50} + H_{86.6})$, (3.19) where H_0 , H_{50} and $H_{86.6}$ represent values of H corresponding to $B = 0$, $B = 0.5B_m$ and $B = 0.866B_m$. This is shown in Fig. 3.7.

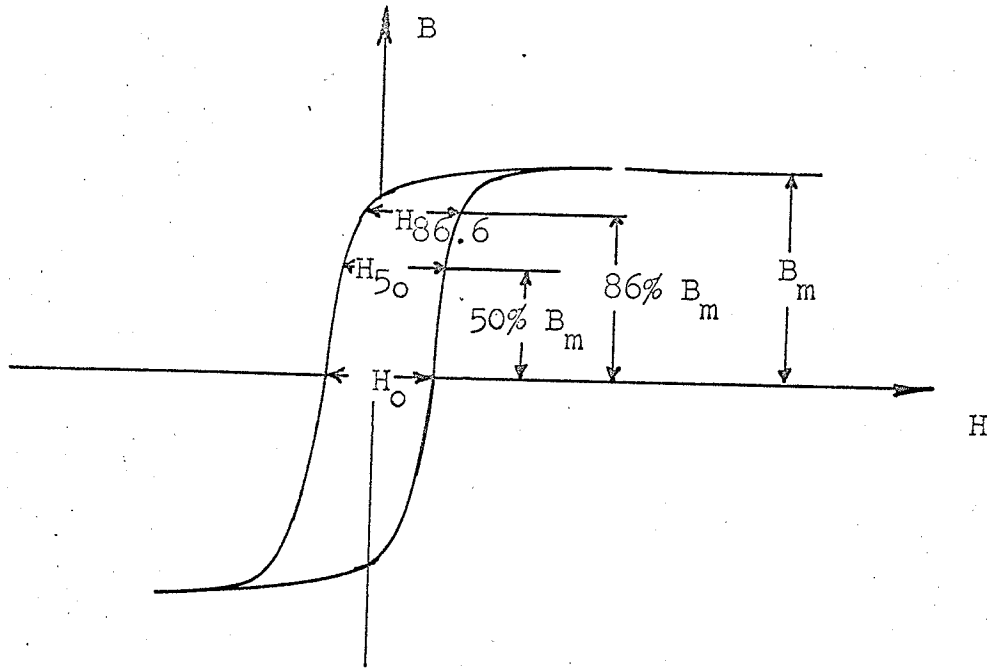


Fig. 3.7: Parameters used to estimate loop area.

Therefore, the area would be

$$S = \frac{\pi}{6} (H_0 + \sqrt{3} H_{50} + H_{86.6}) B_m \quad (3.20)$$

and the losses would be

$$W = \frac{\pi}{6} (H_0 + \sqrt{3} H_{50} + H_{86.6}) B_m 10^{-8} \text{ Joules per cubic inch per cycle.} \quad (3.21)$$

If the loop is square enough (compare with Fig. 2.2(d), 2.2(e), p.7; and Photo 6, for Deltamax characteristics), we can assume $H_c \approx H_{50} \approx H_{86.6}$, so that (3.21) can be written as

$$W = K_L \cdot B_m \cdot H_c, \text{ where } H_c \text{ is the coercive force.}$$

When equating the two expressions arrived at for the losses for a particular value of B_m , we get

$$K_1 \cdot f + K_2 f^2 = K_3 H_c. \quad (3.22)$$

This means that the relation between H_c and the frequency for a particular input amplitude might be approximated by

$$H_c = af + bf^2. \quad (3.23)$$

For each input amplitude, one first has to use graph 3.1, p.33, to find the value of H_c corresponding to this amplitude; then, to calculate a_1 and a_2 and to add the correction for f .

It is easily seen that due to the extreme differences between the types of materials being used, it becomes useless to adopt this formula generally. On the other hand, the formula shows that the frequency should be accounted for. The only way to cope with this problem is to obtain particular results for particular types of nonlinear elements.

III.10 Summary

From the theory presented thus far, the following conclusions concerning the behaviour of the hysteresis loop in magnetic materials should be noted.

- (1) For low fields the magnetization curve is approximately retraced when the field is diminished, thus not giving rise to a hysteresis loop.
- (2) For low fields both H_c and B_r are approximately proportional to H_m^2 .

- (3) For low fields the loop may be approximated by parabolic segments.
- (4) For intermediate fields the relation between H_c and H_m may be taken as linear.
- (5) There are saturation values for H_c and B_r known as "coercivity" and "retentivity".
- (6) The value of H_c depends upon the frequency and increases rapidly with increases in frequency.

It is obvious that when forming models, it is impossible to account for all these factors together.

The next chapter will present some attempts to derive the describing function by considering some of these properties. As can be expected, these functions will yield satisfactory results only where these assumptions hold.

CHAPTER IV

EXTENSION OF DESCRIBING FUNCTION TECHNIQUES TO GENERALIZED FORMS OF HYSTERESIS NONLINEARITY

From the theory that was previously presented, it is obvious that a more complete model for magnetic hysteresis should be used in order to obtain satisfactory results. In this chapter, models of hysteresis nonlinearity are presented, and their validity is later checked by experiments.

IV.1 Piece Wise Linear Model in Which The Width of The Loop is Linearly Proportional to The Input Signal

The model itself is basically the same as shown in Fig. 2.3, p.9, the only difference being that the width b depends linearly upon the input amplitude A (23 and 24). This relation may be represented as a straight line. (See Fig. 4.1.

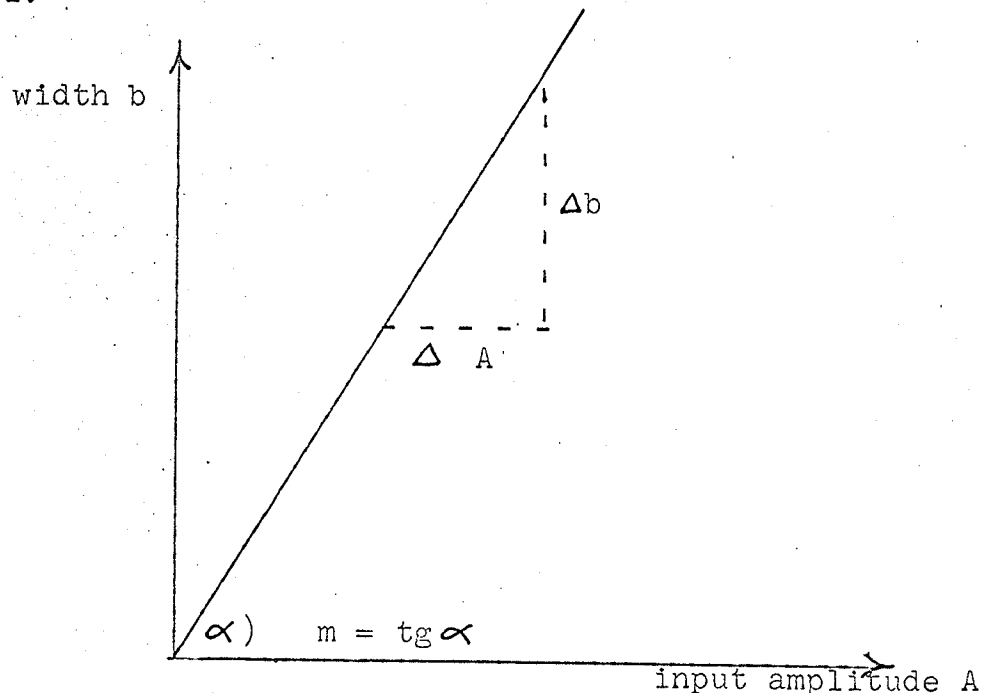


Fig. 4.1: The variation of the width of the hysteresis loop with amplitude

The slope 'm' might have any positive value and depends on the nonlinear element under discussion. Under this assumption, the hysteresis loop begins from a mere point located at the origin with a zero input amplitude and expands linearly with the input signal. That this model does not represent the actual behaviour of magnetic material can easily be seen by comparing the straight line approximation (Fig. 4.1) with the curves representing the relation between H_c and H_m (Graph 3.1, p.33). The main differences are:

(i) The actual curve starts with a zero slope, i.e. there is a region in which the hysteresis loop has no width, that is, the nonlinear element actually behaves as a linear element having the gain $\frac{dB}{dH} = \mu_0 + 2\sqrt{H}$, (4.1) which is equal to μ_0 for $H = 0$.

(ii) The coercive force reaches a saturation value and does not increase significantly for signals exceeding the saturation level. This is also illustrated in Graph 3.1, p.33. That is to say, the relation between the coercive force and the input amplitude is not linear, at least, not near the origin or beyond the saturation knee.

Although these facts suggest a rejection of the linear model, it is proved in experiments to follow that under certain conditions, there is ample justification to allow for the use of this model within a certain amplitude range of the input signal.



Therefore, we will again adopt the model used in Section II.2, p.9, and substitute into (2.6) and (2.8) the relation $b = mA$. (4.2)

Some doubt may arise concerning the legitimacy of this procedure, since, in the integrals which were derived in Sec. II.2, p. 9, b was assumed as constant, while now it is a variable; and that therefore the validity of the previously derived expression is not, in this case, consistent. However, referring to the principles upon which the describing function technique is based, we recall that time varying elements are not included in the nonlinear characteristic. Therefore, in order to perform the integration in the first case, we used the assumption upon which the technique of Krylov and Bogoliubov is based - that A , the amplitude, is a slowly varying function of time which may be considered to be constant at its average value over a single cycle. But, if A is constant, it implies also that b is constant over one cycle. Hence, we can modify the previous formulae using the relation (4.2).

Assuming that saturation does exist, we previously found that:

$$G(A) = f_1(U_1, U_2)$$

and

$$B(A) = f_2(U_1, U_2),$$

where

$$U_1 = \arcsin \frac{b_1}{A}, \quad U_2 = \arcsin \frac{b_2}{A},$$

and

$$b_1 = \frac{c-bk}{k}, \quad b_2 = \frac{c+bk}{k}$$

If we now substitute mA for b , we get

$$U_1 = \arcsin(c/kA-m), \quad U_2 = \arcsin(c/kA+m). \quad (4.3)$$

Thus, the describing function becomes a function of the input amplitude A and the slope of Fig. 4.1, p. 40; that is, of m .

Rather interesting results occurred while checking the behaviour of our model when saturation is not present. Under this assumption, we previously had (2.9) and (2.13). These now become:

$$G(A) = \frac{k}{\pi} \left[\arcsin(1-2m) + \frac{\pi}{2} + \frac{1}{2} \sin 2(\arcsin(1-2m)) \right]. \quad (4.4)$$

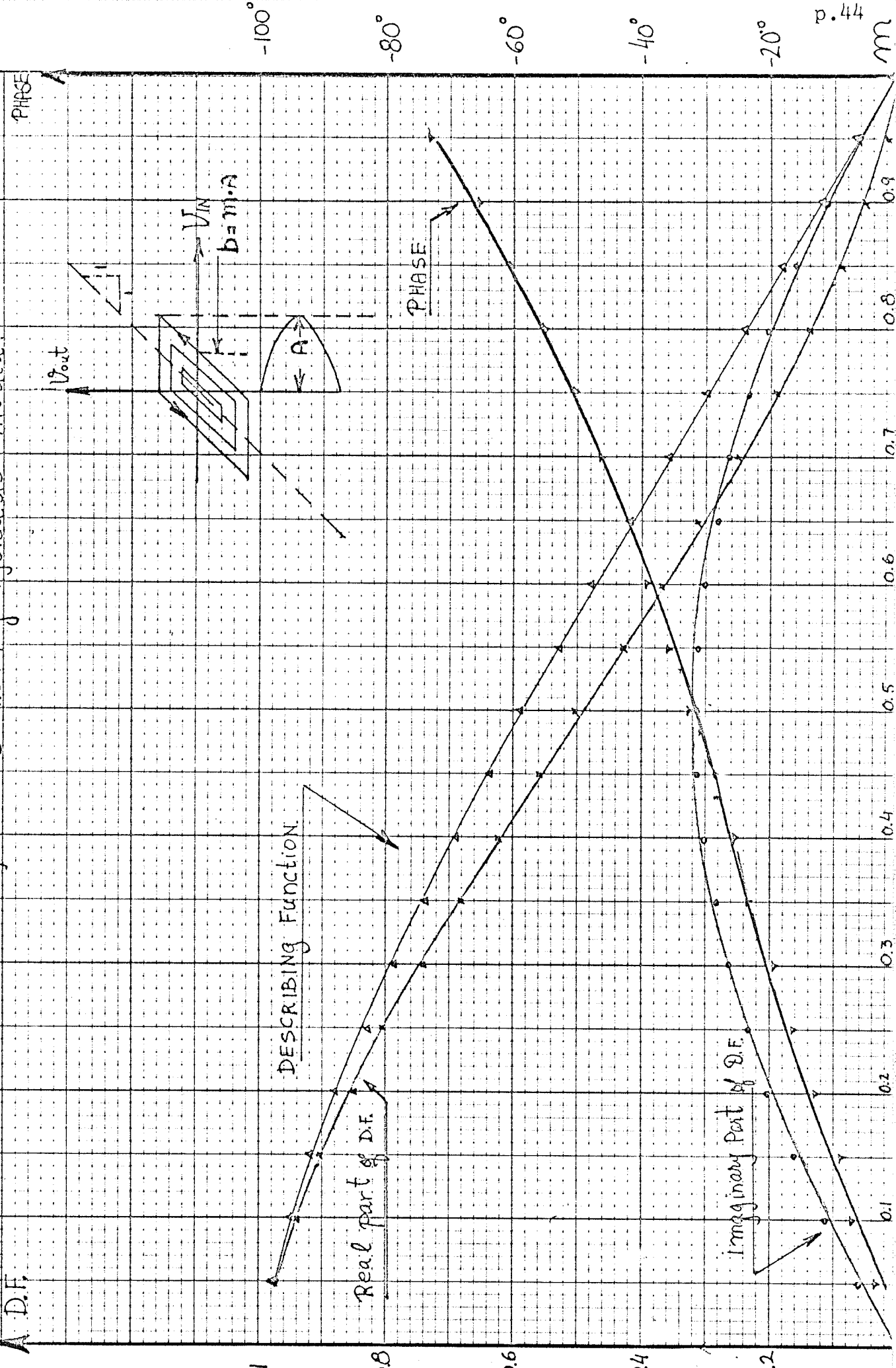
$$B(A) = \frac{-4km}{\pi} (1-m). \quad (4.5)$$

It is now evident that the describing function is not dependent upon the input amplitude. That is, the describing function shrinks into a point in the Nyquist plane. This point changes its position according to variations of the slope m in Fig. 4.1, p. 40. This is a rather interesting result which clearly utilizes the distinction which should be made between various types of hysteresis nonlinearities.

Digital computer* evaluation of the formulae (4.4) and (4.5) resulted in graphs 4.1, p.44, and 4.2, p.45. The critical loci for both cases is shown in Graph 4.3, p. 46. In obtaining these results, the gain of the piecewise linear model was, for the sake of convenience, taken as $k=1$ with a saturation value of $c=5$.

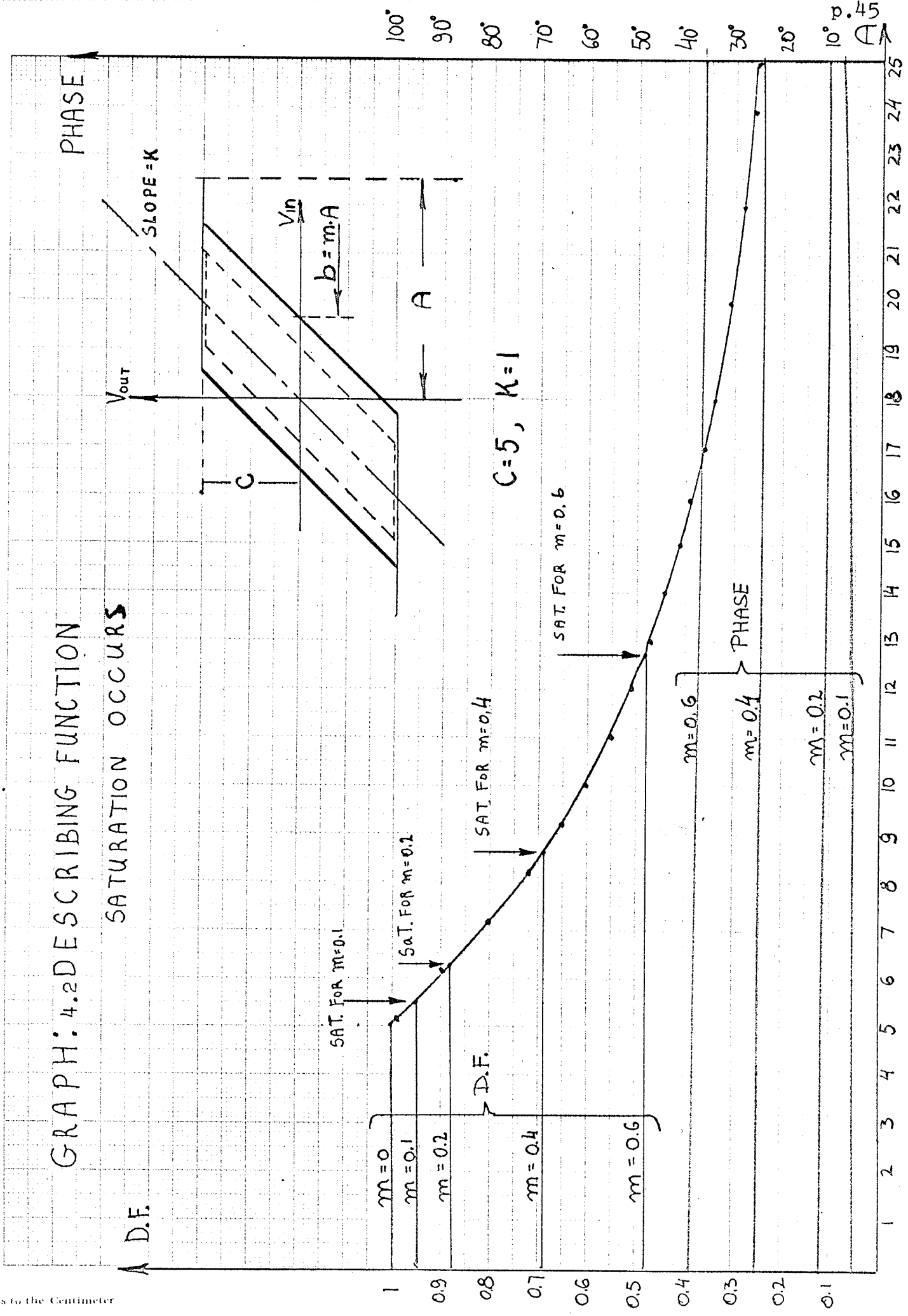
* The computer used is the I.B.M. 1620.

GRAPH: 4.1: DESCRIBING FUNCTION
for non saturating hysteresis model.

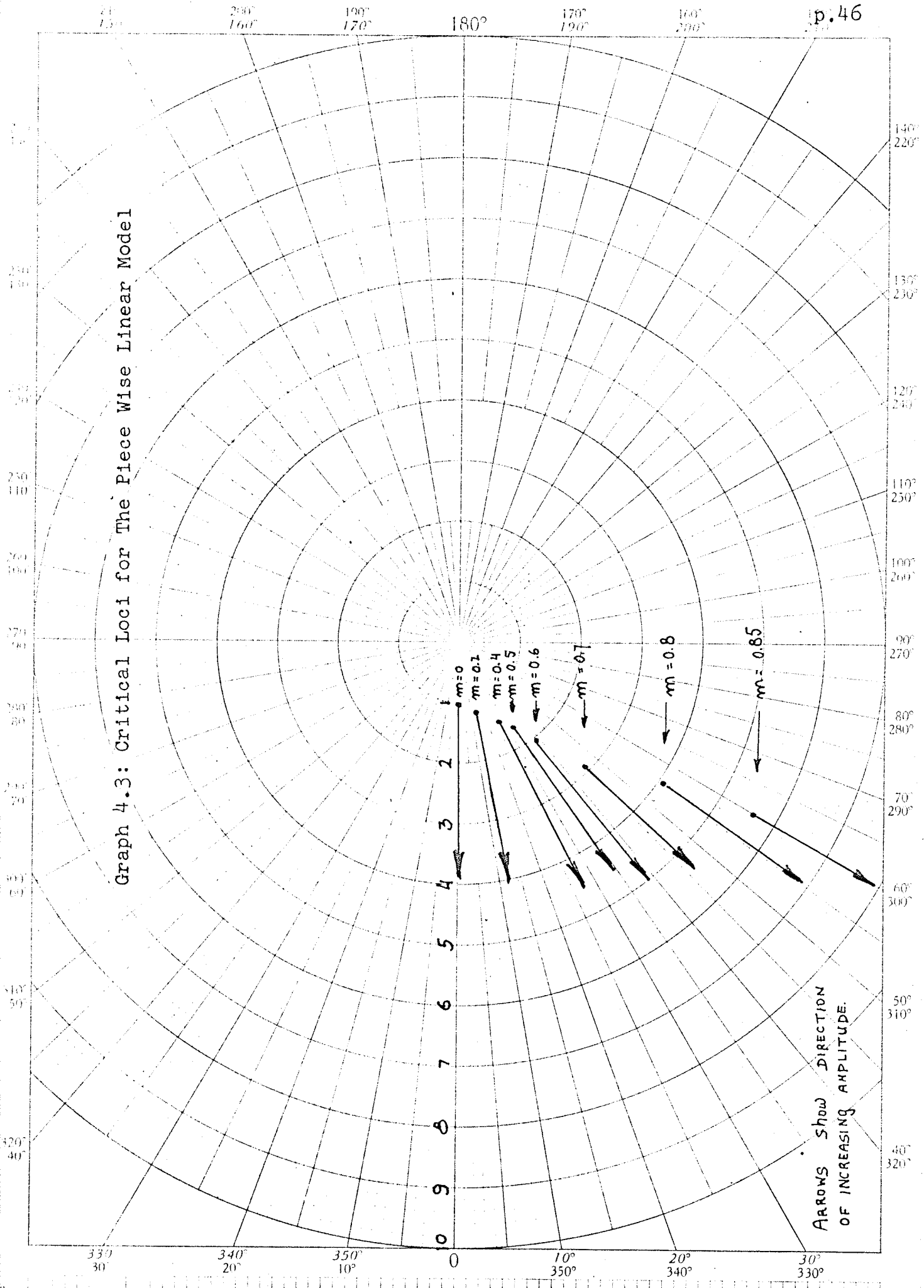


GRAPH: 4.2 DESCRIBING FUNCTION

SATURATION OCCURS



Graph 4.3: Critical Loci for The Piece Wise Linear Model



ARROWS SHOW DIRECTION OF INCREASING AMPLITUDE.

Graph 4.1, p. 44, gives the variation of the describing function together with its real part, imaginary part, and phase, as functions of the parameter m . The amplitude A is not present, since it has no effect on the describing function in this range.

It should be noted that when $m=0$, we have a simple case of linear gain, and the describing function is represented by $1 < 0$ as can be seen from graph 4.1, p.44, or directly from formulae (4.4) and (4.5).

Graph 4.2, p.45, presents the situation when saturation does occur. The describing function now varies with the input amplitude as previously shown. For any value of m , the describing function begins from an initial value given in graph 4.1, p.44. The representation of this value on graph 4.2, p.45 is actually a straight horizontal line, due to the fact that the independent variable is now A rather than m . As the input amplitude reaches saturation value, (this value depends upon the value of m , and may be calculated by: $A_{\text{sat.}} = \frac{(c/k)}{(1-m)}$), the gain of the nonlinear element is reduced according to the illustrated curve. It is interesting to note that the phase shift remains relatively constant throughout amplitude changes.

In this case, by letting $m=0$, we get the known describing function for simple saturation nonlinearity with gain equal to 1.

The results of these graphs are combined in graph 4.3, p.46, which illustrates the critical loci for the nonlinear element in the Nyquist plane. The describing function remains as a point for amplitudes lower than the saturation value. Once the input amplitude exceeds the saturation value, the points would move along the lines in the direction indicated by the arrows.

Another model using the same relationship between b and H_m might also be used. The necessity for such a model arises because of the differences between typical hysteresis loops of different materials. While the first model might adequately represent the hysteresis loop for Deltamax, it does not, for example, represent the true behaviour of the Supermalloy loop. The latter may be represented in a better way by either using ellipses or parabolae as approximations (21, 25 and 32) which would yield unwieldy algebraic expressions, or, by other piece wise linear approximations as shown in Fig. 4.2.

Using the same method as before, we arrive at the following expressions for this model, when saturation is present:

$$G(A) = \frac{2}{\pi} \left[\left\{ 1 - \frac{m}{\sin U_1} \right\} U_1 + (\sin U_1 - m) \cos U_1 \right] . \quad (4.6)$$

$$B(A) = \frac{-2}{\pi} m \cdot \sin U_1 . \quad (4.7)$$

If saturation is not present, we get:

$$G(A) = \frac{2}{\pi} \left[(1-m) \frac{\pi}{2} \right] = 1-m,$$

$$B(A) = \frac{-2}{\pi} \cdot m .$$

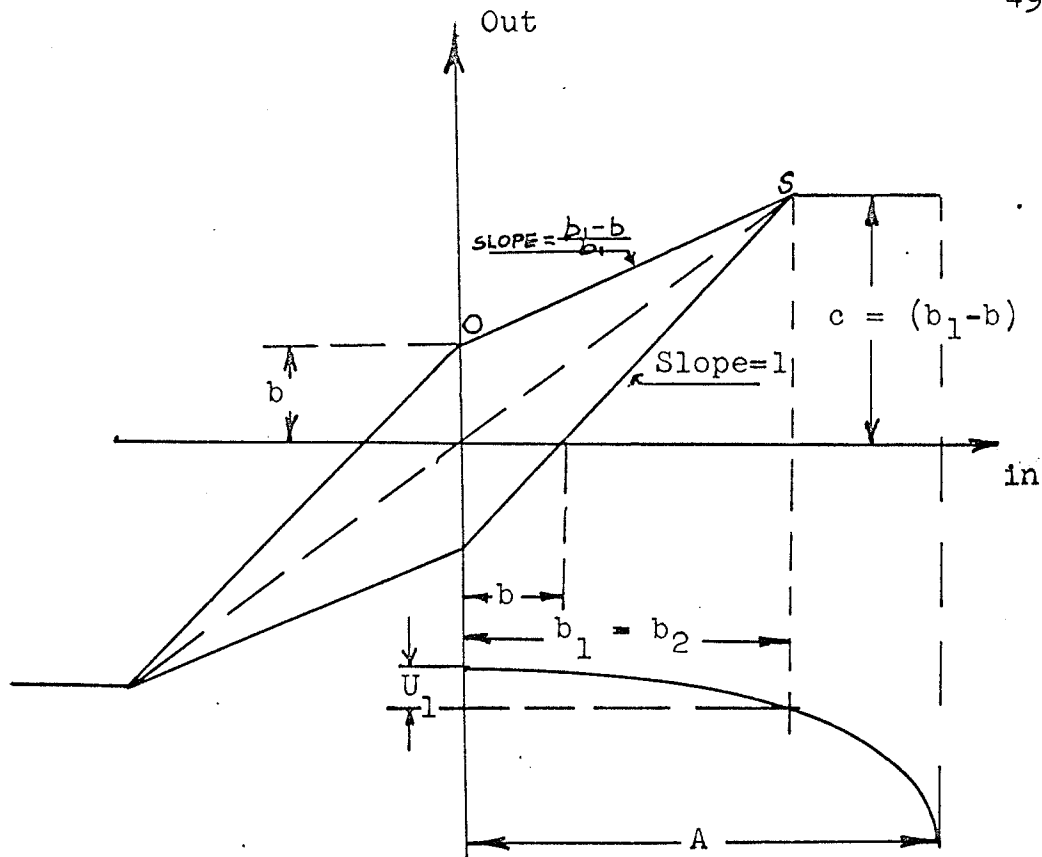
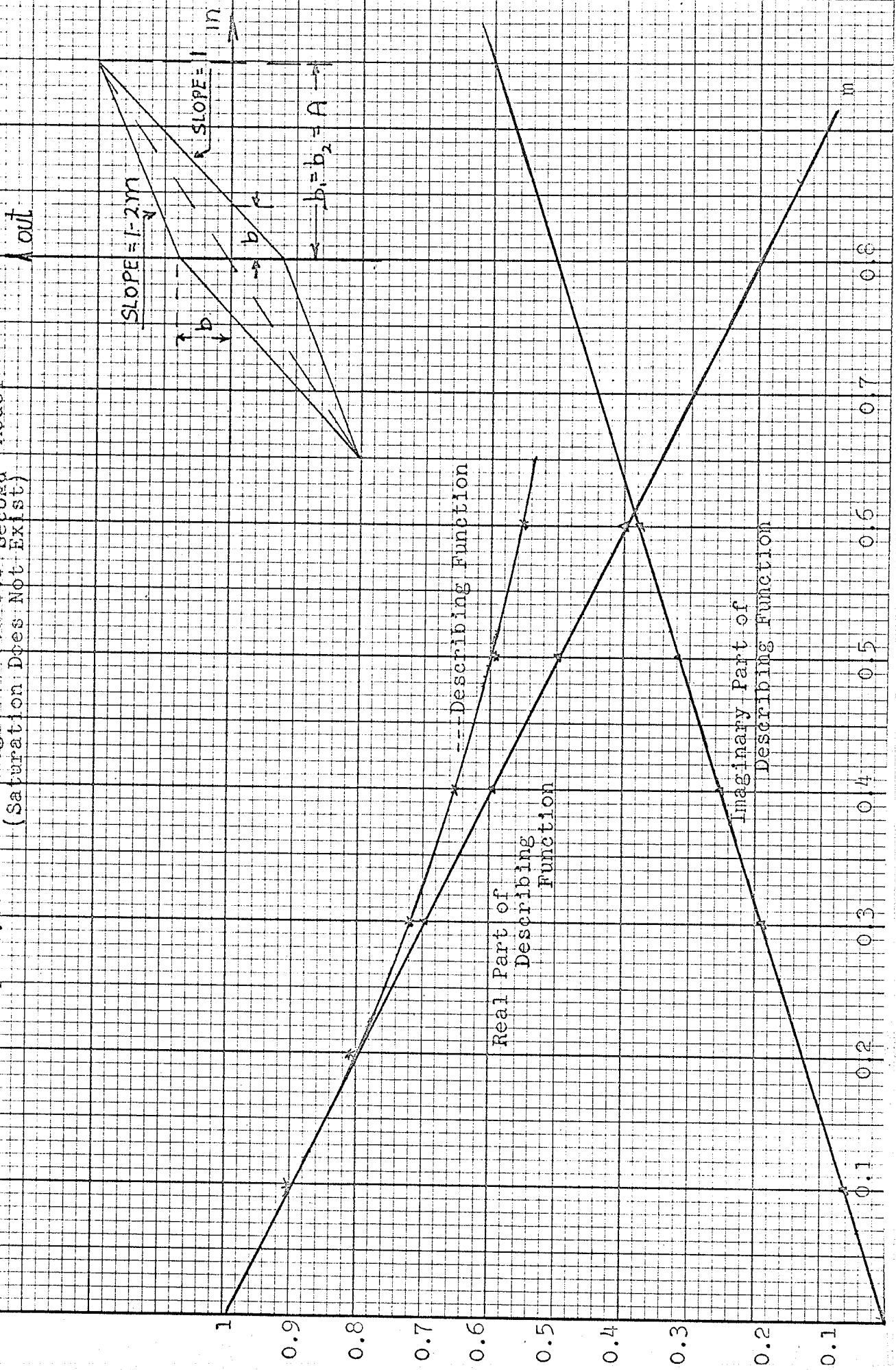


Fig. 4.2: Piece wise linear approximation for hysteresis loop.

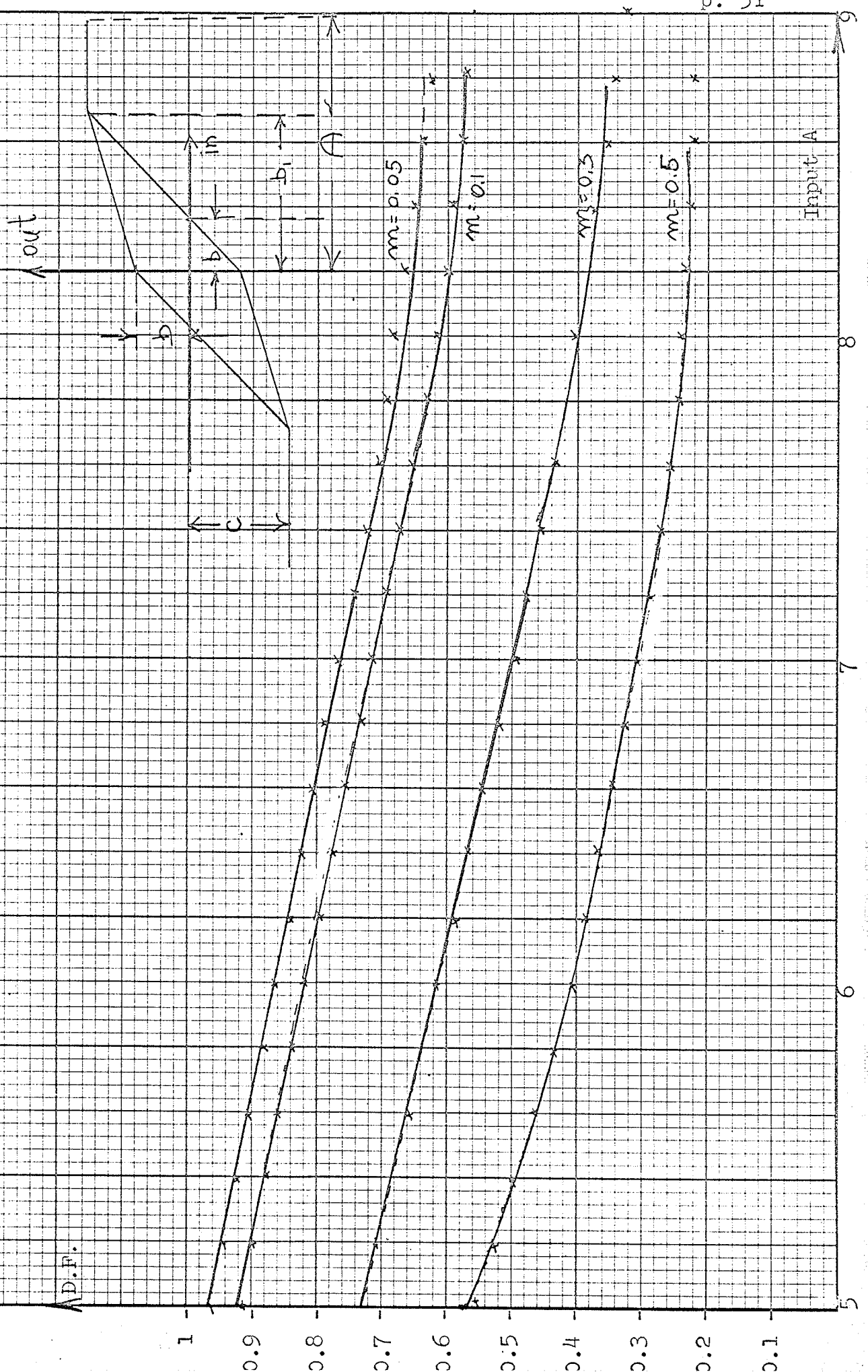
Comparing these results with the previously derived expression, we see that for amplitudes lower than the saturation amplitude, this model yields a describing function which is also a mere point in the Nyquist plane. However, for values exceeding saturation value, the behaviour is somewhat different, see Graph 4.5, p. 51. Because the slope of the segment $O - S$ in Fig. 4.2 is $1-2m$ *, this model yields impractical results for $m > 0.5$. Also, for $m = 0.5$, this model coincides exactly with the previous model, and by comparing 4.1, p.44 and 4.4, p. 50, we see that the describing function for this case is the same for both models. (The describing function for this model was obtained from the computer as shown in graphs 4.4 and 4.5).

* For $A \leq b$.

Graph 4.4: Describing Function for Second Model
 (Saturation Does Not Exist)



Graph 4.5: Describing Function for Second Model (Saturation Exists)



A.D.P.

IV. 2 Piecewise Linear Model in Which the Width of the Loop Is a Nonlinear Function of the Output Signal

From the theory previously presented, we concluded that the coercive force behaves in the following manner:

- (1) H_c is zero for very low amplitudes.
- (2) H_c is proportional to H_m^2 for low amplitudes.
- (3) H_c increases linearly with H_m for mid-range amplitudes.
- (4) H_c behaves according to Kennelly formulae when approaching the "knee".
- (5) H_c depends on the frequency of the input signal.

It is impractical to consider all these facts together. Instead, one can try to represent the curves of graph 3.1, p.33 mathematically, and then substitute this relation into previous formulae. This particular type of analytical representation permits the utilization of known results of nonlinear analysis.

It should be noted that formula (3.12), which may be written as $H_c = \frac{H_m}{a_2 + b_2 H_m}$, is empirical. In addition, it fails to represent the H_c curve for negative values of H_m . In order to represent these curves analytically, we first observe that the actual curves of H_c and H_m (Graph 3.1, p.33) show that the dependence between H_c and H_m (excluding the low values of H_m) may be represented by an odd function. Therefore, generally one could write:

$$H_c \approx \alpha H_m - \beta H_m^3 + \gamma H_m^5 + \dots \quad (4.7)$$

To simplify, we use only the first two terms, and arrive at:

$$H_c \cong \alpha H_m - \beta H_m^3. \quad (4.8)$$

This analytical representation is also an empirical approximation which might be used to obtain the "best fit" to the experimental curve in the region of interest.

The coefficients α and β may be evaluated in terms of the Kennelly formulae; this can be done for a given range of values as an approximation. For example, we note:

$$\frac{dH_c}{dH_m} = \frac{a_2}{(a_2 + b_2 H_m)^2}.$$

From this we see that if $H_m = 0$, the slope will be $1/a_2$ and if $H_m = \infty$, the slope will be zero. On the other hand, differentiating (4.8) we have $\frac{dH_c}{dH_m} = \alpha - 3\beta H_m^2$.

For $H_m = 0$, the slope is α .

Thus, using $\alpha = 1/a_2$ would give the same initial slope.

Also, H_c can be written as

$$H_c = 1/a_2 H_m - \frac{b_2}{a_2 (a_2 + b_2 H_m)} H_m^3. \quad (4.9)$$

If the maximum possible value of H_m in a certain problem is $H_m \text{ max.}$, we can substitute for β in (4.8) the value

$$\beta = \frac{b_2}{H_m \text{ max. } a_2 (a_2 + b_2 H_m \text{ max.})}. \quad (4.10)$$

Using these values of α and β , the two approximations will have the same initial slope and the same amplitude for $H = H_m \text{ max.}$

In order to check the behaviour of the describing function under such relations between H_c and H_m , an experimental curve showing the relation between H_c and H_m for K - S magnet steel, as shown in Graph 4.6 was chosen. This curve was approximated by use of the following three relations:

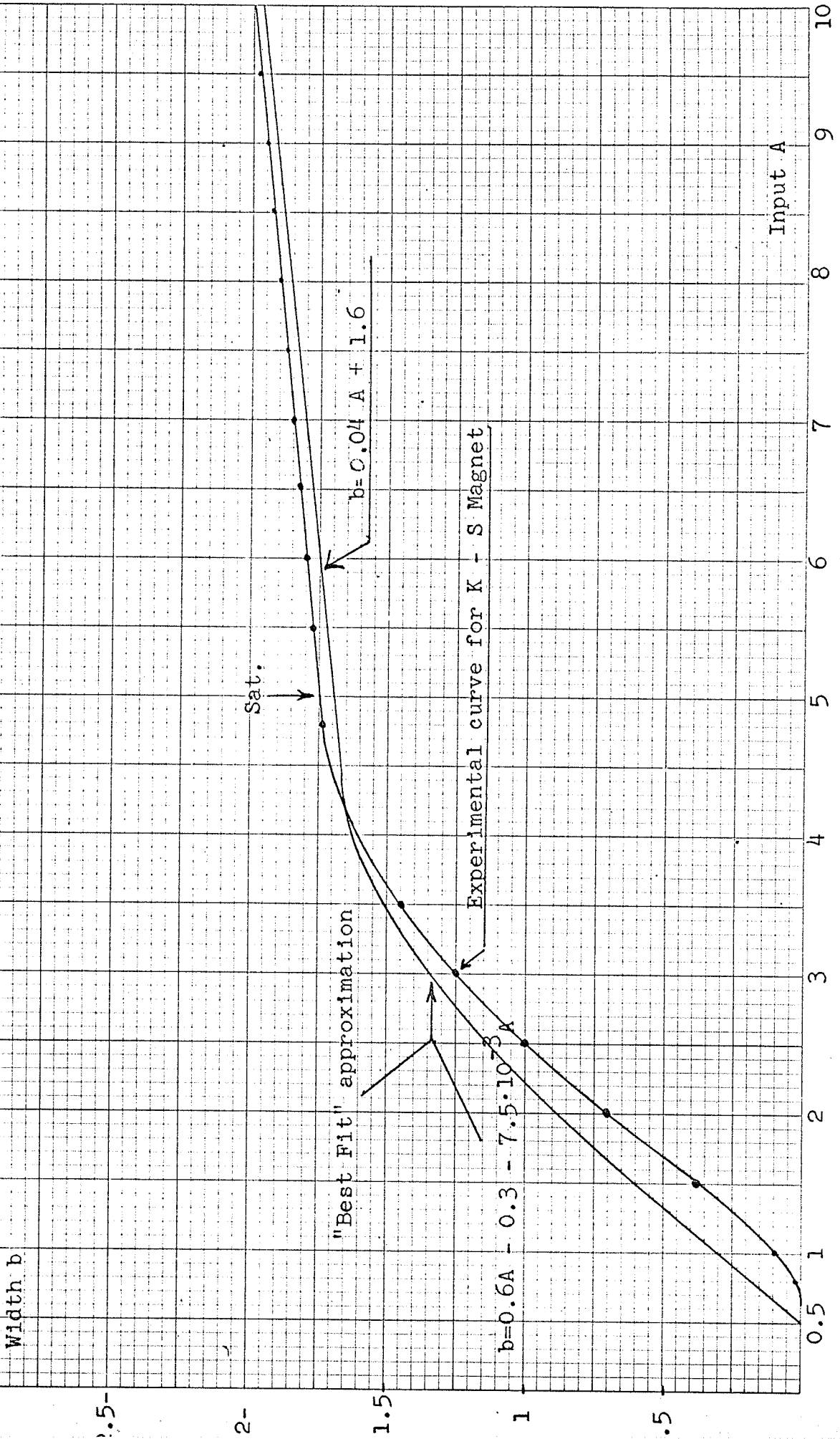
- (1) $H_c = 0$ for $H_m \leq 0.5$.
- (2) $H_c \cong 0.6 H_m - 0.3 - 7.5 \cdot 10^{-3} H_m^3$ $0.5 \leq H_m \leq 5$.
- (3) $H_c = 0.04 H_m + 1.6$ $5 \leq H_m$. (4.11)

The coefficients for these expressions were calculated experimentally to achieve the "best fit" with the experimental curve. The experimental curve and the approximated curve are shown in Graph 4.6.

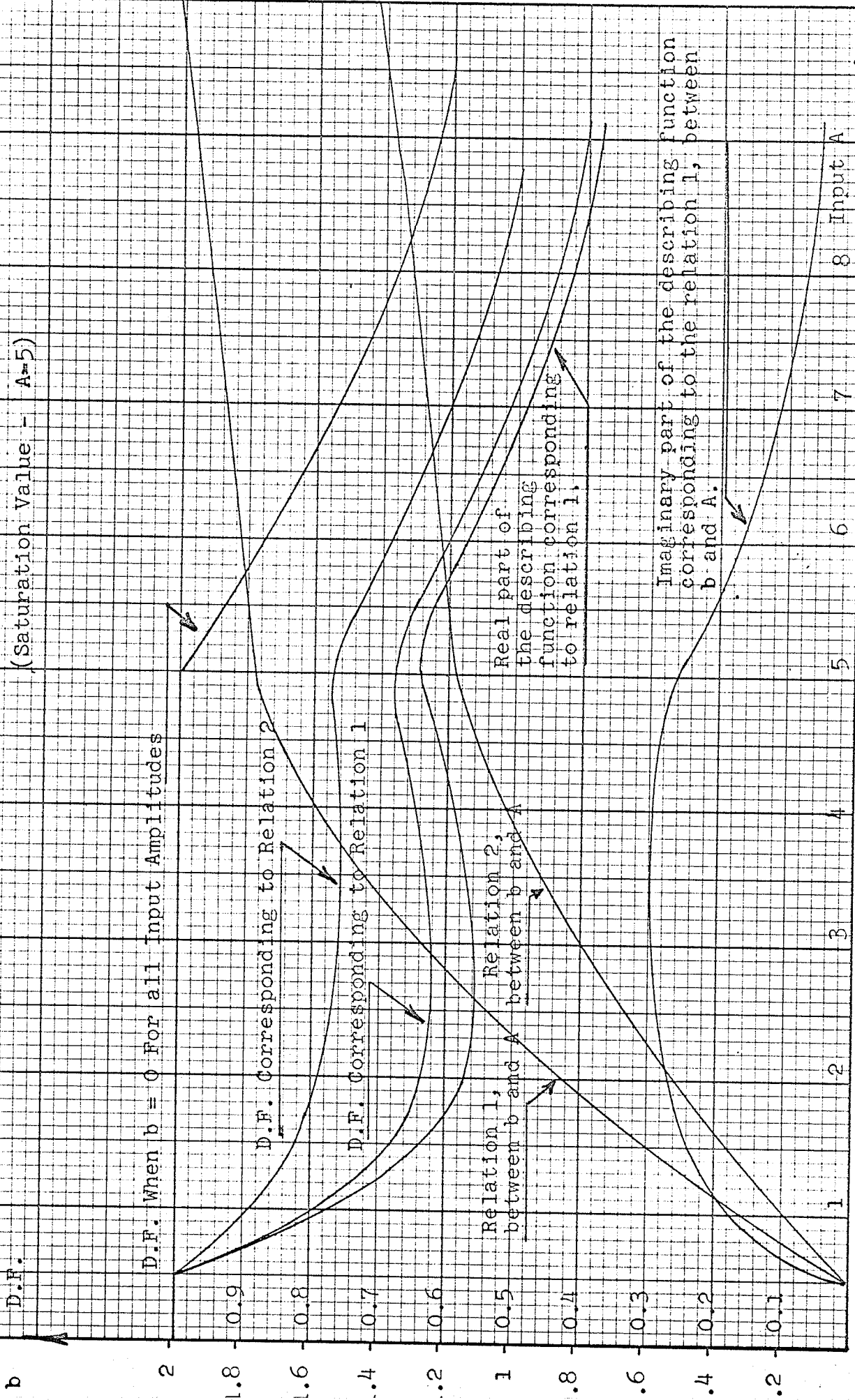
Relations (4.11) were substituted into equations (4.6 and 4.7) and represent the dependence of b upon A . The results which were obtained by the computer are shown in Graph 4.7. It should be noted that any type of $H_c - H_m$ curve might be applied for this check, noting that relations (4.11) should be changed accordingly.

As may be predicted, the describing function depends upon the amplitude for all regions in which the width of the loop is not linearly proportional to the input amplitude. By setting $H_c = 0$ for all input amplitudes, we will again arrive at the describing function for single value saturation nonlinearity.

Graph 4.6: Approximated Relation Between b and A



Graph 4.7: Describing Function for Hysteresis Nonlinearity, When The Relation Between b and A is Not Linear (Saturation Value - $A=5$)



Although this model is more complete than previous models, it does not hold for the whole range of input signals, due to the fact that the input is not sinusoidal for large input signals.

In order to check the validity of the proposed models, we can use either an analog computer simulation for such nonlinearity or actual physical elements.

An experimental analog computer set-up is shown in Fig. 4.3.

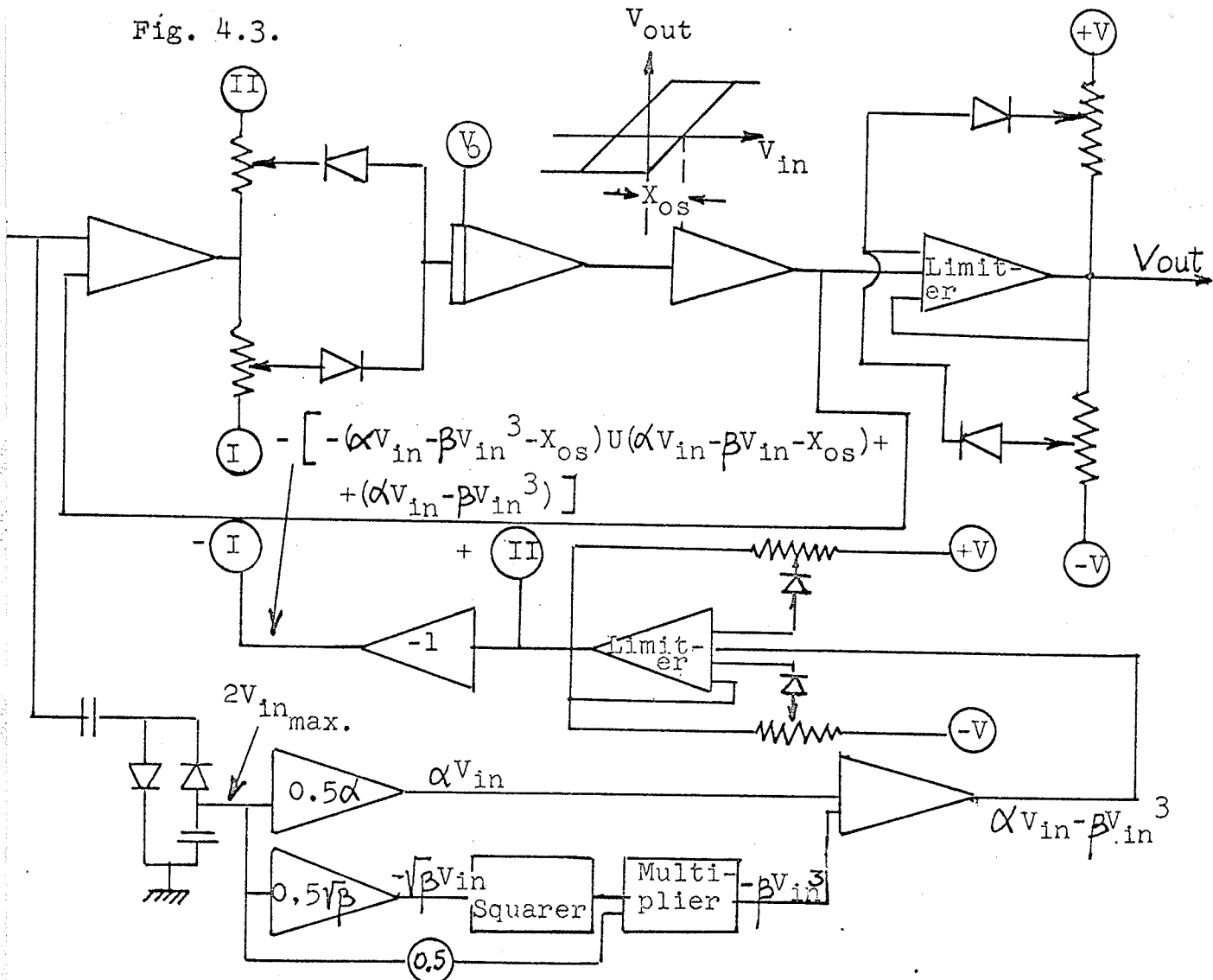


Fig. 4.3: Analog computer set-up for simulating general forms of hysteresis nonlinearity.

This set-up can be adjusted to the shape of any of the models previously used. However, from a practical point of view it is preferred to perform experiments on actual elements rather than on simulated ones. For this reason, three magnetic cores were chosen. The experiments are described in the following chapter.

CHAPTER V

EXPERIMENTAL DERIVATION OF THE DESCRIBING FUNCTION FOR NONLINEAR MAGNETIC CORES

This chapter presents a series of experiments which were carried out in order to determine the actual describing function for nonlinear magnetic cores. The difference between the actual results and the calculated results is then pointed out and the reasons for these deviations are explained.

V.1 The Nature of The Chosen Cores

Three typical high permeability cores were chosen for the experiment. These cores are usually used for magnetic amplifiers, and therefore may be found in numerous instruments, i.e., instrument amplifiers, control relays, modulators, voltage regulators, frequency meters, magnetometers, light dimmers, speed control systems, etc. The materials used for each of the three cores were:

(1) Deltamax. A 50% nickel-iron alloy having a rectangular hysteresis loop. This material is widely known for its use in saturable core reactors, and particularly in magnetic amplifiers.

Heretofore, very little a.c. data on this material has been published. The Deltamax characteristics shown in Figs. 5.1 and 5.2 were selected from measurements made on many different samples, and represent what may be expected as average for Deltamax.

DELTAMAX

Specimen Core
4168-D-2

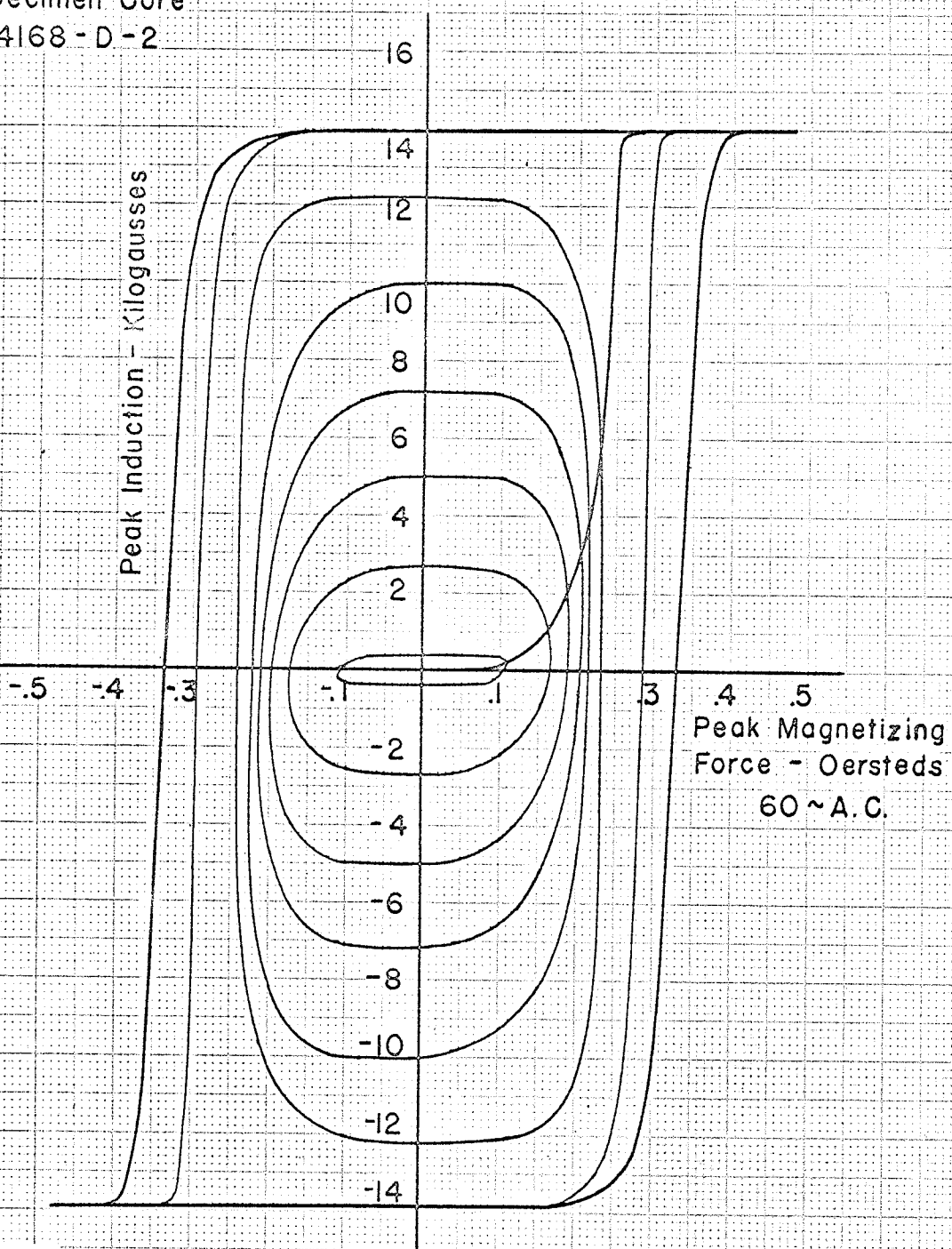
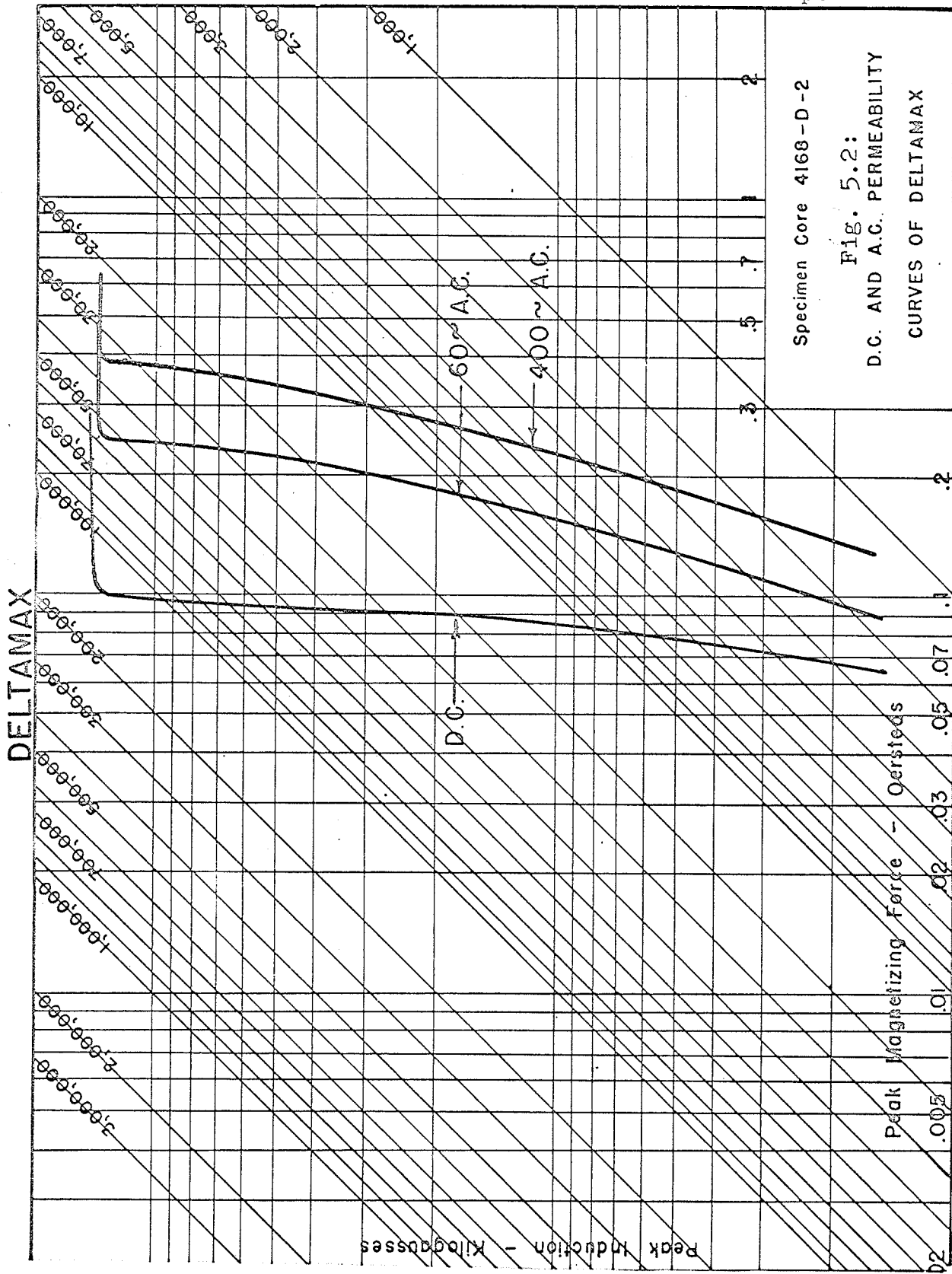


Fig. 5.1: VARIATION OF DELTAMAX HYSTERESIS LOOP WITH PEAK MAGNETIZING FORCE



Specimen Core 4168-D-2

Fig. 5.2:

D.C. AND A.C. PERMEABILITY

CURVES OF DELTAMAX

All the a.c. data was taken under conditions of sinusoidal exciting current with a peak magnetizing force slightly greater than that required to reach saturation in the core material. Under test conditions of sinusoidal flux in the core, the hysteresis loop would appear substantially narrower than those shown. Fig. 5.1 shows the family of hysteresis loops for Deltamax measured at various values of peak magnetizing force. Comparison of this family of loops with the curves for 4-79 Mo Permalloy, shown in Fig. 5.3, merely accentuates the rectangularity of the Deltamax hysteresis loop.

(2) 4-79 Mo Permalloy. This alloy has found many applications where high permeabilities at moderate to low magnetizing fields are required. The material consists of approximately 4% molybdenum, 79% nickel, and the balance is iron. Similar data representative of the average properties of this alloy are shown in Figs. 5.3 and 5.4.

(3) Supermalloy. This alloy is closely related to 4-79 Mo Permalloy in chemical composition, exhibits the highest initial and maximum permeability of any known commercially available material, and has the lowest hysteresis loss.

The cores are of the tape wound variety and are readily available under the manufacturer's designation of

4178-S4	Supermalloy,
4178-P1	4-79 Mo Permalloy,
and 4168-D2	Deltamax.

The actual cores installed for testing are shown in Photos 3 and 4, p₆₈ (See Appendix A for technical data.)

4-79 MO - PERMALLOY

Specimen Core
#4178-P-1

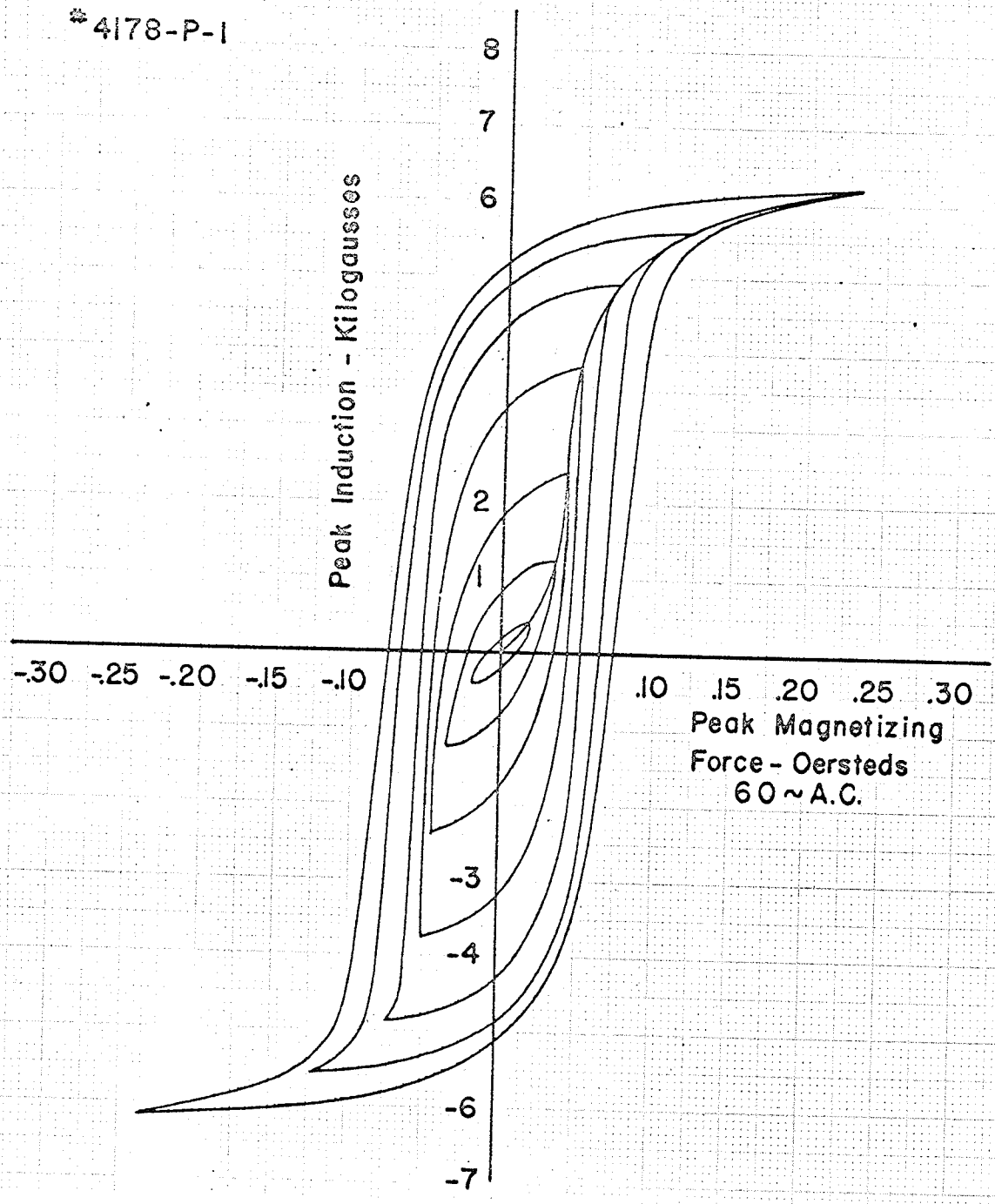
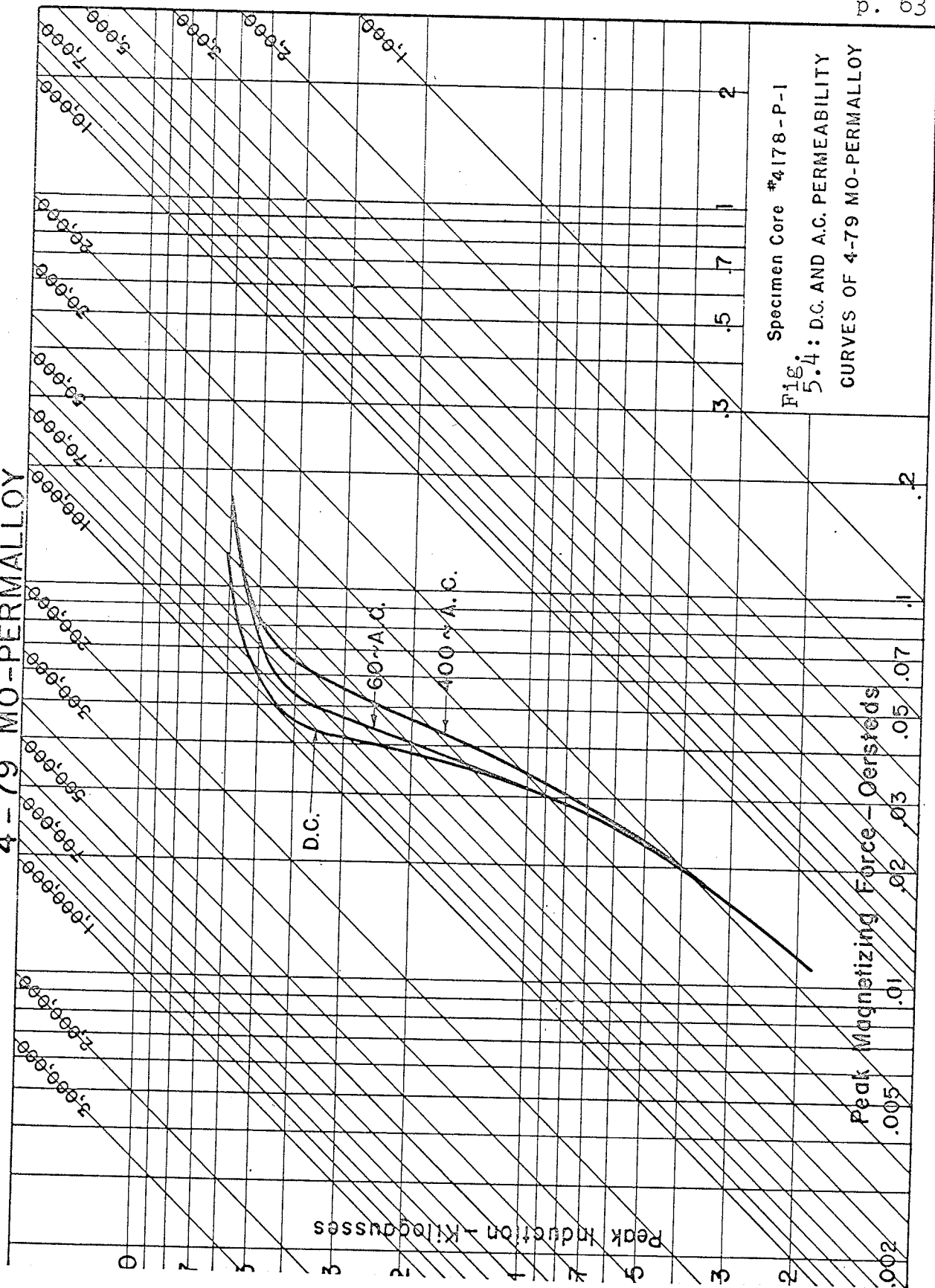


Fig. 5.3: VARIATION OF 4-79 MO-PERMALLOY HYSTERESIS LOOP WITH PEAK MAGNETIZING FORCE

4-79 MO-PERMALLOY



Specimen Core #4178-P-1

Fig. 5.4: D.C. AND A.C. PERMEABILITY CURVES OF 4-79 MO-PERMALLOY

V. 2 Set-Up of The Cores for Testing

A transfer function analyzer* was used in order to find the first harmonic of the output signal from the core. This instrument operates in a manner similar to that of a conventional wave analyzer, but, in addition, supplies information concerning the phase shift between the first harmonic component of the output signal and the input signal. Also, it incorporates an internal computing device which gives direct indication of the value of the square root of the in-phase component squared plus the quadrature component squared. A schematic of the set-up used is shown in Fig. 5.5, and the actual set-up is shown in Photo 1, p. 65.

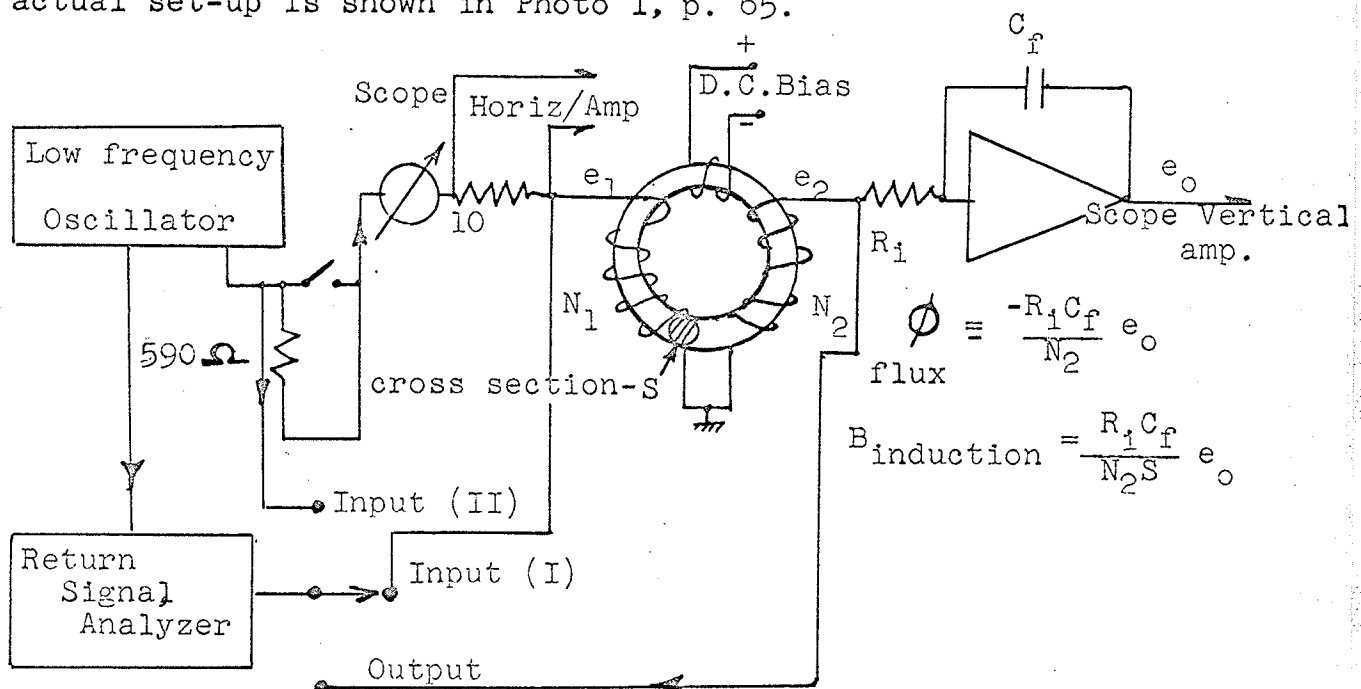


Fig. 5.5: Experimental set-up for derivation of the describing function for the cores.

*The transfer function analyzer is manufactured by Boonshaft and Fuchs Inc., Hatboro, Pennsylvania.

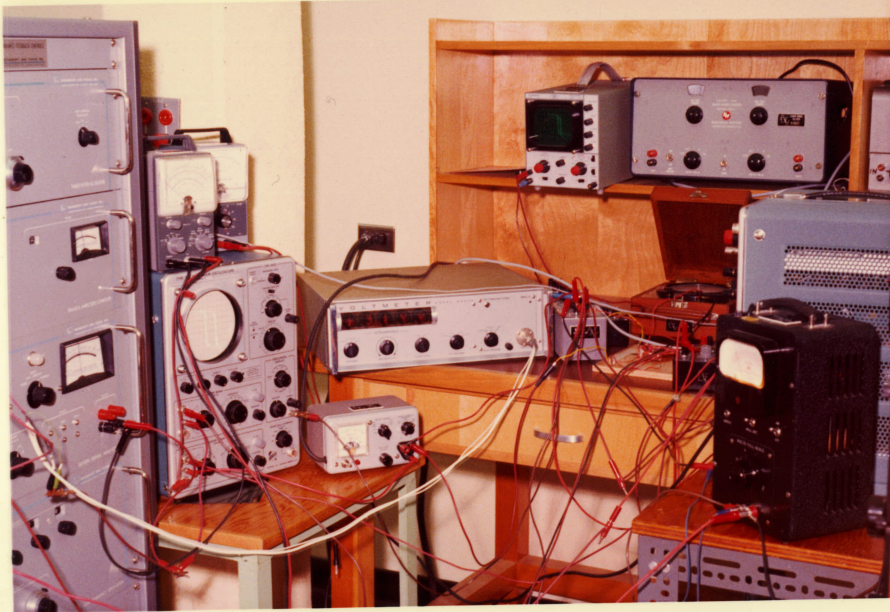


PHOTO #1
Instrument Set-Up for
Testing Cores

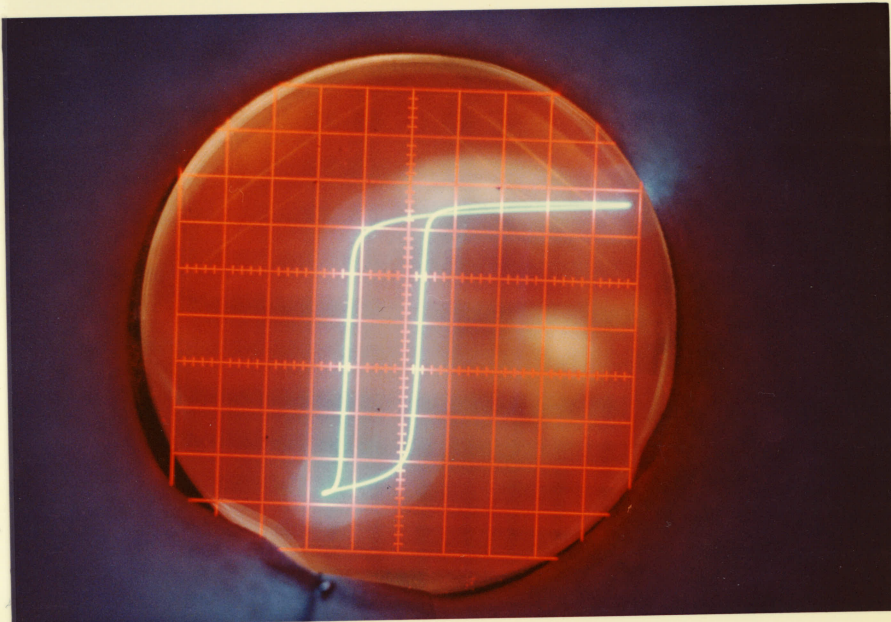


PHOTO #2
D. C. Bias Effect on The
Cores

V. 3 Tests That May be Performed

A variety of tests were made on the cores, due to the fact that a plot of B vs. H is not a complete description of the magnetic characteristic of the cores for all modes of operation.

In linear systems, it is sufficient to know the response to a sinusoidally applied signal in order to determine the behaviour of another arbitrary wave form. However, for magnetic material, the losses are so dependent upon the amplitude and frequency of the driving signal, that generally, many sets of curves of B vs. H are needed in order to form a clear picture of the magnetic behaviour. For example, Fig. 5.6 is a typical hysteresis loop occurring when the flux density B is maintained sinusoidal throughout the entire cycle. Fig. 5.7 is a plot of the hysteresis loop when the current is maintained as a square wave. The loop in the second case appears to have become more "squared".

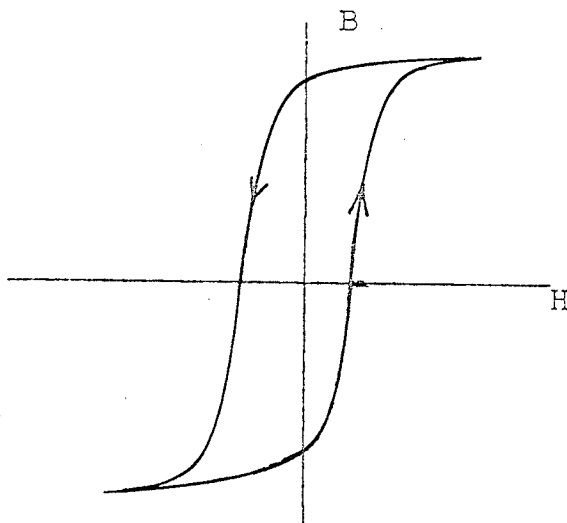


Fig. 5.6: Magnetic hysteresis loop.

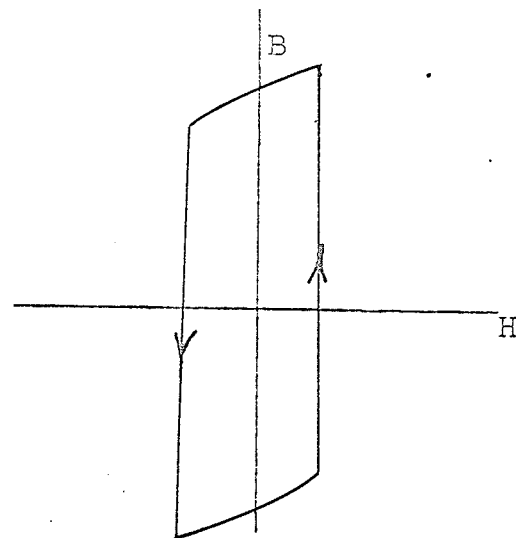


Fig. 5.7: Hysteresis loop obtained under square-wave current drive.

Under certain conditions, the current might have a sinusoidal wave shape or square wave shape (compare photos 7, p. 70 and 12, p. 72).

Another example which demonstrates the changes a static square hysteresis loop might undergo when different driving signals are applied is shown in Figs. 5.8 and 5.9. The effect of sinusoidally applied voltage and sinusoidally applied current is evident.

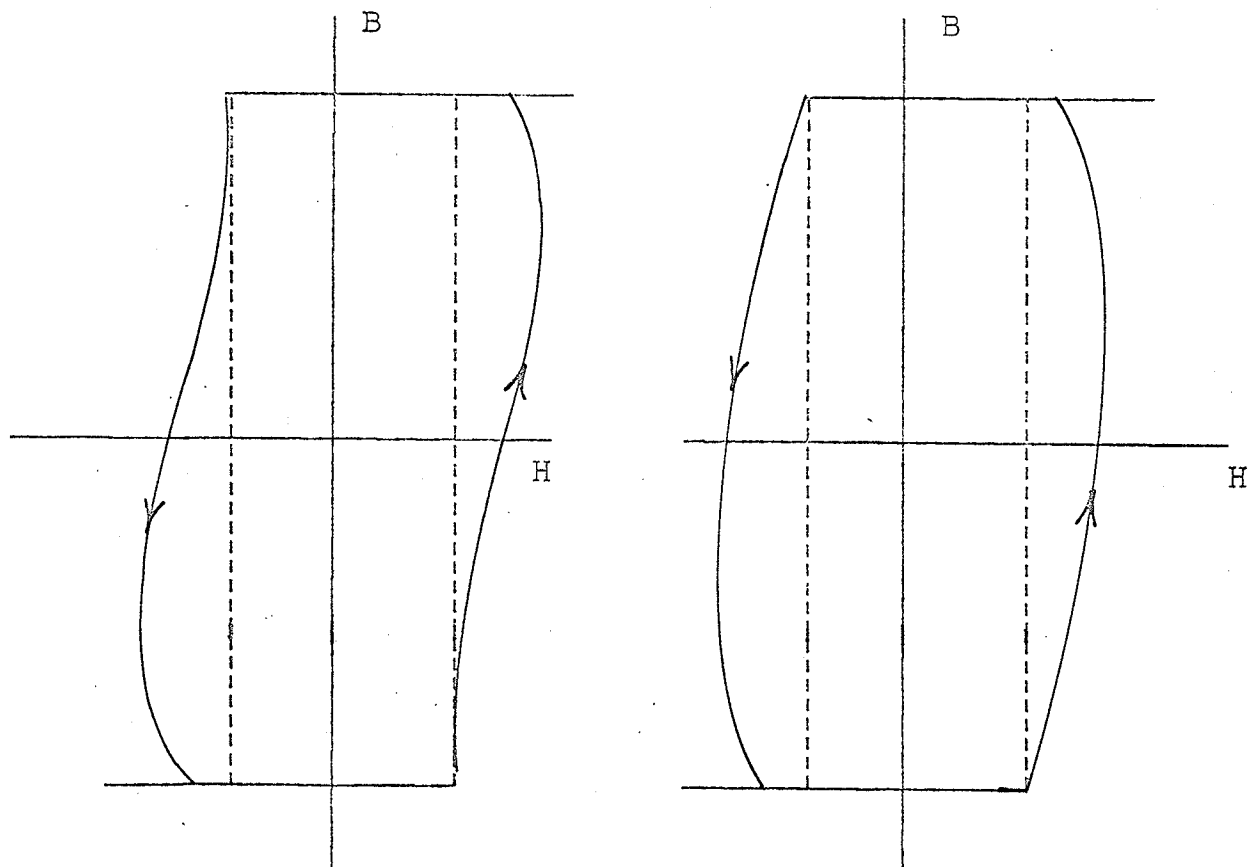


Fig. 5.8: Loop distortion with sinusoidal applied voltage.

Fig. 5.9: Loop distortion with sinusoidal applied current.

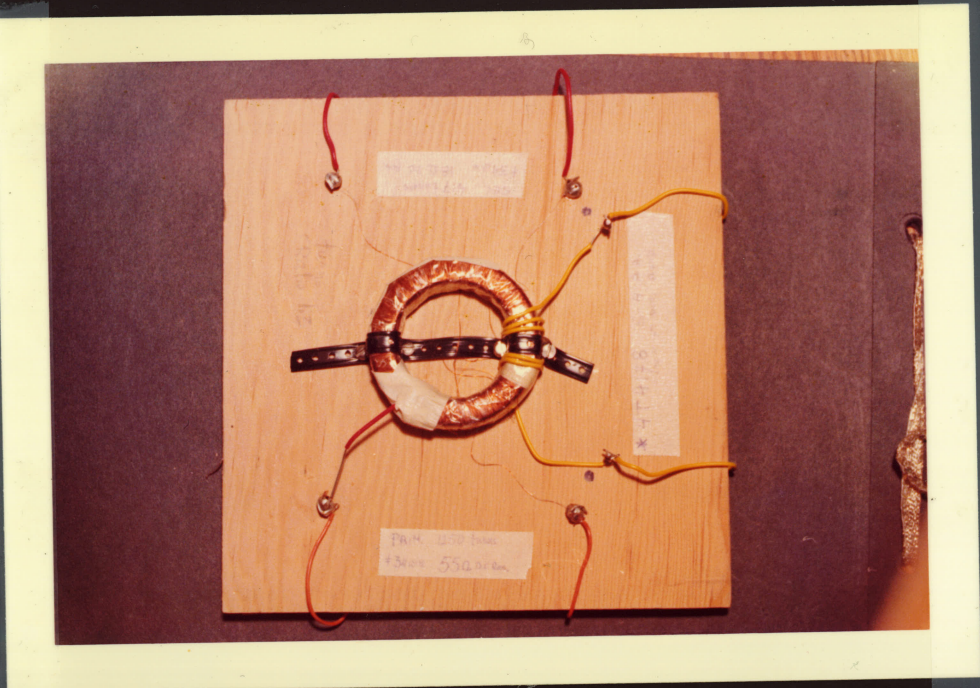


PHOTO #3
4T4178-S4 Installed for
Testing

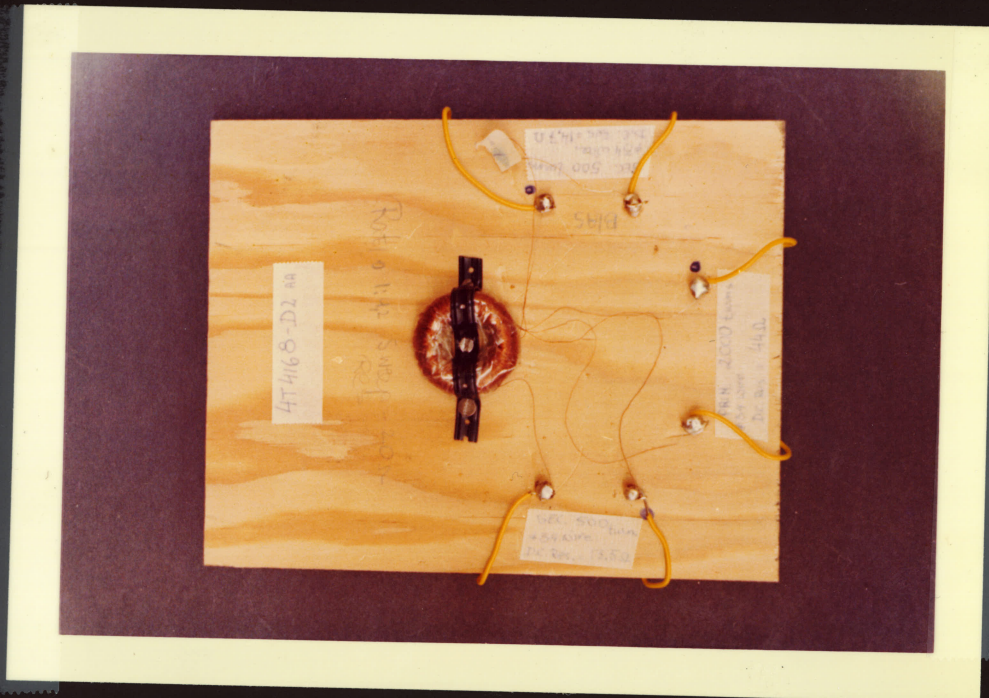


PHOTO #4
4T4168-D2 Installed for
Testing

Therefore, while testing the cores, the following questions arise:

How is the describing function going to be measured -

- (a) as a ratio of output voltage to input voltage?
- (b) as a ratio of flux density to input current?
- (c) as a ratio of output voltage to input current?
- (d) as a ratio of output current and input voltage?

It is obvious that each of these measurements would yield completely different results. More than this, at times we cannot measure certain types of transfer functions due to there not being enough cases in which we can force the current through the core to be sinusoidal. In actual application, it is usually far from being sinusoidal. (See Photos 8 - 13; pp. 71, 72.)

Thus, it becomes meaningless to define a describing function for a nonlinear element of this kind without clearly stating for which type of driving signal it was calculated.

From a practical viewpoint, we chose the describing function for the above mentioned cores under the conditions of sinusoidally applied voltage measured between the input voltage and the output voltage, since this situation is the most frequently encountered in actual control systems.

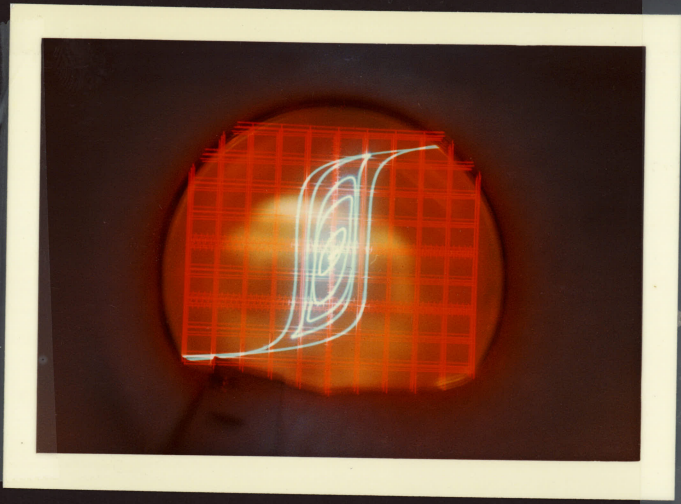


PHOTO #5
Dynamic hysteresis loops
for Supermalloy. $f=30$ c/s

PHOTO #6
Dynamic Hysteresis Loop
for Deltamax $f = 20$ c/s

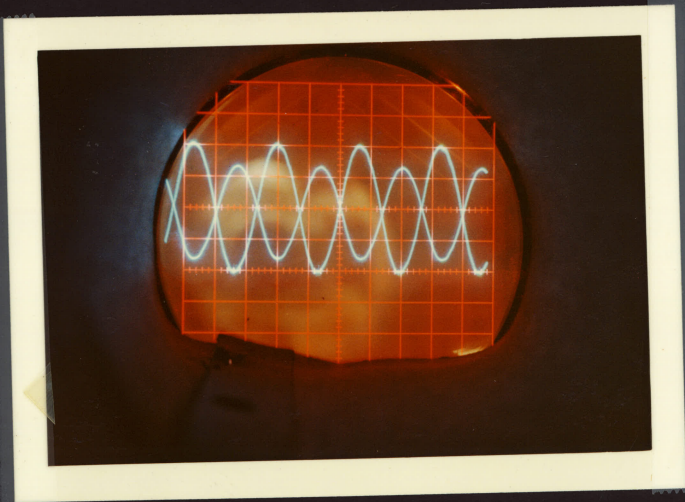
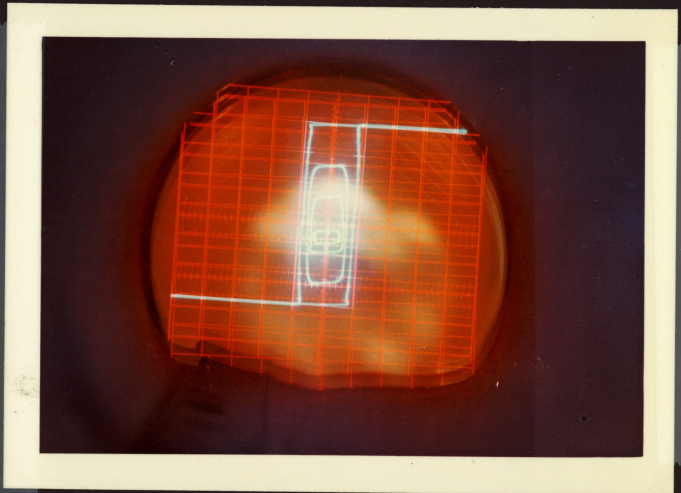


PHOTO #7
Input Current (Smaller) and
Voltage to Deltamax Core
for Low Signals. 20 c/s/

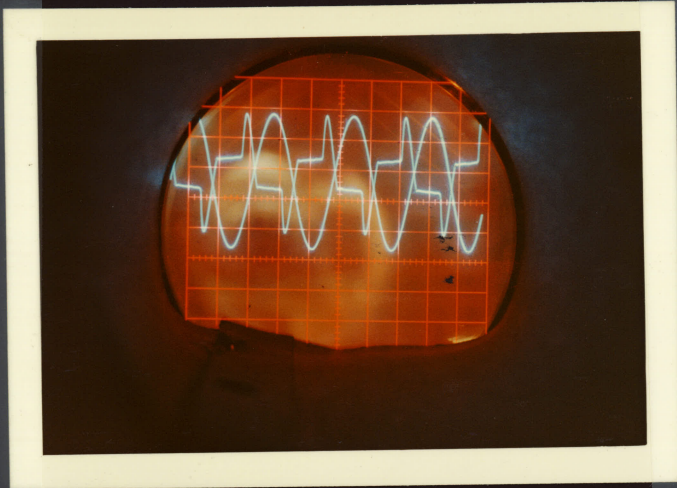


PHOTO #8
Input Voltage (sin) and
Input Current for Deltamax
for Large Signals.
600 ohms in series

PHOTO # 9
Input Voltage and Input
Current for Deltamax, for
Large Signal.
(No. Resis. in Series)

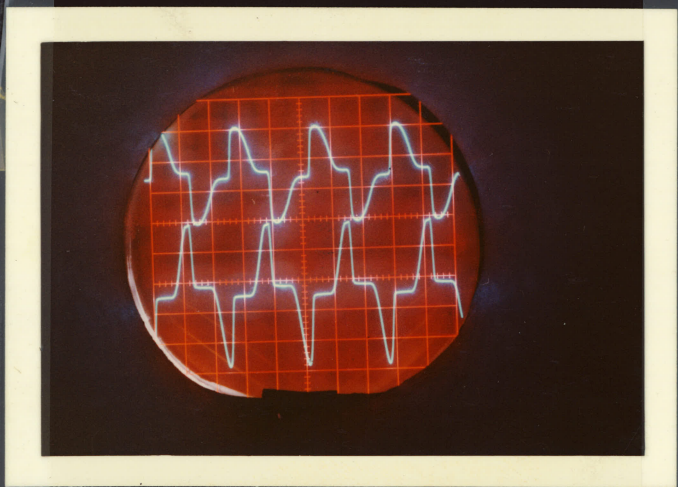
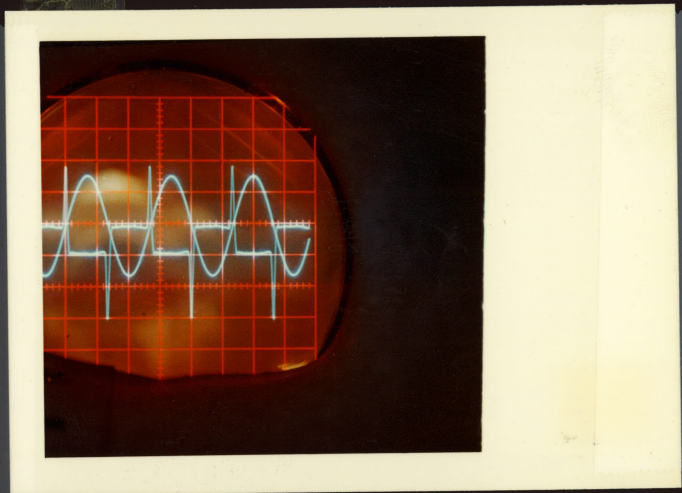


PHOTO #10
out put Voltage (Lower) and
Input Current for Permalloy
for 20 c/s

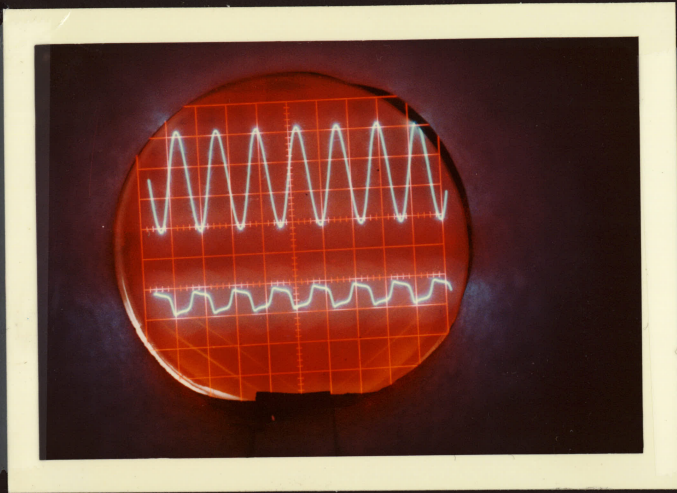


PHOTO #11
Input Voltage (Lower) and
Input Current for Permalloy
for 30 c/s

PHOTO #12
Input Voltage (Lower) and
Input Current for Permalloy
for 40 c/s

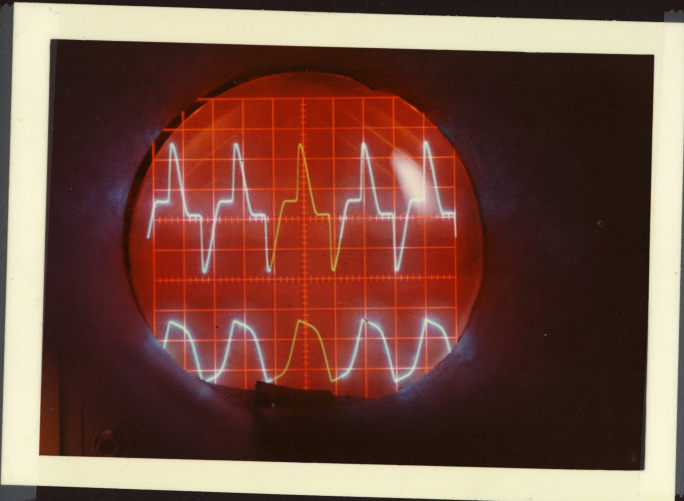
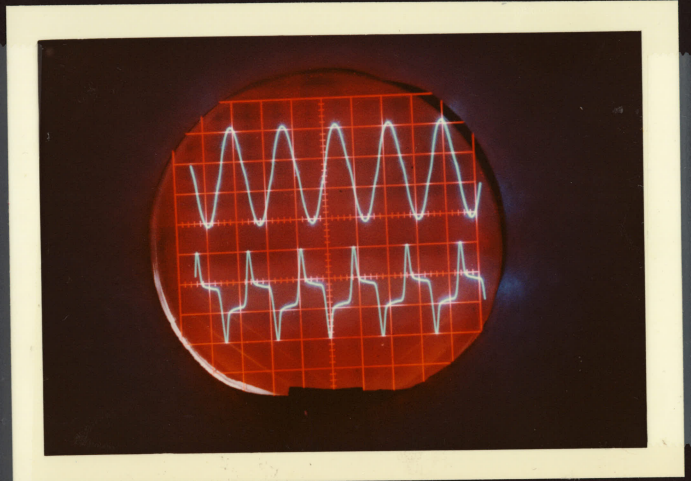


PHOTO # 13
Current through Permalloy
Core (up) and flux

V. 4 Describing Function Measurements Under Sinusoidal Applied Voltage to Cores

V. 4.1 Tests on 3T4178-P1

Tests conducted on this specimen yielded the results shown in Graph 5.1, p. 75. (See Appendix B for numerical data.) It should be noted that it is impractical to normalize the input voltage with respect to the loop width, since the latter does not remain constant, but changes according to the amplitude and frequency of the input signal as shown in Graph 5.2, p. 76. Measurement of this curve cannot be performed with sufficient accuracy to justify normalization with respect to the loop width.

Normalization of the input signal can be performed with respect to the saturation voltage. However, it should be noted that this voltage is linearly dependent upon the frequency of the input signal as shown in Graph 5.3, p. 77. Normalization with respect to this quantity is made later. Because the actual results obtained for the cores under test cannot be applied to any other magnetic core, it was preferred to calibrate the graphs in terms of actual input voltages. This calibration proves extremely useful in checking the results obtained by means of an analog computer, as in this manner, the amplitude of the oscillation may readily be predicted.

Graph 5.1, p. 75, presents the phase and magnitude of the describing function for three different frequencies.

It may be seen that no similarity exists between these curves and the curves to be found in many textbooks dealing with hysteresis type nonlinearities, (See Fig. 2.5, p. 14).

On the other hand, there is, to some extent, agreement between the experimental and theoretical results. Comparing Graph 5.1, p.75 with Graphs 4.2, p. 45 and 4.4, p. 50 (which were obtained through digital computer calculations of the theoretical models), it is seen that for fluxes less than the saturation value, the describing function remains constant in amplitude and phase (excluding very low fields), as was predicted by these models. However, over the saturation point, the first two models do not yield satisfactory results, but the third model (in which the relation between the coercive force and applied field approximates the actual experimental curve), predicts quite similar behaviour, but not accurately enough to be used in practical application. The reason for the similarity and dissimilarity between calculated and measured results is given below.

For low input signals, the input current remains sinusoidal (see Photo 7, p. 70), hence satisfying one of the assumptions under which the describing function was calculated; while for large signals the input current ceases to be sinusoidal (see Photos 8 through 13, pp. 71 and 72). Hence, our model is no longer valid, since for its derivation we assumed a sinusoidal input signal.

WORKING P.P.: DESCRIBING FUNCTION FOR 4-79 MO-PERMALLOY
(374178)

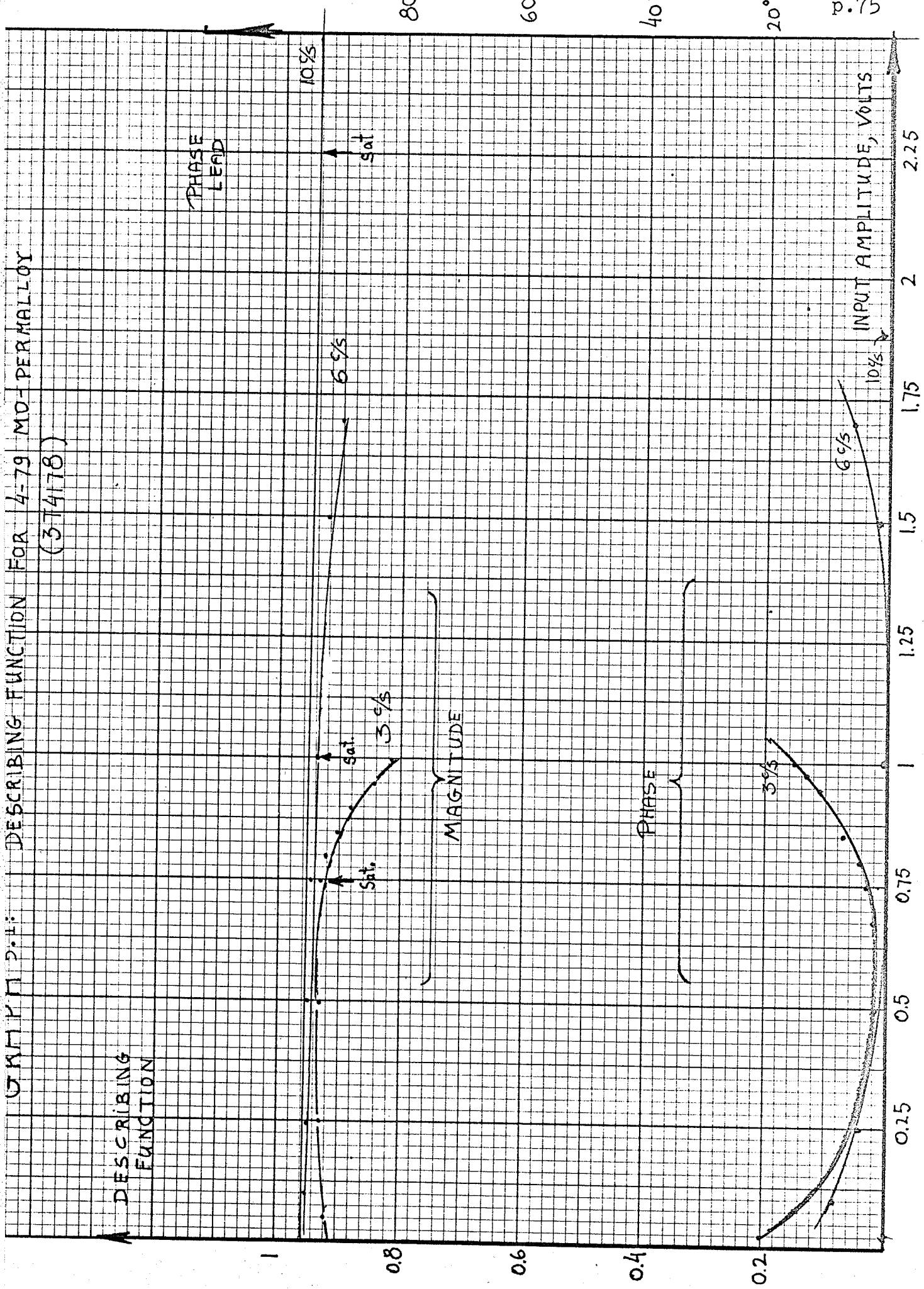
DESCRIBING
FUNCTION

PHASE
LEAD

MAGNITUDE

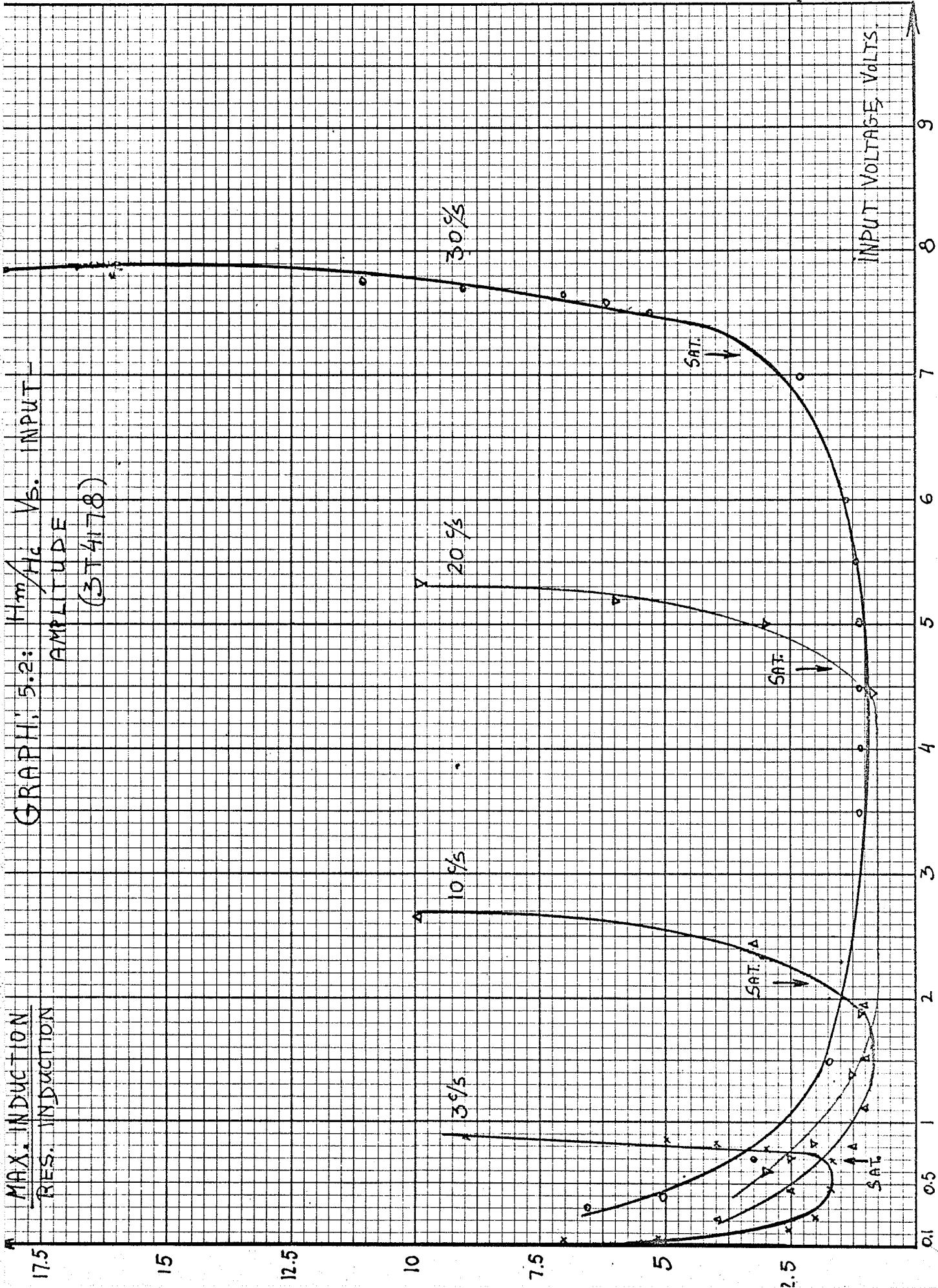
PHASE

INPUT AMPLITUDE, VOLTS



MAX. INDUCTION
RES. INDUCTION

GRAPH 5.2: H_m/H_c Vs. INPUT
AMPLITUDE
(3T4178)

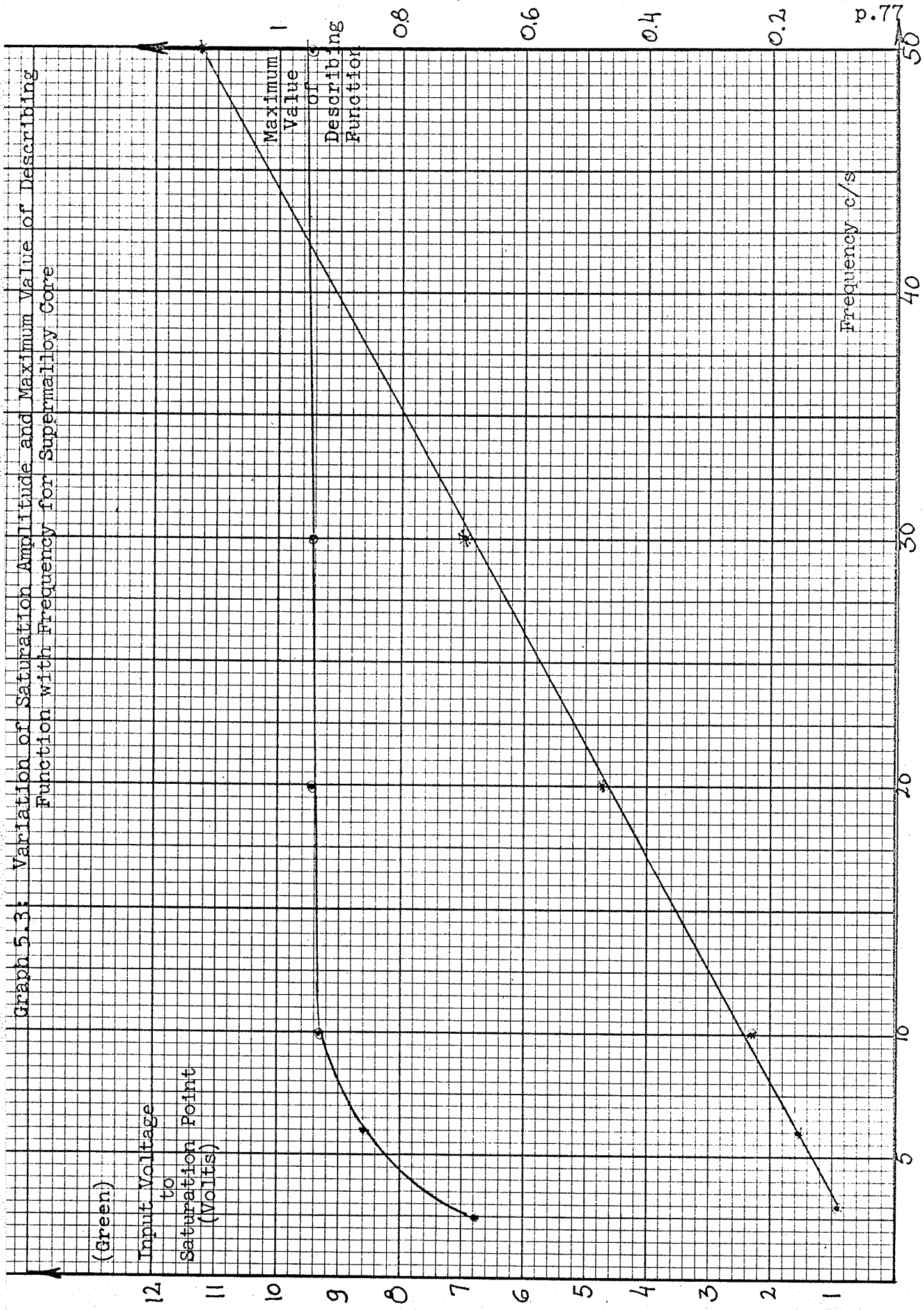


Graph 5.3: Variation of Saturation Amplitude and Maximum Value of Describing Function with Frequency for Supermalloy Core

(Green)

Input Voltage
to
Saturation Point
(Volts)

Maximum Value
of
Describing
Function



Frequency c/s

Concerning the mid-range of input signals, although the current is not purely sinusoidal (See Photo 15, p.79), there is still reasonable agreement between the theoretical and the experimental models, that is, the describing function remains constant. The reason for this is illustrated in Graph 5.2, p.76. This graph shows the ratio between the maximum induction and the coercive force as a function of the input amplitude for various frequencies.

It is seen that these curves assume approximately constant values for certain ranges. In these ranges, the ratio of the applied field to the coercive field is constant, i.e., the coercive force changes linearly with the input amplitude. Examination of Graph 5.1, p. 75, reveals that the describing function remains constant only within this range. This coincides with the theoretical results.

It should be noted that our third model, eq.(4.6) and (4.7) should be properly adjusted in order to obtain the best results; that is, the relation between H_c and H_m should be as close as possible to the H_c vs. H_m curve of the actual core under test.

The effect of frequency on the properties of the non-linear element is shown in Graphs 5.1 through 5.3, pp. 75 - 77. One can try to normalize graphs 5.1 and 5.2 with respect to frequency, in order to exclude the linear frequency dependent element, (the self-inductance of the coil) from the nonlinear element.

PHOTO # 14
Analog Computer Set-Up

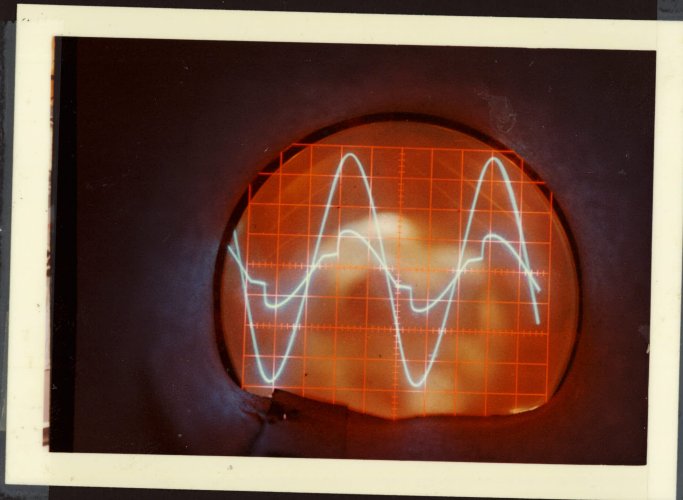
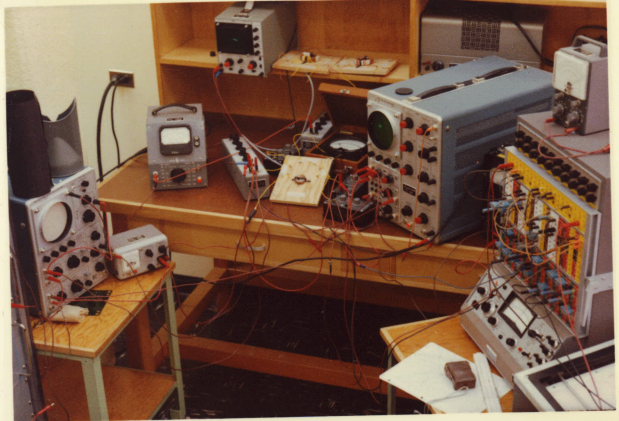
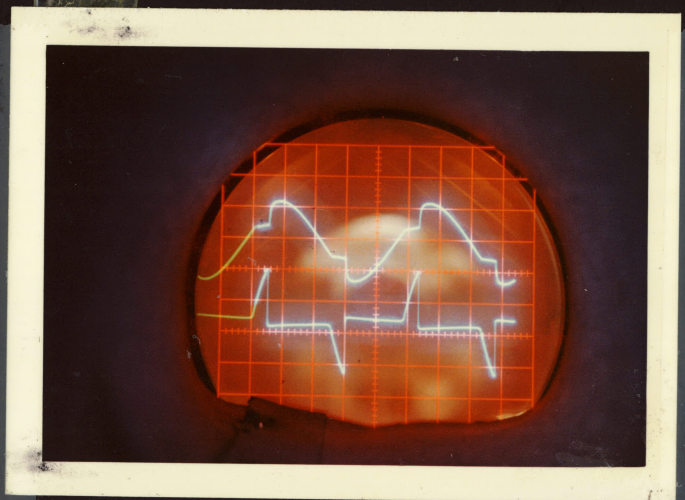


PHOTO # 15
Limit Cycle with Deltamax
Core.
Source Impedance 600 ohms
Gain = 7200

(50 ms/cm)
Current (Smaller) 1 mA/cm
Voltage 2 V/cm

PHOTO # 16
Limit Cycle with Deltamax
Core.
Current through core (up)
and output voltage from
core (50 ms/cm)



However, as will later be shown, it is unfortunate that the self-inductance of the coil depends on input amplitude and thus cannot be separated from the hysteresis nonlinearity.

As previously mentioned (Section II.4), a hysteretic element tends to cause a lag in the phase of the output component. All the methods and techniques previously described give the phase shift of the hysteresis element as a lag. This holds true when dealing with mechanical hysteresis and measurement of the transfer function is made between the input and output positions, but, is not the case when dealing with nonlinear elements having characteristics similar to those of magnetic cores.

A phase diagram illustrating what actually takes place while driving the cores is shown in Fig. 5.10.

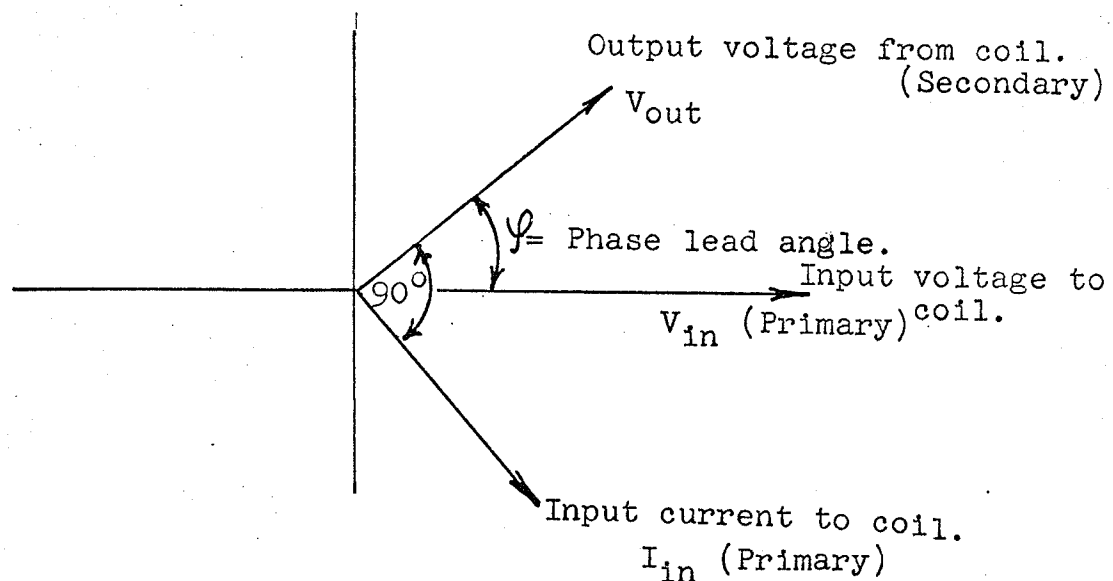


Fig. 5.10: Phase shift between input voltage and output voltage.

It is evident that while the current lags behind the input voltage, the output voltage leads the input voltage, (or, in the lossless case where the coil is a pure inductor in the same phase as the input voltage). Thus, the critical locus is not in the third quadrant as would normally be expected, but is in the second quadrant. The critical loci are shown in Graph 5.4, p. 82.

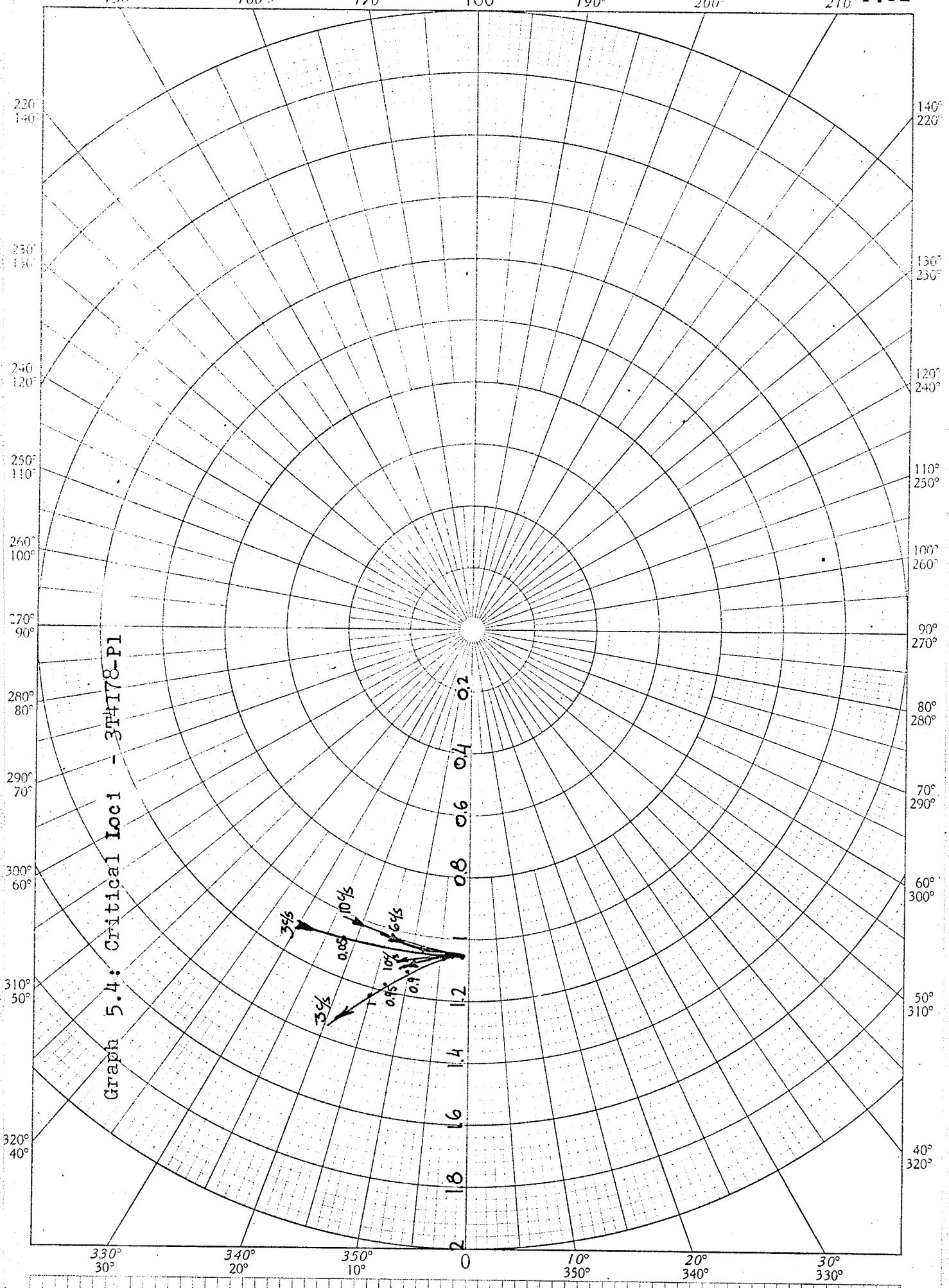
V. 4.2 Tests on 4T4162-D2

Up to this point, we have seen that to some extent both theory and practical application have been in agreement with one another, but, from this point and continuing onward we unfortunately find increasing differences between theory and practice; these will be discussed on the following pages.

The behaviour of the Deltamax specimen is shown in Figs. 5.1, p.59, and 5.2, p.60, as well as Photo 6, p.70. The results of the measurements in this specimen are illustrated in Graph 5.5, p. 83. (See Appendix B for numerical data.)

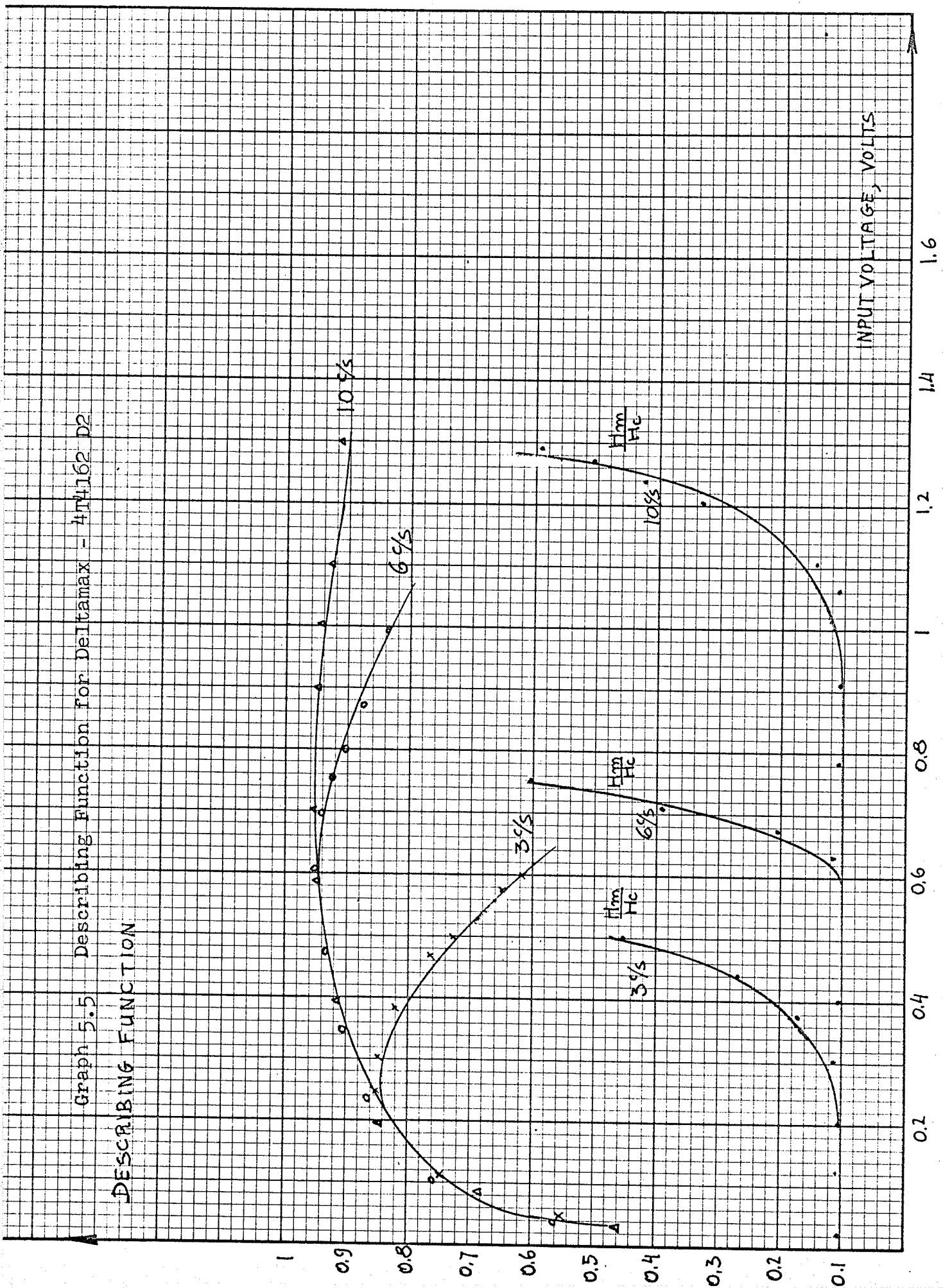
The behaviour of the describing function for this case differs considerably from either the describing function of 4-79 Mo Permalloy or the theoretical results obtained in Chapter IV, because the describing function starts from zero, rather than from its maximum value, reaches a peak value, and decreases again. These differences lie in the characteristic behaviour of the individual specimens under examination.

Graph 5.4: Critical Loci - 3T4I78-P1



Graph 5.5 Describing Function for Deltamax - 4M4162 D2

DESCRIBING FUNCTION

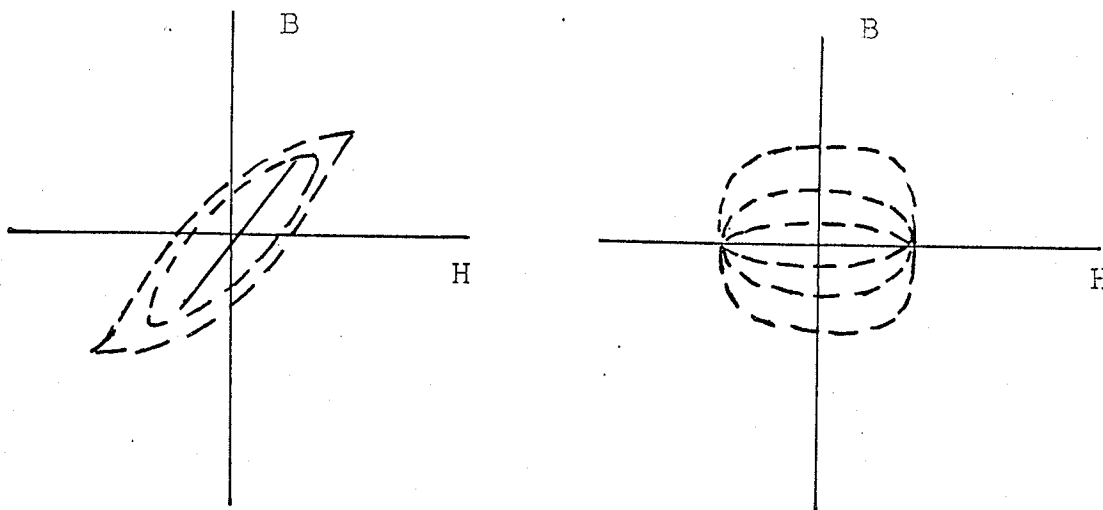


The gain in the reversible region is given by

$$\frac{dB}{dH} = \mu_0 + \sqrt{H}.$$

That is, for $H=0$, the gain is μ_0 . By looking at Figs. 5.2, p.60 and 5.4, p. 63, it is seen that while the magnetization curve for Permalloy has $\mu_0 \approx 20,000$ (Supermalloy has $\mu_0 \approx 100,000$) Deltamax has an initial permeability of $\mu_0 \approx 1,000$. This means that while the hysteresis loop for Permalloy and Supermalloy begins to build up as shown in Fig. 5.11(a), the Deltamax loop begins as shown in Fig. 5.11(b).

Thus, there is a range for which there is no output for a given input.



(a) Permalloy and Supermalloy

(b) Deltamax

Fig. 5.11: Behaviour of hysteresis loops near the origin.

That is, there is a kind of backlash effect for small amplitudes, and therefore, in the initial range the shape of the describing function for such cores would be similar to the describing function derived for backlash. The behaviour of this core for intermediate and large signals is similar to Permalloy. Graph 5.5, p. 83 also presents the relation between H_c and H_m . The describing function remains approximately constant over the range in which $\frac{H_m}{H_c} = \text{const.}$, that is,

$$H_c = mH_m \quad (\text{excluding of course the region near the origin}).$$

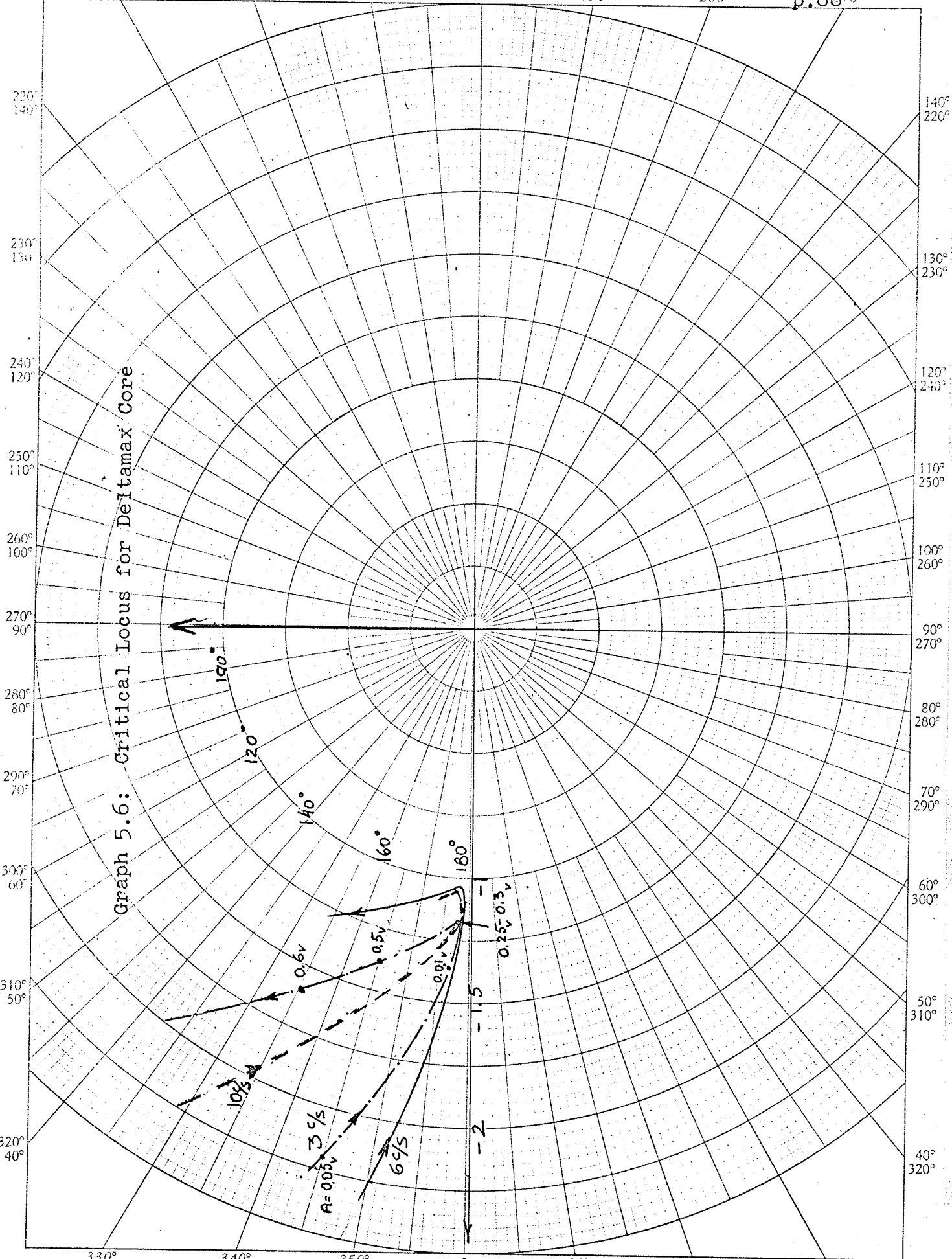
The critical loci for this core are shown in Graph 5.6, p.86.

V.5 Source Impedance Influence on The Derivation of The Describing Function

It was previously mentioned that for most applications, the transfer function in which we are mainly interested should be measured between the input and output voltage.

Previous experiments show that when the input voltage is sinusoidal, the theoretical models yield satisfactory results (some types of cores only) for inputs which were beyond the saturation level. However, magnetic nonlinear elements usually have low input impedance (i.e. generators, motors, amplidynes, transformers) and therefore require a larger current drive. If the driving generator has no internal impedance the input voltage to the nonlinear element would remain sinusoidal, although the current supplied by the generator

Graph 5.6: Critical Locus for Deltamax Core



is not sinusoidal, also, no attenuation in the magnitude of the applied voltage would take place between the generator and the driven element.

On the other hand, if the source does have an output impedance, the applied voltage would no longer be sinusoidal due to non-sinusoidal voltage drop across this impedance. Also, due to the formation of a voltage divider between the internal impedance of the source and the input impedance of the nonlinear element, attenuation between the driving and driven element will occur.

Unfortunately, the attenuation of this voltage divider is not a constant quantity that can readily be accounted for, but rather changes in an intricate manner. Obviously, under such conditions the describing function would differ considerably from the describing function measured before.

The problem is of great importance in cases when one tries either to limit the current through nonlinear elements having low input impedance by placing a resistor in series, or, while using driving generators of high output impedance in order to obtain sinusoidal current drive.

When dealing with control systems, one should be aware that when placing impedance in series with such elements, the stability of the system may be affected.

In order to predict operation under such conditions, a series resistance of 600 ohms was placed in series with the coils (thus representing an artificial source impedance). This value was chosen because it is a typical output impedance

of many standard sources. Results of these experiments are shown on the following pages.

V. 5.1 Tests on 3T4178-P1

Graph 5.7, p. 89, shows the shape of the describing function for various frequencies. (See Appendix B for data corresponding to this graph.) Comparison with Graph 5.1, p. 75 accentuates the differences between the two. The phase shift for low input signals is much larger than previously, and while the previous describing function began from its maximum value, it now begins from a lower value. The effect of frequency on the describing function is much more noticeable, and for low frequencies the gain of the nonlinear element is considerably decreased.

A plot of the input voltage required to drive the core into saturation vs. the frequency, and maximum equivalent gain of the nonlinear element vs. frequency are shown in Graph 5.3, p. 77. It is seen that the saturation value varies linearly with frequency. Thus, normalization with respect to this value is actually the same as normalizing the curves from a frequency point of view.

If, by so doing, all the curves shown in Graph 5.8, p.90 were to coincide, this would prove that the nonlinear element could be separated into a linear storage element (self-inductance of the coil) whose impedance linearly increases with frequency,

Graph 5.7: Describing Function for Permalloy Core

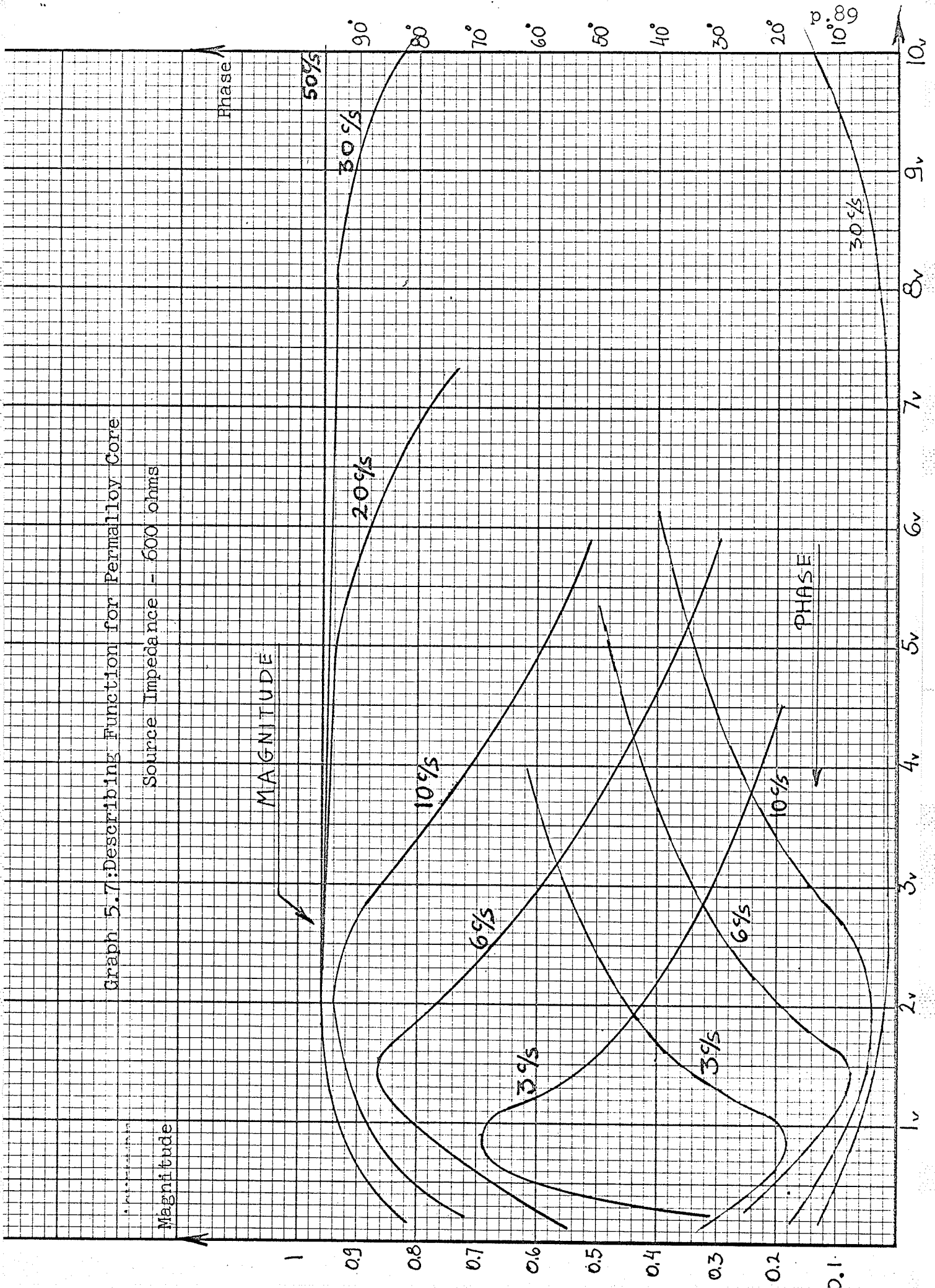
Source Impedance - 600 ohms

Magnitude

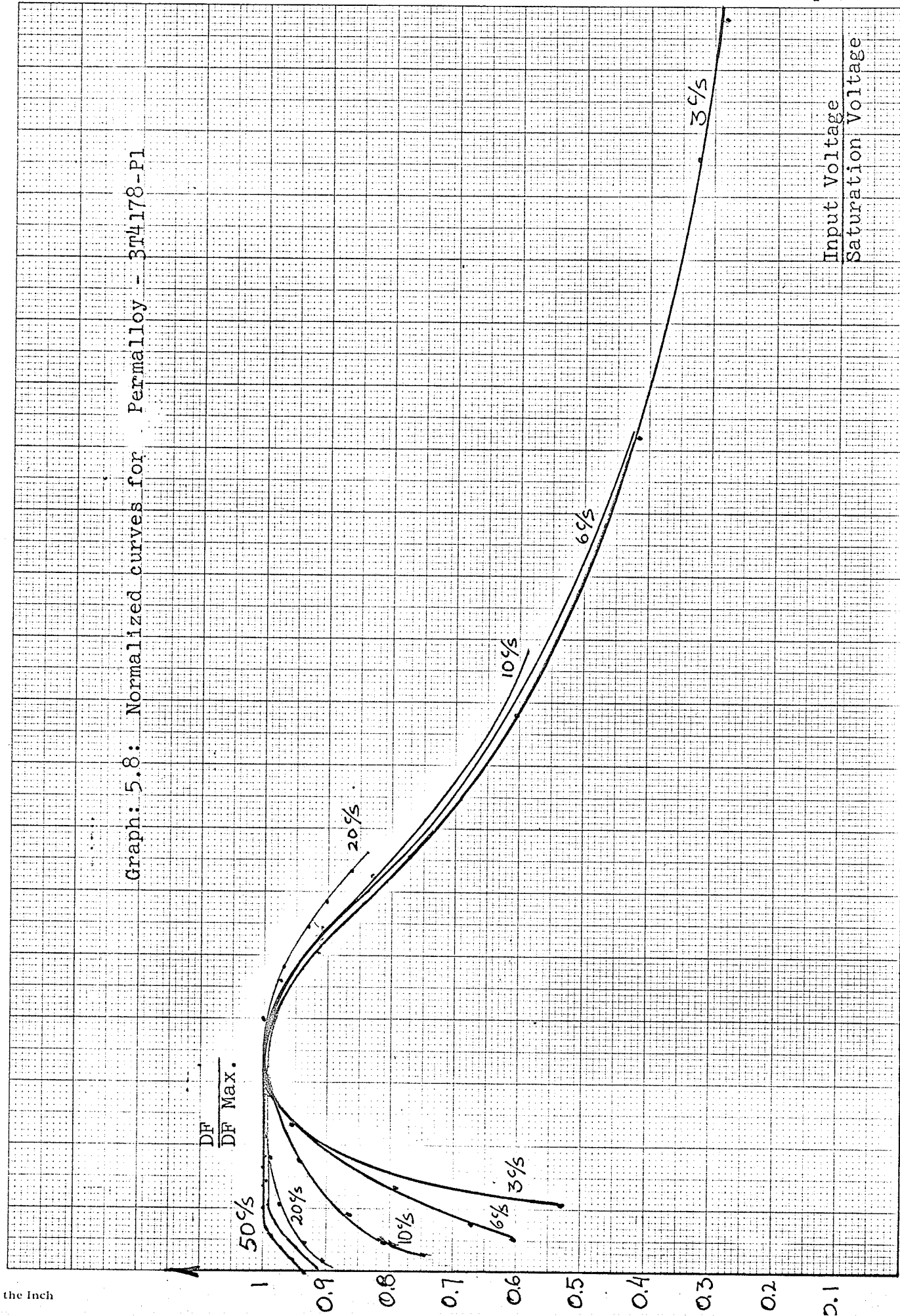
Phase

MAGNITUDE

PHASE



Graph: 5.8: Normalized curves for Permalloy - 3T4178-P1



5

4

3

2

1

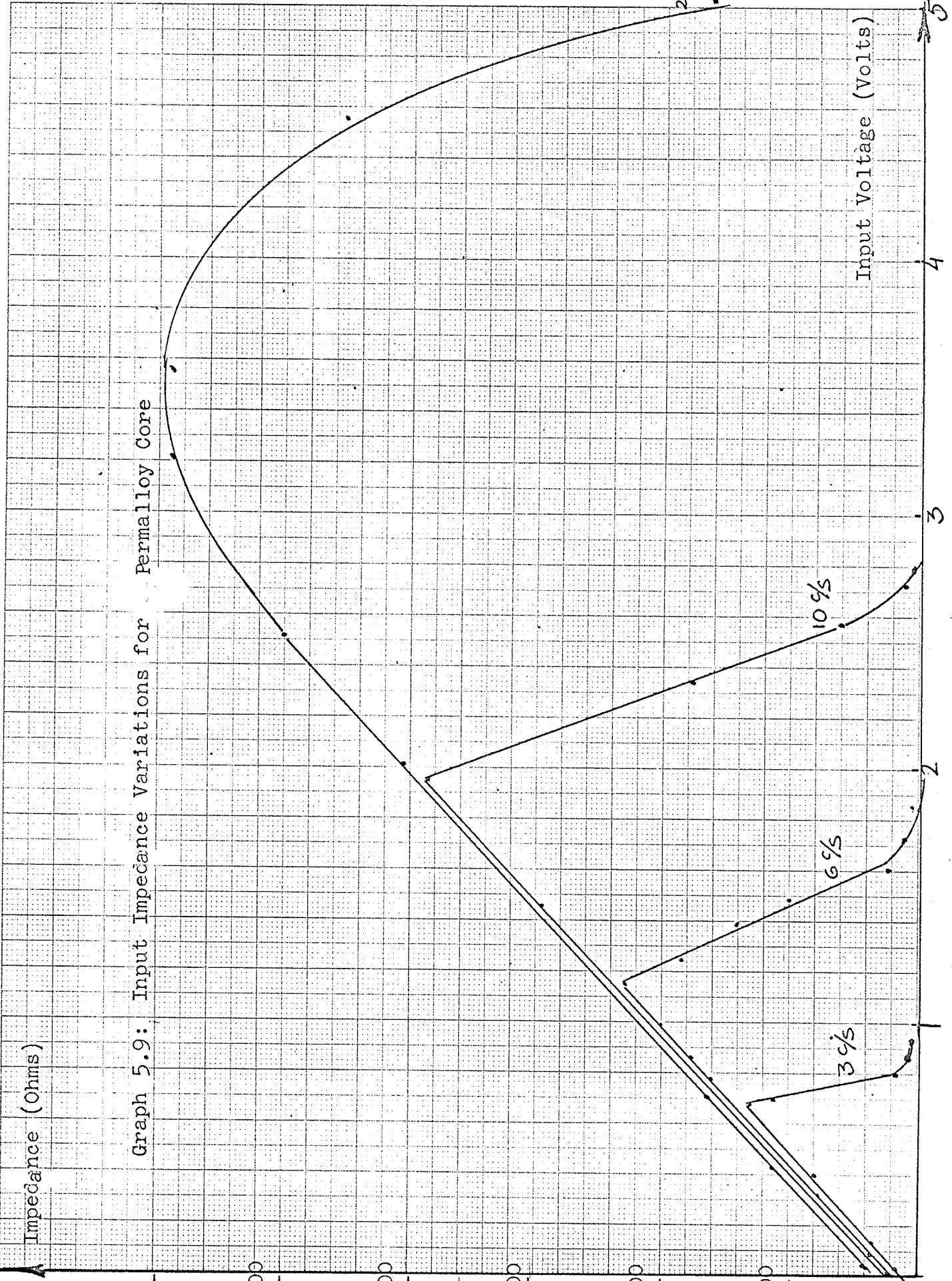
Input Voltage
Saturation Voltage

and a hysteretic nonlinearity having an output dependent only on the amplitude of the input signal.

Graph 5.8, p. 90 shows the normalized curves from which it is seen that such an assumption (found in most textbooks) is, in this case, not valid. Graph 5.8 also shows that the effect of frequency on the cores is especially noticeable for inputs below the saturation level. For high frequencies the describing function becomes similar to the describing function of the theoretical models.

Let us examine the reasons for these deviations more closely. As mentioned before, one of the reasons for the discrepancy between the two series of tests is due to the presence of a nonlinear voltage divider between the driving generator and the non linear element. Graph 5.9, p. 92 shows curves for input impedance of the coil vs. input amplitude for various frequencies. (The input impedance was calculated by dividing the input amplitude (R.M.S.) by the first harmonic of the input current.)

From these curves it is seen that for low signal inputs the impedance is very low because the permeability of the core in this region is low. Thus, much of the applied voltage appears across the 600 ohm resistance and the input to the coil is very low. Increasing the input amplitude moves the working point into the high permeability region, thus increasing the coil impedance.



Graph 5.9: Input Impedance Variations for Permalloy Core

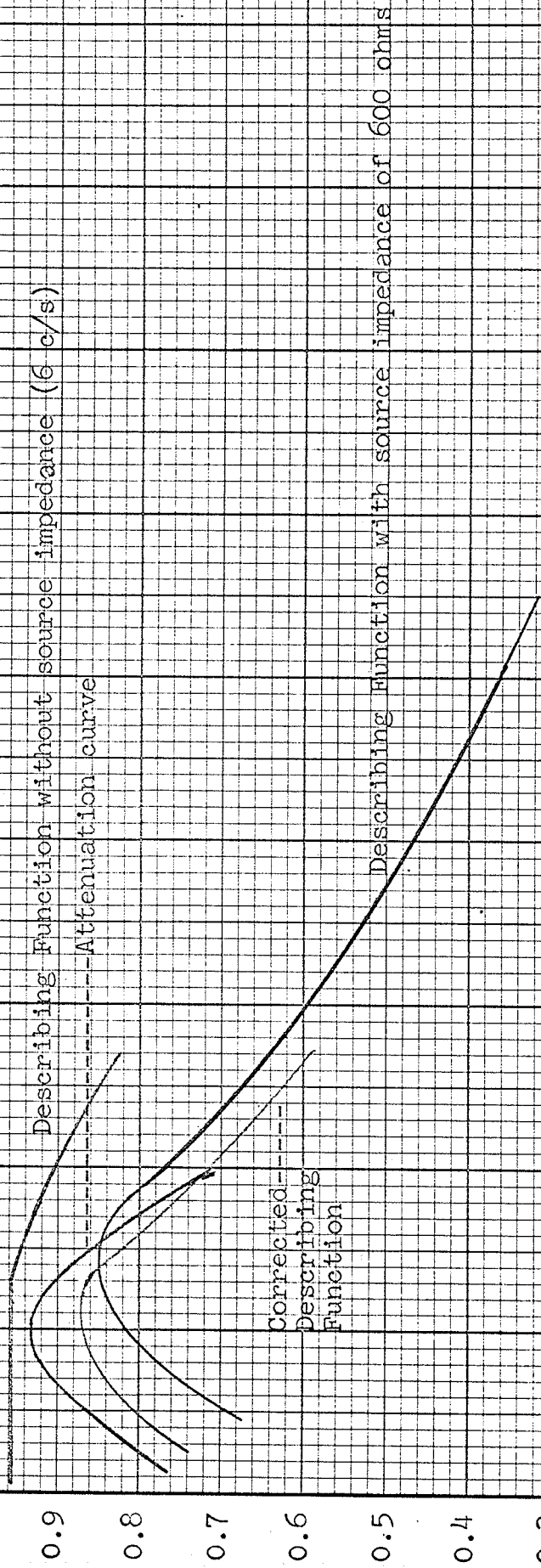
Hence, the value of the describing function is increased. Once the saturation point is exceeded, the permeability of the core becomes very low and its impedance drops considerably. As a result, the value of the describing function is rapidly decreased. Using Graph 5.9, p. 92 and the value of the source impedance, it is possible to construct an attenuation curve which will show the attenuation for each frequency and input amplitude. Then, by multiplying Graph 5.1, p. 75 by the attenuation curve shown in Graph 5.9, p. 92, one arrives at a corrected form for the describing function. (See Graph 5.10, p. 94.)

It is shown that the original graph and the corrected graph do not completely overlap. This is because introducing resistance in series also changes the current wave shape. (See Photos 8 and 9, p. 71.)

The describing function and the factors affecting it are shown in Graph 5.11, p. 95, and it is thus shown that the describing function is more or less constant where H_m/H_c assumes a constant value. Its maximum value and rate of increase or decrease depend closely upon the input impedance and variations of coil impedance with amplitude and frequency.

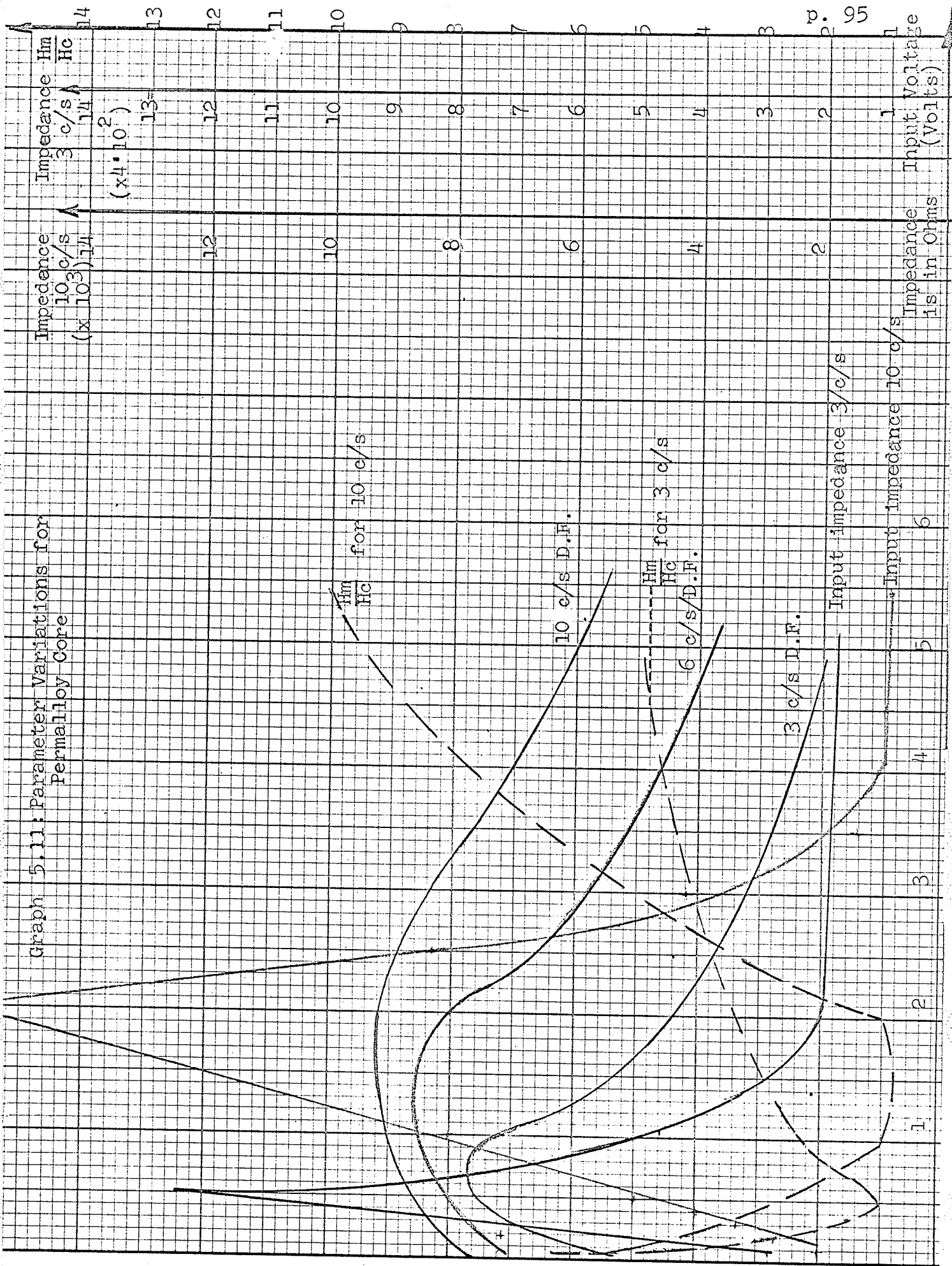
Graph 5.12, p. 96 shows the critical locus for this new case. Comparison with Graph 5.4, p. 82 shows that it is not difficult to arrive at a system which would be stable in the one case and unstable in the other.

Graph 5.10: Effect of Source Impedance on The Describing Function for Permalloy Core

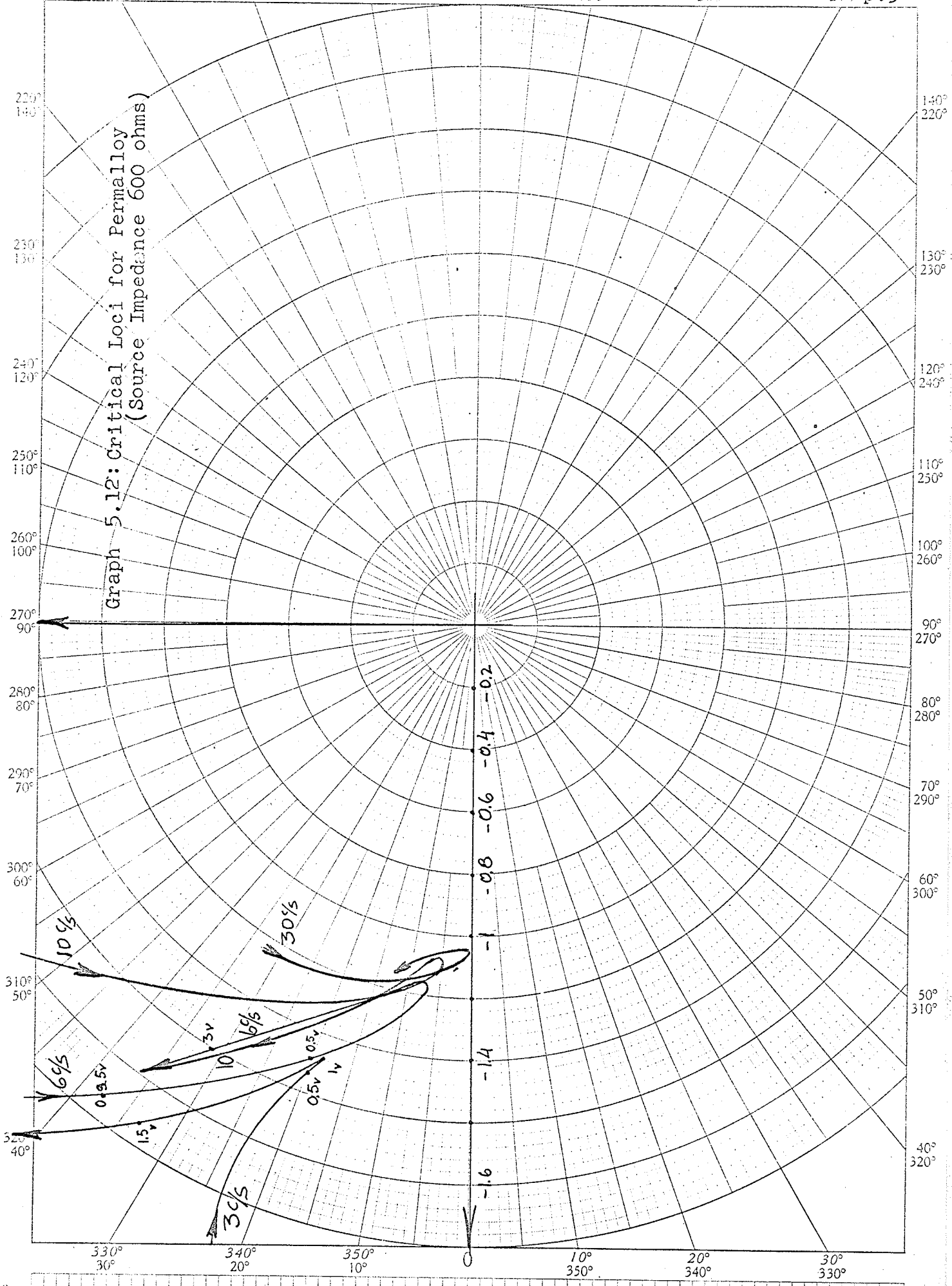


1 2 3 4 5

Graph 5.11: Parameter Variations for Permalloy Core



Graph 5.12: Critical Loci for Permalloy
(Source Impedance 600 ohms)



V. 5.2 Tests on 4T4178-S4

A similar set of tests was conducted on Supermalloy. Because of the similar behaviour of these two materials, the results obtained are much the same as for 4-79 Mo Permalloy. These results are displayed in Graphs 5.13 through 5.15, pp. 98 - 100. The data for these graphs is given in Appendix B.

V. 5.3 Tests on 4T4168-D2

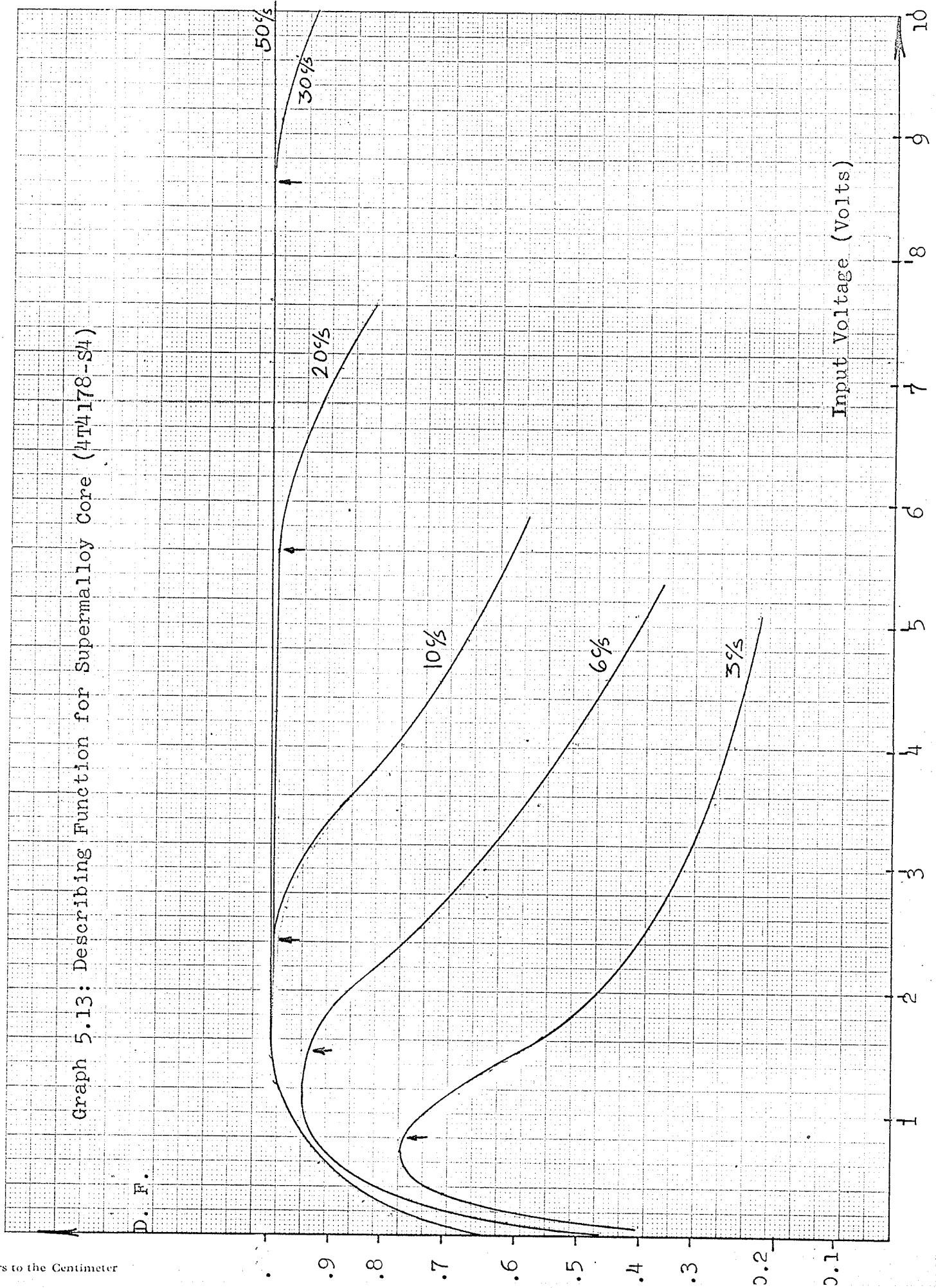
Somewhat different results were obtained for Deltamax. As mentioned before, the initial slope of the magnetization curve for this material is relatively low. Hence, for a certain range of input amplitudes there is actually no output. As a result, this element acts much the same as a backlash nonlinearity.

Verification of this conclusion may be obtained by examination of Graph 5.16, p. 101 (See Appendix B for data), where the combined effects of series resistance are added. As expected, the curves develop from zero gain due to "backlash" effects and the high attenuation which is caused by the nonlinear voltage divider.

Normalization of these curves with respect to saturation amplitudes (i.e. with respect to frequency) and to the maximum gain is given in Graph 5.17, p. 102. It is again seen that any attempt to deliberately separate the linear storage device from the nonlinear characteristic would not yield satisfactory results.

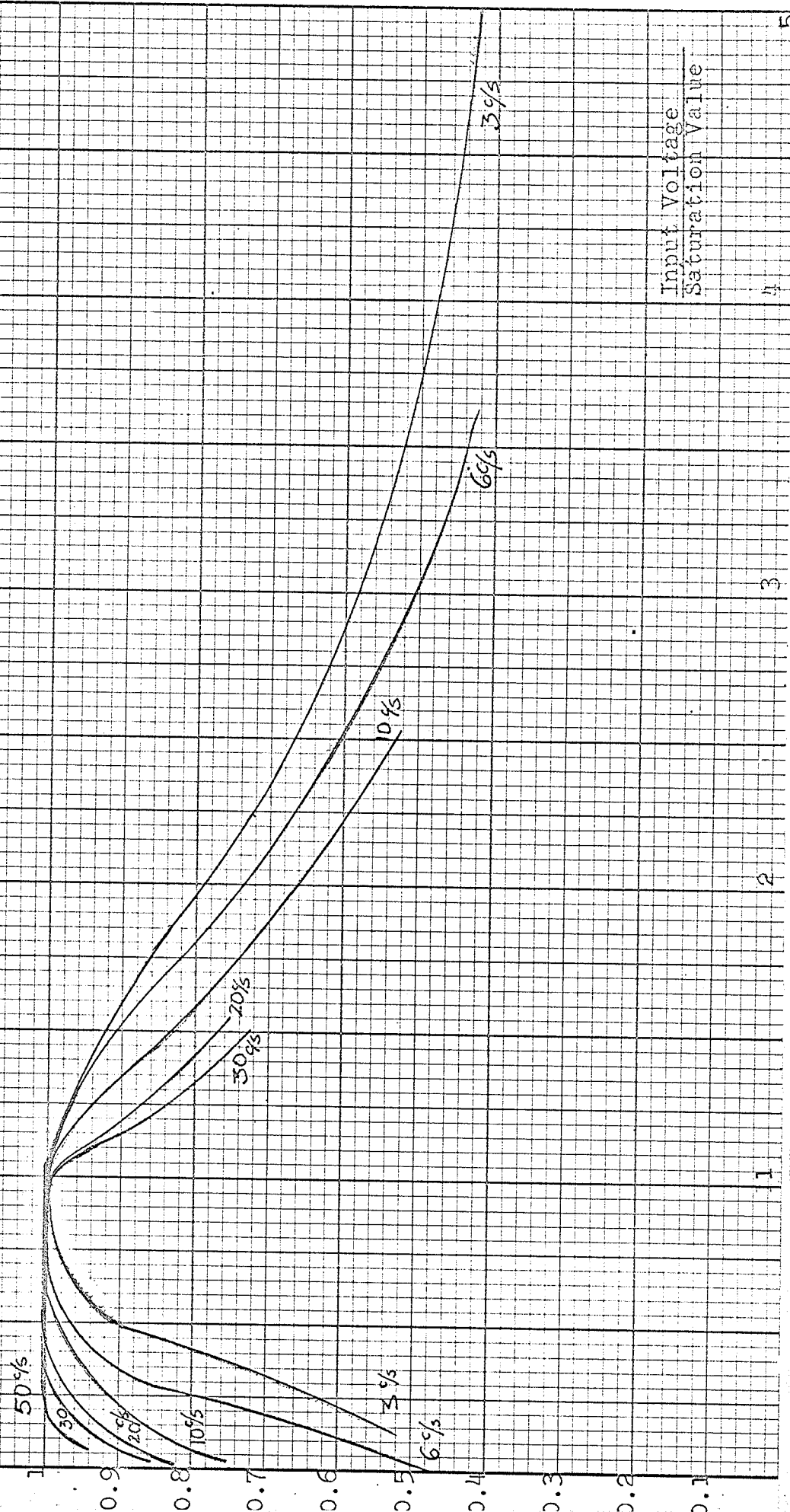
Graph 5.13: Describing Function for Supermalloy Core (4T4178-S4)

D. F.



Graph 5.14: Normalized Describing Function for Superalloy

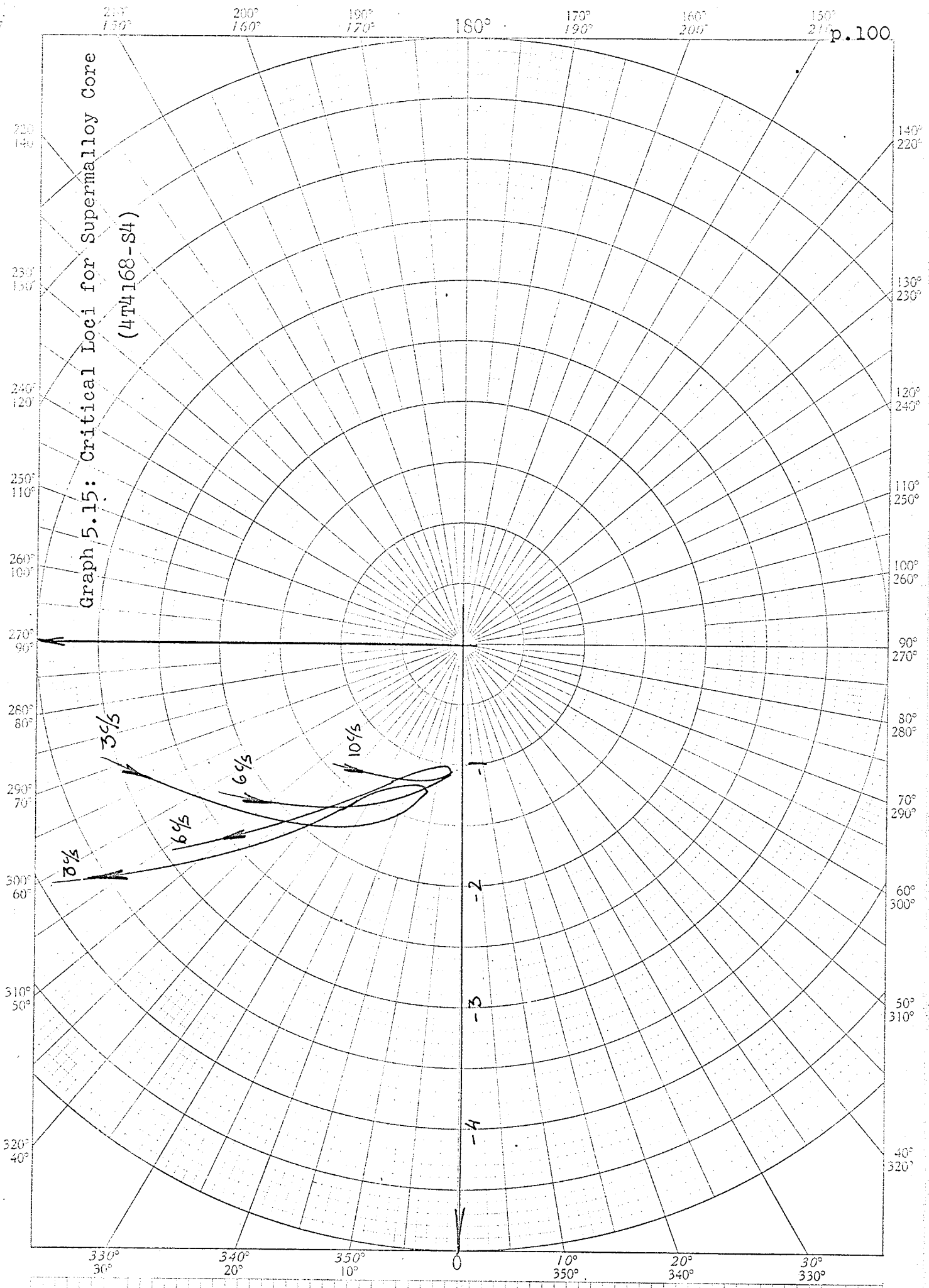
D.F.
D. F. Max.



Input Voltage
Saturation Value

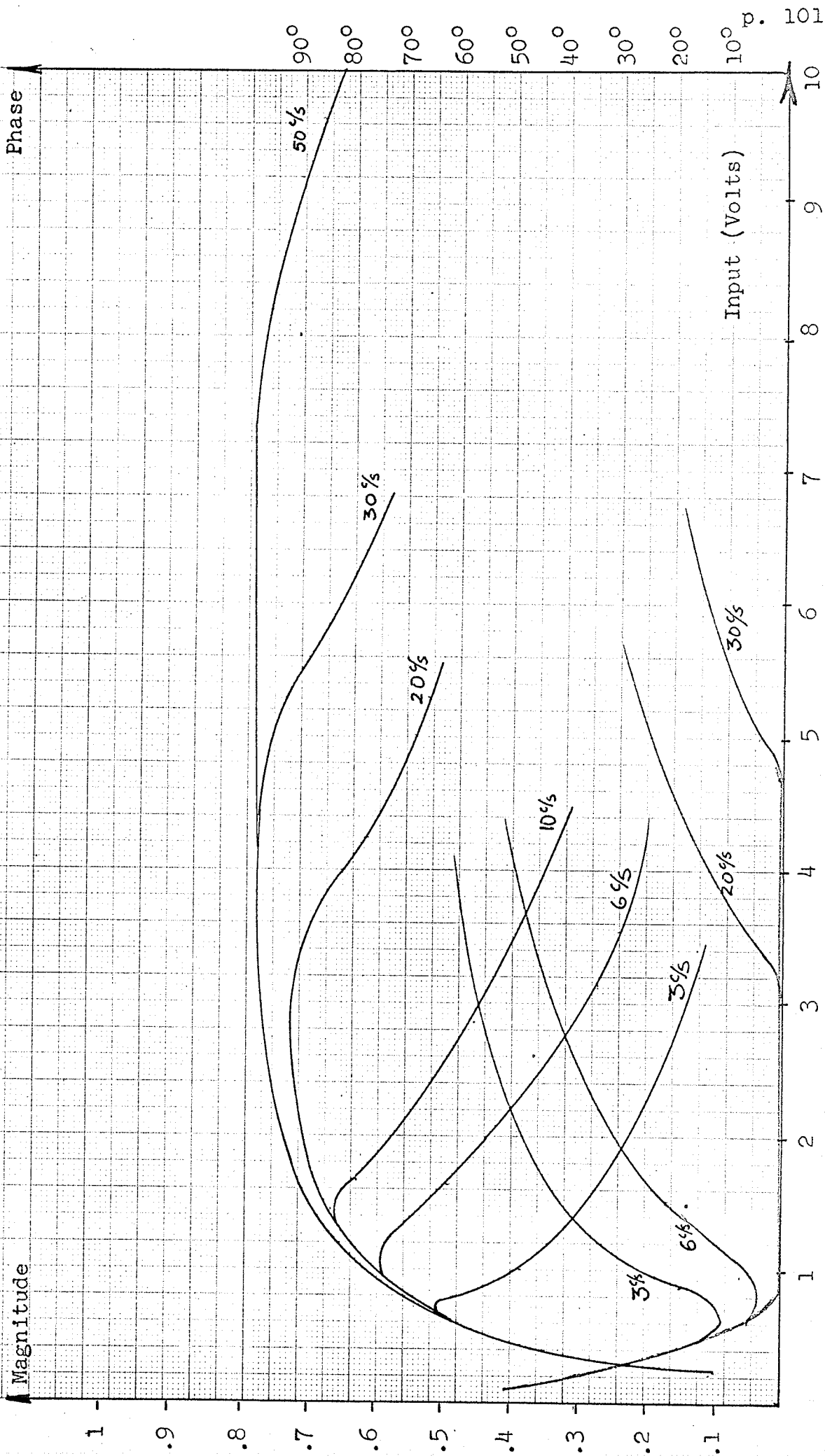
1 2 3 4 5

Graph 5.15: Critical Loci for Supermalloy Core
(4T4168-S4)



Graph 5.16: Describing Function for Deltamax Core - 4T4168-D2

Source Impedance - 600 ohms



Magnitude

Phase

Input (Volts)

1

.9

.8

.7

.6

.5

.4

.3

.2

.1

1

2

3

4

5

6

7

8

9

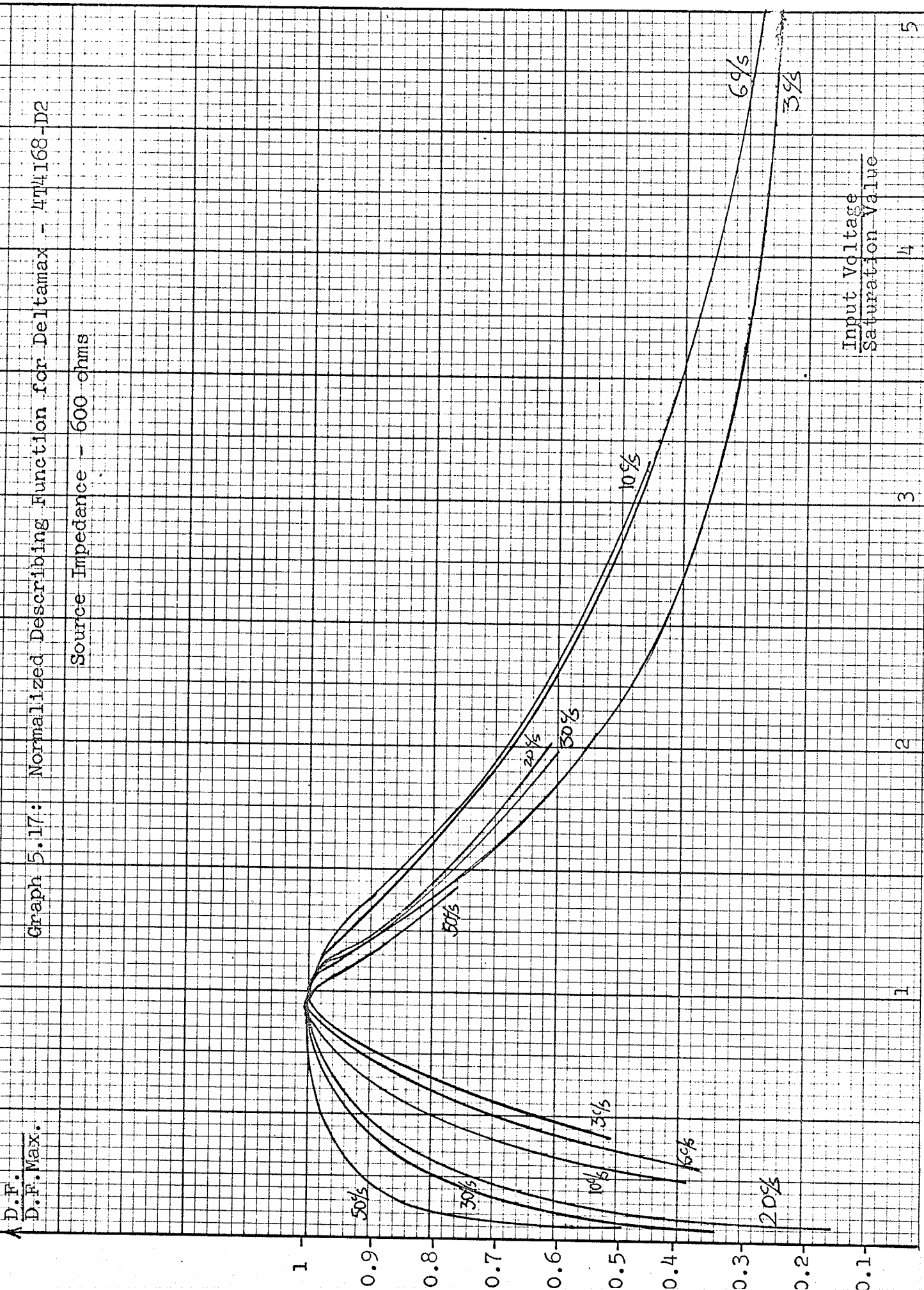
10

101

Graph 5.17: Normalized Describing Function for Deltamax - 4T4168-D2

Source Impedance - 600 ohms

D.F.
D.F. Max.



Input Voltage
Saturation Value

The input impedance for this material is given in Graph 5.18, p. 104 . Again we can form an attenuation curve by using these graphs with the value of input impedance from which one set of curves may be derived from the other set. (Although the derived curve and the measured curve do not coincide with each other completely, still, this curve can be employed if one wishes to take into account the influence of source impedance.) Graph 5.19, p. 105 shows the two sets of measured curves - the attenuation curve and a derived curve for 6 and 10 cps.

Graph 5.20, p. 106 shows the critical locus for this case. It is seen that the relative location of these loci is approximately the same as previously, however, the amplitude scaling is different. Also, in this case, a stable system may become unstable when source impedance is varied.

V. 6 Analog Computer Verification of The Results

In order to verify the results for the measurements referred to in previous chapters, a typical control system was simulated on an analog computer*. A transfer function of a voltage regulator having as its elements an amplidyne and generator was chosen, and the cores were inserted in series with the system as shown in Fig. 5.12, p. 107.

*The computer used was: Pace TR-10, Electronics Associates, Inc. Long Branch, New Jersey, U.S.A.

Graph 5.18: Input Impedance Variations for Deltamax Core
(474102-D2)

Core Impedance (ohms)

Ohms)

1000

900

800

700

600

500

400

300

200

100

Input Voltage to Core

0.2

0.4

0.6

0.8

1

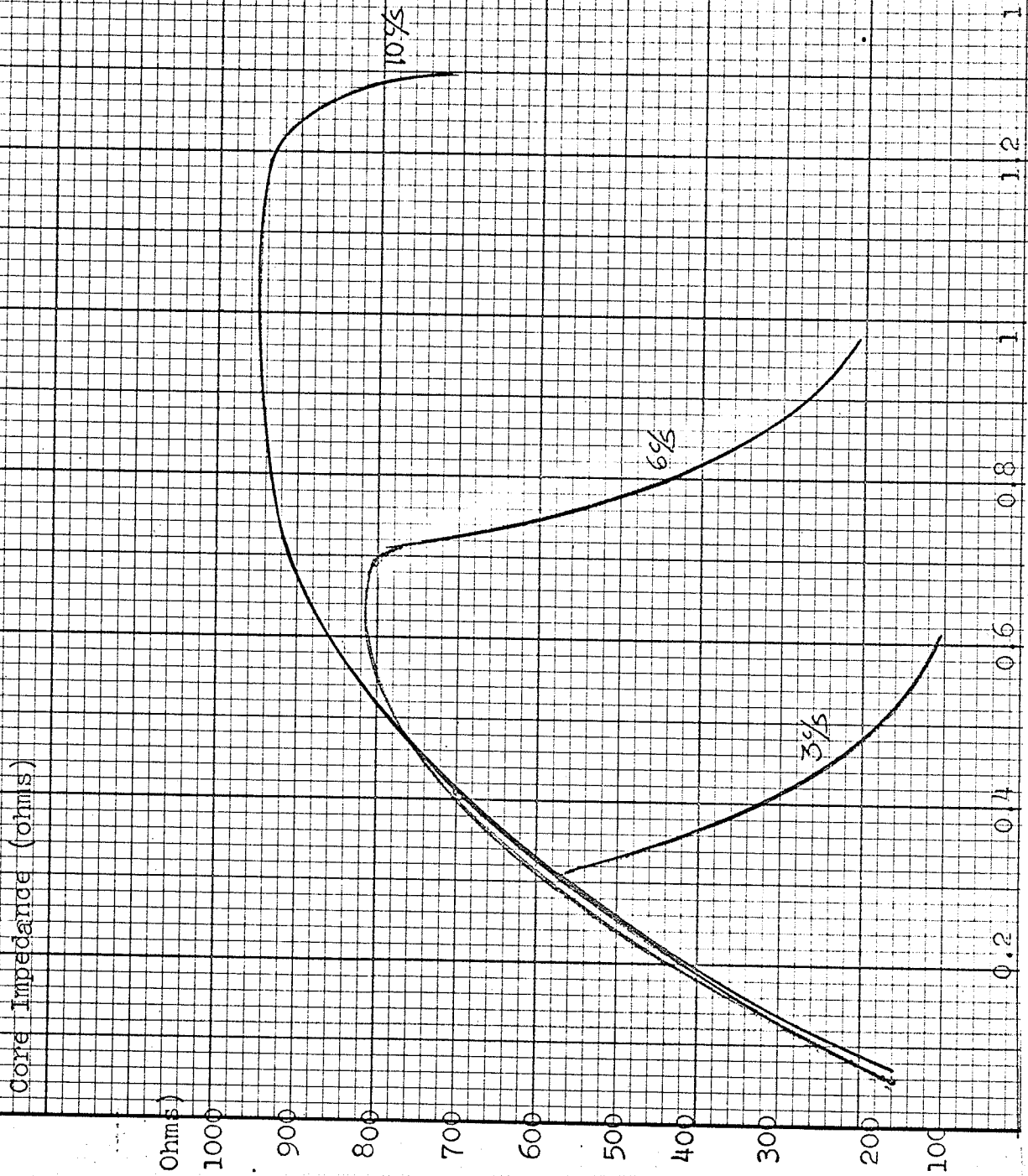
1.2

1.4

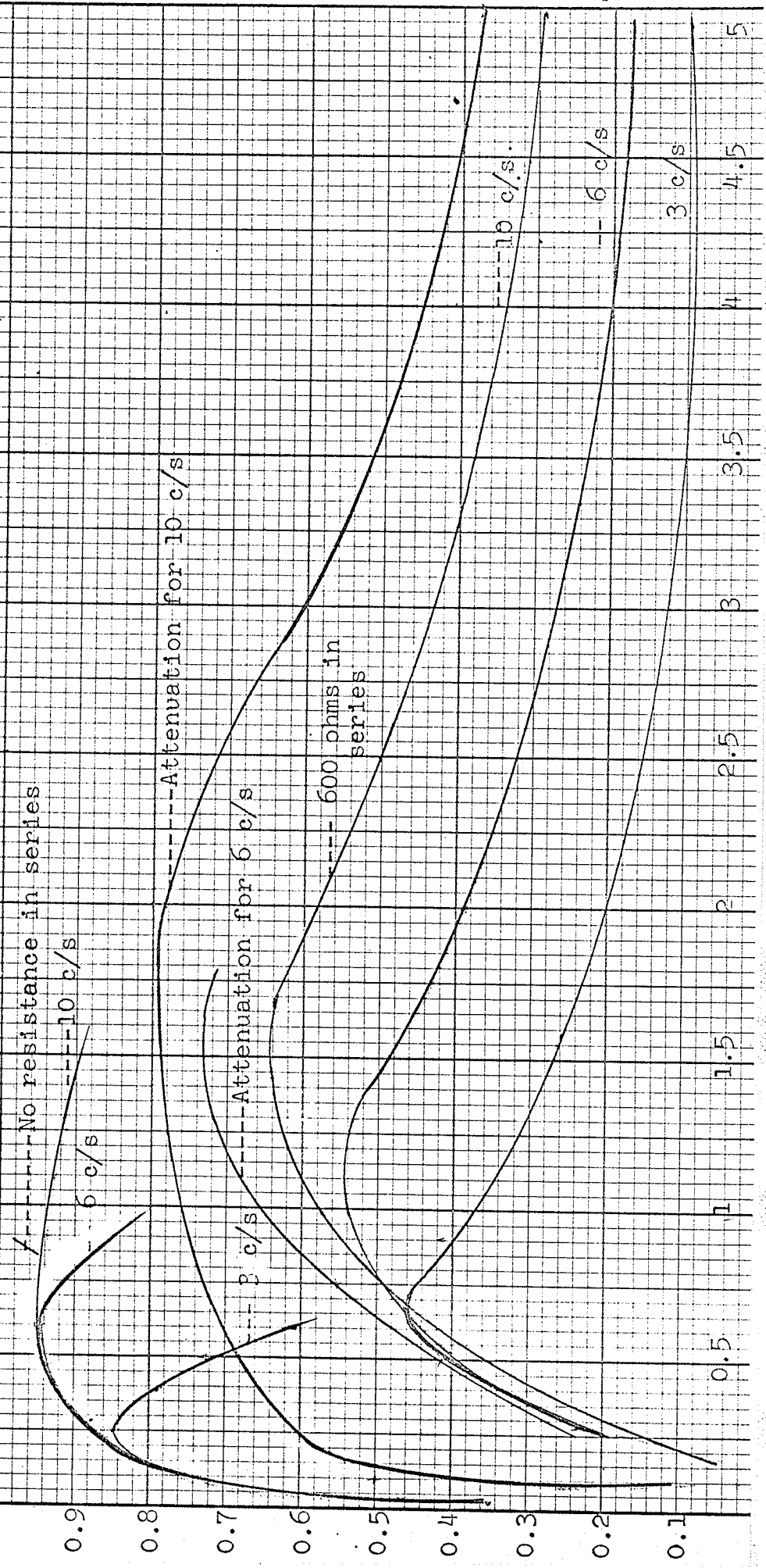
1.6

1.8

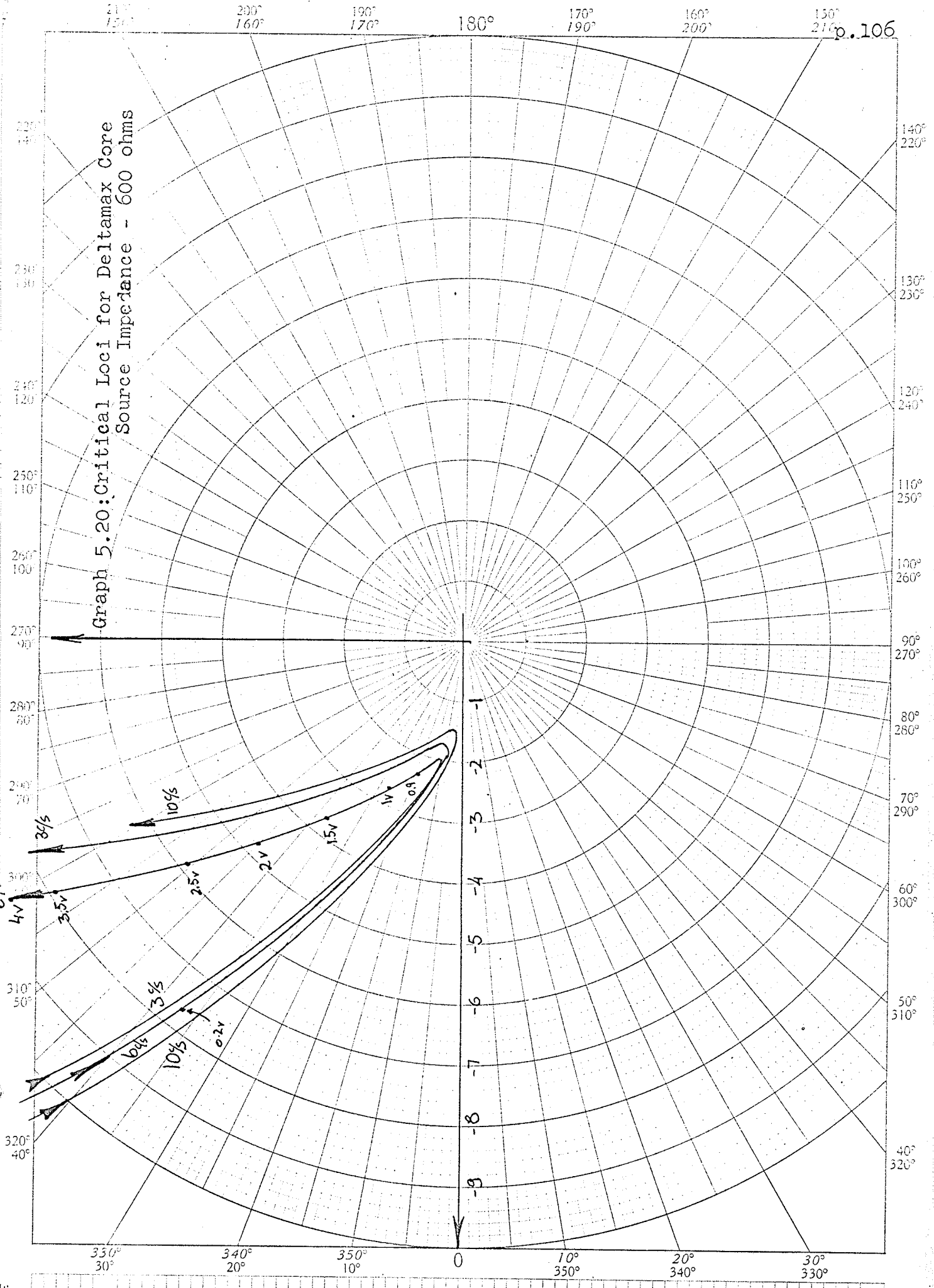
2



5.19
Graph - Comparison Between Two Sets of Describing Functions



Graph 5.20: Critical Loci for Deltamax Core
Source Impedance - 600 ohms



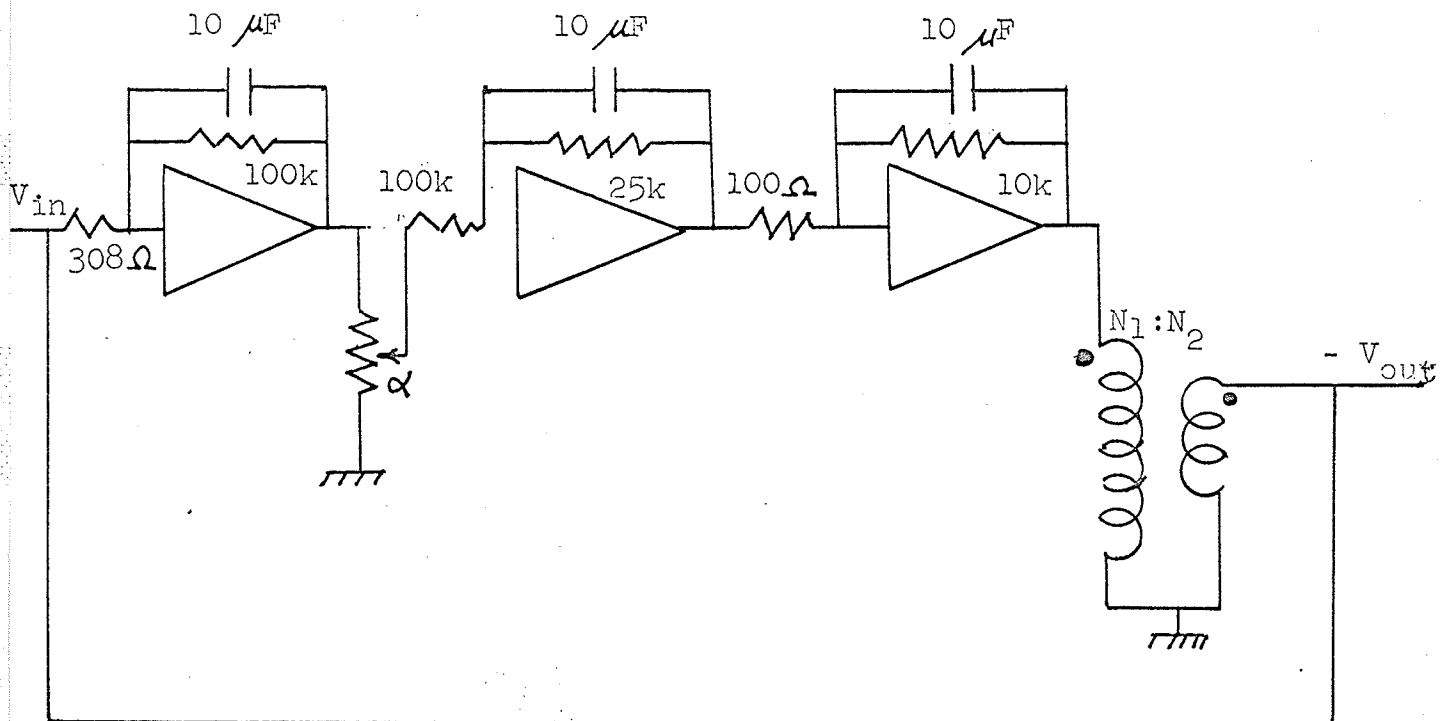


Fig. 5.12: Simulated control system.

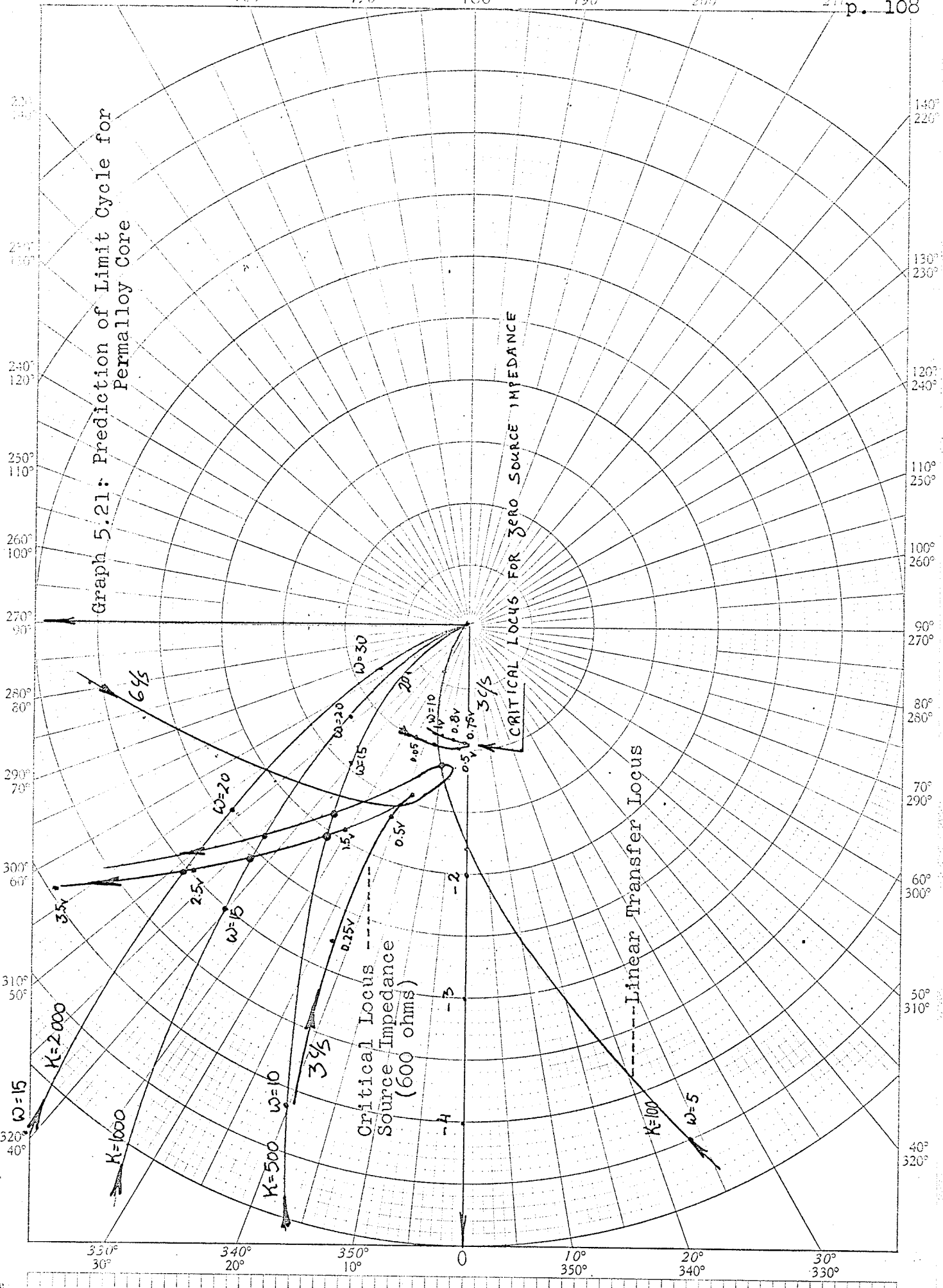
Tests were carried out for the Permalloy and Deltamax cores, and the gain of the system was varied in order to obtain a limit cycle within the closed loop. The transfer function of the linear elements is

$$G(s) = \frac{K}{(1+s)(1+0.25s)(1+1.1s)}$$

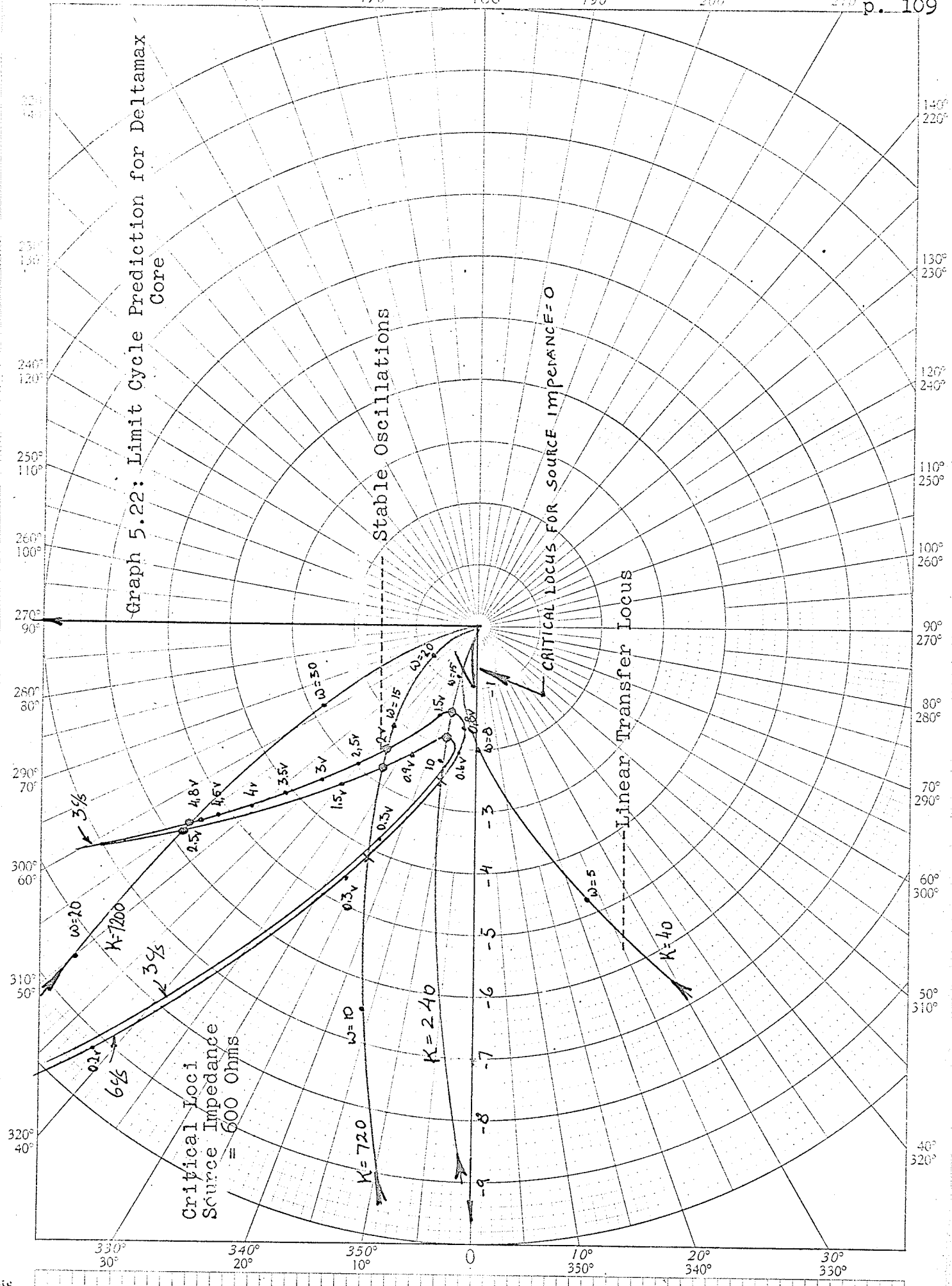
The Nyquist diagram for this function is plotted in Graphs 5.21, p. 108, and 5.22, p. 109, together with the critical loci for Permalloy and Deltamax respectively.

It is clearly seen that intersection between the critical loci and transfer loci occurs in the second quadrant rather than in the third, due to phase lead rather than phase lag of the output voltage from the nonlinear elements.

Graph 5.21: Prediction of Limit Cycle for Permalloy Core



Graph 5.22: Limit Cycle Prediction for Deltamax Core



Critical Loci
Source Impedance
= 600 Ohms

Stable Oscillations

CRITICAL LOCUS FOR SOURCE IMPEDANCE=0

Linear Transfer Locus

By comparing Tables 5.1 and 5.2, pp. 110 and 111, which represent results obtained from the computer, with Graphs 5.21 and 5.22, pp. 108 and 109 respectively, it is seen that the predicted results conform with the measured results. Slight differences occur due to the fact that the input to the non-linear element is not purely sinusoidal, and also because for each limit cycle frequency we must use a critical locus corresponding to this frequency. This can be done only by the "cut and try" method.

The effect of the source impedance on the stability of the system is also illustrated in Graphs 5.21 and 5.22, pp. 108 and 109.

<u>System Gain</u>	<u>Oscillations Amplitude</u>	<u>Frequency c/s</u>	<u>ω rad/sec.</u>
Source Impedance = 600 Ohms			
2500	3.17 Volts	3.58	22.5
2000	2.65	3.33	20.9
1500	2.16	3.12	19.6
1000	1.7	2.86	17.9
500	1.06	2.38	14.9
325*	.95	2.08	13.0
Source Impedance = 0 Ohms			
675	2.65 Volts	2.78	17.4
500	2.27	2.63	16.5
350	1.77	2.38	14.9
250	1.43	2.28	14.3
200	1.23	2.08	13
150	1.06	1.92	12
100	.706	1.79	11.2
50*	.354	- -	- -

* Oscillations die out.

Table 5.1: Frequency and Amplitude of Limit Cycle for Permalloy Core.

<u>System Gain</u>	<u>Oscillations Amplitude</u>	<u>Frequency c/s</u>	<u>w rad/sec.</u>
Source Impedance = 600 Ohms			
7520	6.55 Volts	4.16	26.1
6250	6.37	3.85	24.2
5000	5.65	3.7	27.2
3750	4.95	3.45	21.7
2500	3.89	3.23	20.3
1250	2.48	2.78	17.5
1000	2.12	2.63	16.5
750	1.9	2.38	14.9
500	1.42	2.18	13.7
375	1.24	1.85	11.6
250*	- -	- -	- -

Source Impedance = 0 Ohms

1250	1.77 Volts	3.33	21
1125	1.77	3.12	19.6
1000	1.7	3.04	19
875	1.59	2.94	18.4
750	1.43	2.94	18.4
625	1.27	2.78	17.5
500	1.06	2.63	16.5
375	.74	2.5	15.7
250	.706	2.27	14.2
125	.495	1.92	12
100	.39	1.75	11
75	.354	1.66	10.4
50*	.24	1.43	9

* Oscillations die out.

Table 5.2: Frequency and Amplitude of Limit Cycle for Deltamax Core.

In order to check the low amplitude branch of the critical locus, one needs to simulate a transfer function which would intersect the locus in the manner shown in Fig. 5.13, p.112.

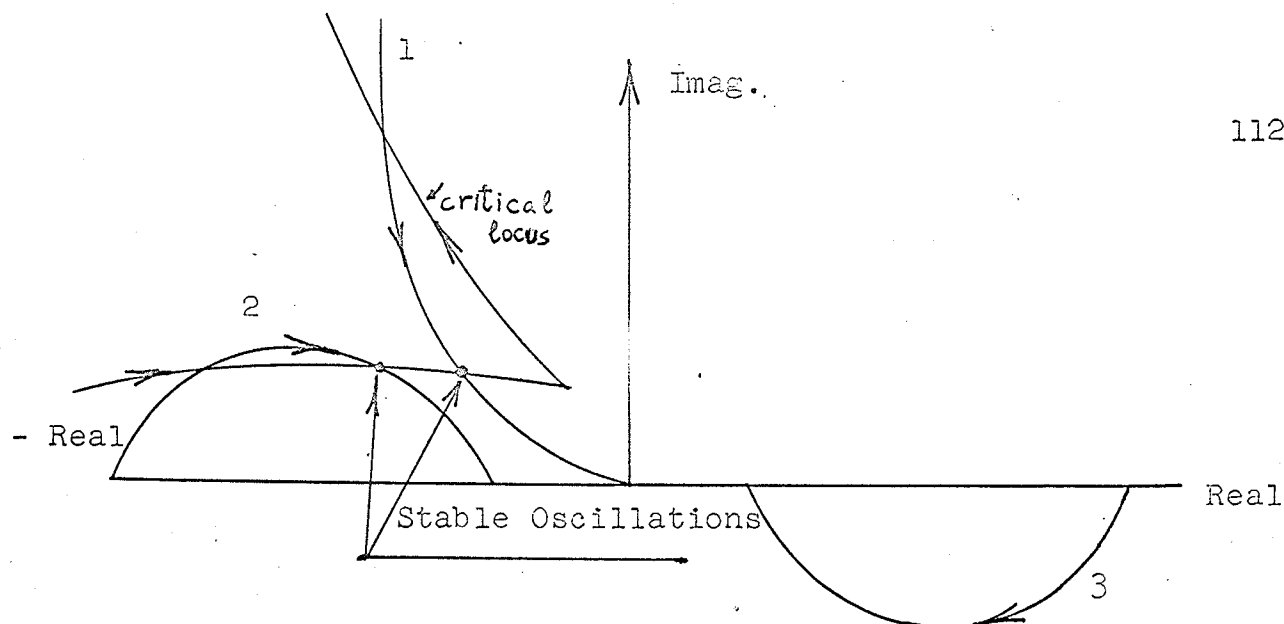


Fig. 5.13: The requirements for low amplitude limit cycle.

Locus (1) may be simulated by a transfer function of the type $\frac{1 + ST}{s^3}$, locus (2) by inverting locus (3) which is the locus of an R-C lag network.

By simulating these models, oscillation took place in the system; however, the results were not in complete agreement with those predicted, as it is difficult to synthesize a transfer function which would intersect the critical locus exactly at the frequency for which this locus was derived. Photo 14, p. 79 shows the computer set-up, and Photos 15 and 16, p. 79, show oscillation when there is a limit cycle in the system.

CHAPTER VI

CONCLUSION

It was shown that the theoretical models representing hysteretic elements would not yield satisfactory results when used generally, and without distinction, to derive the describing function for hysteresis nonlinearities.

A common misconception is to identify a hysteresis nonlinearity with a backlash nonlinearity. This cannot be done in cases where the width of the hysteresis loop is dependent upon the input signal.

Although only magnetic elements were considered in this thesis, it should be noted that the concept of hysteresis covers a multitude of sins in other areas as well. For example, there is the known mechanical hysteresis phenomenon which is to be found in transducer components such as springs or pressure capsules and which arises from the imperfect response of the microscopic crystal grains integrated over the macroscopic dimensions of the strained transducer elements. When load-cycling a steel spring for instance, it is observed that increasing numbers of distorted and partly dislocated crystals do not return to their original shape and position after the load has been restored. The magnitude of the residual deformation depends on the maximum stress applied, but, is independent of time (frequency)(48).

The load deformation diagram is shown in Fig. 6.1.

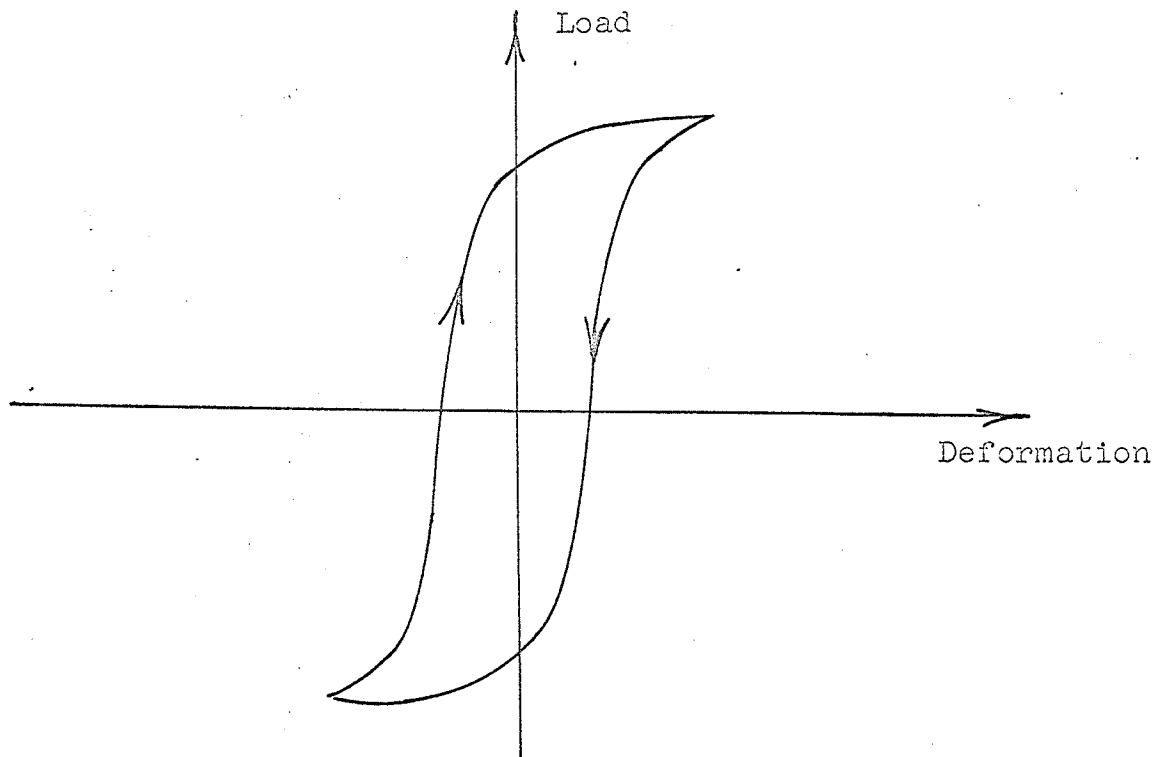


Fig. 6.1: Mechanical hysteresis for a steel spring.

It can be shown that the area of the loop represents the energy dissipated in heat. Another example can be taken from the area of ferro-electric materials which are the dielectric analog of ferromagnetic materials, (that is, they have a high dielectric constant and electrostriction similar to high permeability and magnetostriction, etc.). Thus, their uses are also parallel to those of magnetic materials, and they can be used for electrostrictive transducers, dielectric amplifiers and storage devices.

Ferro-electric materials are dielectrics which exhibit a hysteresis type relation between the applied field and the electrical displacement. (See Fig. 6.2.)

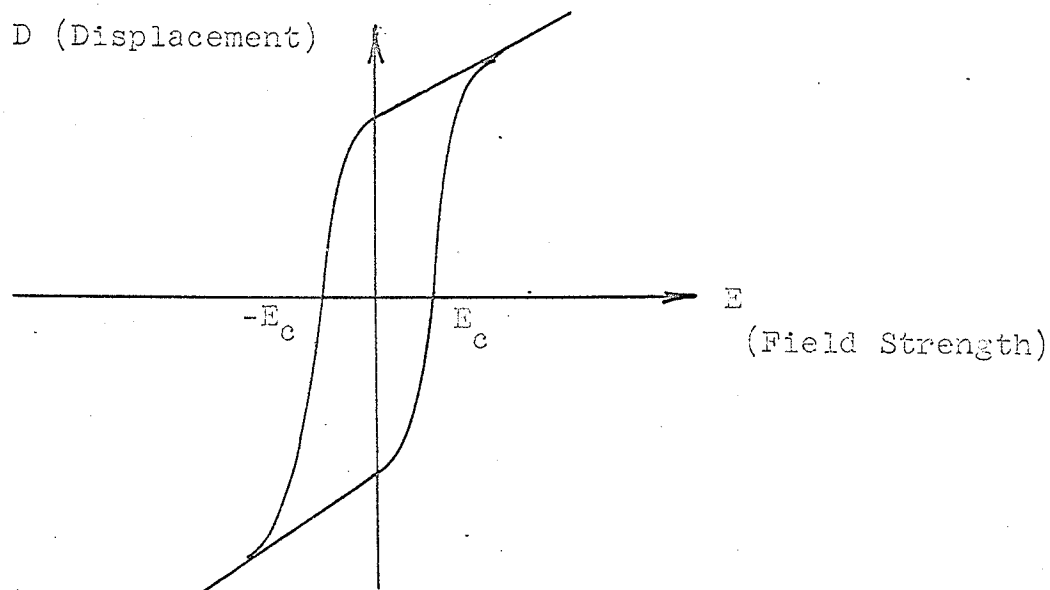


Fig. 6.2: Hysteresis loop for dielectric materials.

The quantity E_c is a function of E , and also, in this case, of the frequency. The area of the loop is again proportional to the heat loss (49).

Thus, it is seen that treatment of such elements by use of the conventional describing function (2.5, 2.8) cannot be justified, since this does not take into account either the relationship between input voltage and input current for example, or the losses which occur in the material.

In order to modify the above mentioned function, one should first derive equivalent parameters which reflect the fundamental nonlinear properties of the element in question. These parameters may depend upon amplitude as well as frequency, and must be found experimentally for the interval of interest, since pure theoretical assumptions do not yield satisfactory results. When investigating the system over wide frequency ranges, it may be advantageous to introduce a suitable number of sub-ranges within which the frequency may be taken as a constant. The derived theoretical models (Chapt. IV) would yield satisfactory results only if the element in question were to behave according to the assumptions made while deriving these models. Since the materials that incorporate the hysteretic phenomena differ greatly from one another, it is felt that rather than make a generalized analysis, a particular analysis for each element in question is required.

- - - - -

REFERENCES

1. Kochenburger, R. J., "A Frequency Response Method for Analyzing and Synthesizing Contactor Servo-Mechanisms". Trans. A.I.E.E., Vol. 69, Part I, pp. 270 - 284, (1950).
2. Goldfarb, L. C., "On Some Nonlinear Phenomena in Regulatory Systems", *Automatika i Telemekhanika*, Vol. 8, No. 5, pp. 349 - 383, September - October, 1947.
Reprinted in "Frequency Response", The Macmillan Company, New York, 1956.
3. Tustin, A., "The Effects of Backlash and of Speed Development Friction on the Stability of Closed Cycle Control Systems", *Journal Institution Electrical Engineers* (London), Vol. 94, Part IIA, No. 1, 1947.
4. Oppelt, W., "Locus Curve Method for Regulators with Friction", *Journal Institution Electrical Engineers* (London), Vol. 94, Part IIA, Nos. 1 and 2, May, 1947; also in Report 1691, National Bureau of Standards, Washington, D. C., 1952.
5. Dutilh, J. R., "Théorie des Servomécanismes à Relais", *L'onde Élect.*, Vol. 30, pp. 438 - 445, 1950.
6. Johnson, E. C., "Sinusoidal Techniques Applied to Non-Linear Feedback Systems", *Proceedings Symposium on Nonlinear Circuit Analysis*, Polytechnic Institute of Brooklyn, New York, N.Y., pp. 258 - 273, 1953.

7. Truxal, J. G., "Control Engineers Handbook," (Book) McGraw - Hill Book Company, Inc., New York, N.Y., 1958.
8. Gibson, J. E., "Nonlinear Automatic Control", (Book) McGraw-Hill Book Company, Inc., New York, N.Y., 1963.
9. Graham, D. and McRuer, D., "Analysis of Nonlinear Control Systems", (Book) John Wiley & Sons, New York, N.Y., 1961.
10. Sridhar, R., "A General Method of Deriving the Describing Function of a Certain Class of Nonlinearities", I.R.E. Transactions on Automatic Control, Vol. AC-5, No. 2, pp. 135 - 141, June, 1960.
11. Grief, H. D., "Describing Function Method for Servo-Mechanism Analysis Applied to Most Commonly Encountered Nonlinearities", Trans. A.I.E.E., Part II (App. & Industry), Vol. 72, pp. 243 - 248, Sept., 1953.
12. West, J. C., "Describing Function Technique", Society Instrument Technology, Vol. 11, No. 1, pp. 1 - 8, March, 1959.
13. Ku, Y. H., "Theory of Nonlinear Control", Journal Franklin Institute, Vol. 27, pp. 108 - 144, 1961.
14. Glinski, G. S. and Ahmed, N. U., "Nonlinear Magnetics", Technical Reports Nos. 64-2 and 64-2-R, University of Ottawa, June, 1964.
15. Lakshmi-Bai, C., "Transformation Method for Study of Non-Linear Components", Trans. A.I.E.E., Vol. 79, Part II (App. & Industry), No. 50, pp. 249 - 254, Sept., 1960.

16. Ku, Y. H., and Chen, C. F., "A New Method for Evaluating The Describing Function for Hysteresis Type Non-Linearities", Journal Franklin Institute, Vol. 27, pp. 108 - 144, 1961.
17. Deekshatulu, B. L., "How to Evaluate Harmonic Response of Nonlinear Components", Control Engineering, Vol. 10, No. 10, pp. 56 - 56, October, 1963.
18. Mahalanobis, A. K. and Nath, A. K., "A Method of Finding The Equivalent Gains of Double Valued Nonlinearities", International Journal of Control, Vol. 1, No. 3, pp. 281 - 295, March, 1965.
19. Mahalanobis, A. K. and Nath, A. K.; "On The Compensation of Hysteresis Effects in Relay Control Systems by Using Positive Hysteresis", Journal of Electronics and Control, Vol. XVII, No. 6, pp. 683 - 695, Dec., 1964.
20. Ewing, J. A., "Magnetic Induction in Iron and Other Metals"(Book) 'The Electrician' Printing and Publishing Co., London, p. 95, London, 1900.
21. Valeese, L. M., "Comparison of Backlash and Hysteresis Effects in Second Order Feedback Systems", Trans. A.I.E.E., Vol., 75, Part II, (App.& Industry), No. 26, pp. 240 - 243, Sept., 1956.
22. Valese, L. M. "Analysis of Backlash in Feedback Control Systems With One Degree of Freedom", Trans. A.I.E.E., Vol. 74, Part II, pp. 1 - 4, March, 1955.

23. Mahalanobis, A. K., "A Describing Function Study of Hysteresis Effects in a Velocity Lag Servomechanism", Proceedings, First Defense Electronics Convention, Bangalore, India, pp. 99 - 103, Sept. 28 - Oct. 1, 1959.
24. Neal, C. B. and Bunn, D. B., "The Describing Function for Hysteresis Nonlinearity", Joint Automatic Control Conference, pp. 185 - 188, June 24 - 26, 1964.
25. Rayleigh, Lord, "The Behaviour of Iron and Steel Under The Operation of Feeble Magnetic Forces", Philosophical Magazine (5) 23, pp. 223 - 245, 1889.
26. Kennelly, A. E., "Magnetic Reluctance", Trans. A.I.E.E., Vol. 8, pp. 485 - 517, 1891.
27. Bozorth, R. M., "Ferromagnetism", (Book) D. Van Nostrand Company, Inc., Toronto, 1953.
28. Ellwood, W. B., "Magnetic Hysteresis at Low Flux Densities", Physics 6, pp. 215 - 26, 483 and 787, 1934.
29. Sanford, R. L., "The Variation of Residual Induction and Coercive Force with Magnetizing Force", National Bureau of Standards (U.S.), Scientific Papers, Papers 383 and 384, 1920.
30. Roters, H. C., "Electromagnetic Devices", (Book) John Wiley & Sons, Inc., New York, N.Y., 1958.
31. Huey, R. M., Pawloff, O. and Glucharoff, T., "Extension of The Dual Input Describing Function Technique to Systems Containing Reactive Nonlinearity", The Institution of Electrical Engineers, Monograph No. 383 M, June, 1960.

32. Armstrong, H. L., "A Simplified Mathematical Approach to Hysteresis Losses", *Electrical Energy*, Vol. 74, No. 12, pp. 1060 - 1062, Dec., 1955.
33. Conover, W. B., "Method for Determination of Hysteresis Loop Area", *Trans. A.I.E.E.*, Vol. 70, Part II, pp. 1485 - 1487, 1951.
34. Katz, H. W., "Solid State Magnetic and Dielectric Devices", (Book) John Wiley & Sons, Inc., New York, N.Y., 1959.
35. Chestnut, H. and Mayer, R. W., "Servomechanisms and Regulating Systems Designs", (Book) John Wiley & Sons, Inc., New York, N.Y., 1959.
36. Nesvizhskiy, Yu, B., "Application of The Harmonic Linearization Method to The Analysis of Forced Oscillations in Circuits Containing Ferrite Cored Coils", *Telecommunications and Radio Engineering*, (English Ed. of 'Electrosvyaz') No. 3, pp. 13 - 17, March, 1964.
37. Nichols, N. B., "Backlash in a Velocity Lag Servomechanism", *Trans. A.I.E.E.*, Vol. 72, Part II, pp. 462 - 468, 1953.
38. Lewis, L. J., "Harmonic Analysis of Nonlinear Characteristics", *Trans. A.I.E.E.*, Vol. 73, Part I, pp. 693 - 699, 1954.
39. Shearder, J. L., "Nonlinear Analog Study of High Pressure Servomechanisms:", *Transactions A.S.M.E.*, Vol. 79, pp. 465 - 472, 1957.

40. Gehmilich, D. K. and Van Valkenburg, M. E., "Measurement of Some Nonlinearities in Servomechanisms", Trans. A.I.E.E., Vol. 73, Part II (App. & Industry), No. 15, pp. 232 - 235, 1954.
41. Satyendra, K. N., "Describing Functions Representing Effect of Inertia, Backlash and Coulomb Friction on Stability of Automatic Control Systems", Trans. A.I.E.E., Vol. 75, Part II (App. & Industry), No. 26, pp. 243 - 249, Sept., 1956.
42. Demczynski, S., "Survey of Methods Available for Analysis and Synthesis of Nonlinear Servo Systems", Electrical Energy, Vol. 1, No. 9, pp. 279 - 284, 10 May, 1957, and pp. 316 - 321, June, 1957.
43. Deekshatulu, B. L., "Approximate Sinusoidal Analysis of Nonlinear Components", Journal Science and Industrial Research, Vol. 21D, No. 6, pp. 175 - 179, June, 1962.
44. Halstenberg, R. V., "Combined Hysteresis and Nonlinear Gains in Complex Control Systems:", I.R.E. Transactions on Automatic Control, PGAC-5, pp. 51 - 58, July, 1958.
45. Akulov, N. A., Ivanovsky, V. I. and Glinka, O. S., "Theory of Hysteresis Loops", Dokl. Akad. Nauk S.S.S.R., 68, No. (5), pp. 833 - 836, 1949.
46. The Arnold Engineering Company, "Technical Data on Arnold Tape Wound Cores", Bulletin TC-101A, June, 1962.

47. "C.R.C. Standard Mathematical Tables", The Chemical Rubber Publishing Company, Cleveland, Ohio, 1962.
48. Neubert, Herman K., "Instrument Transducers, An Introduction to Their Performance and Design", (Book) Clarendon Press, Oxford, England, pp. 15 - 21, 1963.
49. Mason, W. P., "Ferroelectrics", Proceedings of The Symposium on The Role of Solid State Phenomena in Electric Circuits, Polytechnic Institute of Brooklyn, New York, N.Y., pp. 91 - 107, April 23 - 25, 1957.

APPENDIX A

Technical Data for the Tested Cores

	Deltamax (4T4168-D2)	4-79 Mo-Permalloy (4T4178-P1)	Supermalloy (4T4178-S4)
Specific gravity	8.25	8.74	8.77
Electrical resistivity	45	55	65
Initial permeability, μ_i	400 - 1700	10,000 - 40,000	55,000 - 120,000
Maximum permeability	70,000 - 250,000	70,000 - 250,000	300,000 - 900,000
Maximum differential permeability	40,000 - 100,000	40,000 - 100,000	100,000 - 500,000
	100,000 - 400,000	125,000 - 450,000
Residual induction A_{max}	55,000 - 250,000	70,000 - 300,000
B_r (Gausses)	12,500 - 15,000	4,000 - 7,000	4,000 - 5,500
Peak flux density B_p	12,500 - 15,000	4,000 - 7,000	4,000 - 5,500
	12,500 - 15,000	4,000 - 7,000	4,000 - 5,500
B_r/B_p	13,500 - 15,500	6,500 - 8,000	6,500 - 7,800
	13,500 - 15,500	6,500 - 8,000	6,500 - 7,800
	13,500 - 15,500	6,500 - 8,000	6,500 - 7,800
Coercive force H_c (Oersteds)	0.92 min.	0.50 - 0.90	0.50 - 0.80
	0.92 min.	0.50 - 0.90	0.50 - 0.80
Core size	0.04 - 0.16	0.02 - 0.07	0.003 - 0.009
	0.20 - 0.40	0.05 - 0.15	0.02 - 0.06
	0.35 - 0.60	0.075 - 0.25	0.03 - 0.10
Number of primary turns	1.250 in.	2.500 in.	2.500 in.
	1.000 in.	2.000 in.	2.000 in.
	0.125 in.	0.500 in.	0.500 in.
Number of secondary turns	2000 turns of #34 wire	1250 turns of #34 wire	1250 turns of #34 wire
	500 turns of #34 wire	417 turns of #34 wire	417 turns of #34 wire
*Number of bias turns	5 turns	5 turns	5 turns

*These turns were added in order to eliminate the effect of the presence of D.C. voltage in the output of the transfer function analyzer. (The effect of this voltage is shown in Photo 2.)

APPENDIX B

Numerical Data for Graphs

Table B.1: Data for Graph 5.1; p. 75

<u>Input Voltage</u>	<u>1st Harmonic Output</u>	<u>Phase Lead</u>	<u>D. F.*</u>
<u>f=3 c/s</u>			
0.05 Volts	0.014 volts	22 Deg.	0.922
0.25	0.704	4	0.930
0.5	1.42	1	0.935
0.75**	2.14	3	0.940
0.80	2.25	4	0.925
0.85	2.35	7	0.910
0.9	2.44	10	0.895
0.95	2.45	13	0.850
1	2.50	15	0.825
<u>f = 6 c/s</u>			
0.1	0.029	8	0.955
0.25	0.072	4.5	0.950
0.5	0.143	2	0.945
0.75	0.216	1	0.950
1**	0.285	0	0.940
1.5	0.426	1	0.930
<u>f = 10 c/s</u>			
0.1	0.029	7	0.955
0.25	0.072	4	0.950
0.5	0.143	2	0.942
0.75	0.215	1	0.945
1.25	0.36	1	0.95
1.5	0.435	$\frac{1}{2}$	0.955
1.75	0.501	1	0.945
2	0.575	1	0.947
2.25**	0.65	1	0.955
2.5	0.72	1	0.950
2.75	0.753	4	0.905

* = In order to obtain the describing function (D.F.), multiply the 1st harmonic output by the turns ratio $\frac{1250}{417}$; then divide by the input voltage.

** = Saturation.

Table B.1: (Continued)

<u>Input Voltage</u>	<u>1st Harmonic Output</u>	<u>Phase Lead</u>	<u>D. F.*</u>
	<u>f = 20 c/s</u>		
0.01 Volts	0.003 Volts	6 Deg.	0.99
0.03	0.0088	4	0.970
0.05	0.015	3	0.99
0.2	0.06	2	0.99
0.4	0.12	2	0.99
0.5	0.15	2	0.99
1.5	0.45	0	0.99
2.5	0.73	1	0.982
3.5	1.05	1.5	0.99
4.5**	1.38	1.5	0.99
5	1.35	2	0.98

* = In order to obtain the describing function (D.F.), multiply the 1st harmonic output by the turns ratio $\left(\frac{1250}{417}\right)$; then divide by the input voltage.

** = Saturation.

Table B.2: Data for Graph 5.5, p. 83

<u>Input Voltage</u>	<u>1st Harmonic Output</u>	<u>Phase Lead</u>	<u>D.F.*</u>
<u>f = 3 c/s</u>			
0.01 Volts	0 Volts	0 Deg.	0
0.05	0.0065	15	0.547
0.1	0.018	3	0.755
0.25	0.0502	0	0.845
0.3**	0.060	0	0.84
0.5	0.0865	16	0.726
0.6	0.0865	--	0.605
0.6	0.0865	--	0.605
<u>f = 6 c/s</u>			
0.01	0	0	0
0.05	0.0065	19	0.547
0.1	0.018	4	0.755
0.25	0.051	4	0.85
0.3	0.06	3	0.85
0.4	0.0865	0	0.905
0.5	0.122	0	0.95
0.6	0.136	0	0.95
0.7**	0.16	0	0.957
0.75	0.165	4	0.922
0.8	0.175	8	0.917
0.85	0.175	10	0.862
<u>f = 10 c/s</u>			
0.01	0	0	0
0.02	0.0016	36	0.336
0.05	0.00564	28	0.474
0.1	0.016	13	0.67
0.2	0.040	1	0.84
0.3	0.062	0	0.867
0.4	0.085	0	0.899
0.6	0.13	0	0.91
0.7	0.154	0	0.92
0.8	0.175	0	0.92
0.9	0.205	0	0.955
1	0.225	0	0.945

* = In order to obtain the describing function (D.F.), multiply the 1st harmonic output by the turns ratio $\left(\frac{2000}{500}\right)$; then divide by the input voltage.

** = Saturation.

Table B.2: (Continued)

<u>Input Voltage</u>	<u>1st Harmonic Output</u>	<u>Phase Lead</u>	<u>D.F.*</u>
	<u>f = 10 c/s</u>		
1.1** Volts	0.245 Volts	1 Deg.	0.935
1.2	0.273	1	0.955
1.3	0.285	6	0.92

* = In order to obtain the describing function (D.F.), multiply the 1st harmonic output by the turns ratio $\frac{2000}{500}$; then divide by the input voltage.

** = Saturation.

Table B.3: Data for Graph 5.7, p. 89

<u>Input Voltage</u>	<u>1st Harmonic Output</u>	<u>Phase Lead</u>	<u>D.F.*</u>
<u>f = 3 c/s</u>			
0.25 Volts	0.09 Volts	25 Deg.	0.36
0.5	0.325	21	0.65
1**	0.68	19	0.68
1.5	0.78	35	0.52
2	0.829	43	0.415
2.5	0.845	49	0.34
3	0.845	57	0.28
3.5	0.88	57	0.25
4	0.88	62	0.22
4.5	0.88	62	0.196
5.25	0.91	69	0.158
<u>f = 6 c/s</u>			
0.1	0.0325	82	0.32
0.2	0.114	44	0.57
0.25	0.146	38	0.58
0.5	0.34	20	0.68
1	0.8	10	0.8
1.5**	1.3	6.5	0.865
2	1.56	18	0.78
2.5	1.67	28	0.667
3	1.74	35	0.58
3.5	1.785	39	0.51
4	1.82	43	0.455
4.5	1.835	45	0.407
5	1.85	48	0.37
<u>f = 10 c/s</u>			
0.01	0.065	45	0.6
0.25	0.192	25	0.767
0.4	0.308	16	0.77
0.5	0.706	14	0.81
1	0.875	7	0.875
1.5	1.35	5	0.9
2**	1.85	4	0.925
2.5	2.37	5	0.95
3	2.56	12	0.85
3.5	2.705	20	0.775
4	2.805	25	0.702
4.5	2.87	30	0.637
5.15	2.95	35	0.56

* = In order to obtain the describing function (D.F.), divide the 1st harmonic output by the input voltage.

** = Saturation.

Table B.4: Data for Graph 5.13, p. 98

<u>Input Voltage</u>	<u>1st Harmonic Output</u>	<u>Phase Lead</u>	<u>D.F.*</u>
<u>$f = 3 \text{ c/s}$</u>			
0.1 Volts	0.04 Volts	66 Deg.	0.4
0.2	0.11	40	0.5
0.35	0.25	20	0.71
0.5	0.39	12	0.78
1**	0.77	21	0.77
1.5	0.90	36	0.60
2	0.94	43	0.47
2.5	0.97	49	0.39
3	0.99	55	0.33
3.5	0.99	56	0.28
4	0.99	60	0.26
4.5	0.99	60	0.23
5	0.99	64	0.21
<u>$f = 6 \text{ c/s}$</u>			
0.1	0.045	54	0.45
0.2	0.12	30	0.60
0.35	0.27	20	0.77
0.5	0.42	14	0.89
1	0.93	6	0.93
1.5**	1.42	6	0.94
2	1.74	17	0.87
2.5	1.87	28	0.75
3	1.96	34	0.65
3.5	2.00	38	0.57
4	2.03	42	0.50
4.5	2.05	45	0.45
5	2.07	48	0.41
<u>$f = 10 \text{ c/s}$</u>			
0.1	0.075	39	0.75
0.25	0.21	20	0.84
0.4	0.34	14	0.86
0.5	0.43	12	0.87
1	0.96	4	0.96
1.5	1.45	4	0.97
2**	1.96	4	0.97
2.5	2.49	4	0.99
3	2.88	10	0.96

* = In order to obtain the describing function (D.F.), divide the 1st harmonic output by the input voltage.

** = Saturation.

Table B.4: (Continued)

<u>Input Voltage</u>	<u>1st Harmonic Output</u>	<u>Phase Lead</u>	<u>D.F.*</u>
<u>f = 10 c/s</u>			
3.5 Volts	3.06 Volts	18 Deg.	0.87
4	3.18	24	0.78
4.5	3.27	28	0.72
5	3.31	31	0.66
<u>f = 30 c/s</u>			
0.2	0.165	17	0.825
0.35	0.3	11	0.855
0.5	0.45	9	0.9
1	0.975	5	0.97
1.5	1.47	4	0.97
2	1.96	3	0.97
3	3	2	1
5	5	2	1
7	7	1	1
8**	8	2	1
8.5	8.5	4	1
9	8.9	5	0.99
9.5	9.2	8	0.97
10	9.35	10	0.935
<u>f = 50 c/s</u>			
0.2	0.161	13	0.805
0.35	0.3	9	0.855
0.5	0.455	7	0.91
1	0.95	5	0.95
2.5	2.49	3	0.99
5	5	1	1
8	8	0	1
14	14	2	1
15	14.9	4	0.99
16	15.5	6	0.98

* = In order to obtain the describing function (D.F.), divide the 1st harmonic output by the input voltage.

** = Saturation.

Table B.5: Data for Graph 5.16, p. 101

<u>Input Voltage</u>	<u>1st Harmonic Output</u>	<u>Phase Lead</u>	<u>D.F.*</u>
<u>$f = 3 \text{ c/s}$</u>			
0.1 Volts	0 Volts	58 Deg.	0
0.2	0.02	42	0.1
0.3	0.08	23	0.26
0.5	0.21	12	0.42
0.7**	0.35	10	0.50
0.9	0.37	24	0.41
1	0.38	28	0.38
1.5	0.42	40	0.28
2	0.42	49	0.21
2.5	0.42	52	0.16
3	0.42	56	0.14
3.5	0.42	60	0.12
4	0.42	61	0.10
4.5	0.42	63	0.09
4.8	0.42	63	0.08
<u>$f = 6 \text{ c/s}$</u>			
0.1	0	49	0
0.2	0.021	43	0.105
0.4	0.147	19	0.36
0.6	0.29	5	0.49
0.8	0.46	5	0.57
1**	0.61	5	0.61
1.5	0.79	21	0.52
2.0	0.82	33	0.41
3	0.84	44	0.28
3.5	0.84	48	0.24
4	0.84	50	0.21
4.5	0.86	54	0.19
<u>$f = 10 \text{ c/s}$</u>			
0.2	0.021	44	0.1
0.4	0.126	43	0.31
0.6	0.294	39	0.49
0.8	0.460	35	0.57
1	0.63	30	0.63
1.5**	1.02	23	0.68
2	1.24	12	0.62

* = In order to obtain the describing function (D.F.), divide the 1st harmonic output by the input voltage.

** = Saturation.

Table B.5: (Continued)

<u>Input Voltage</u>	<u>1st Harmonic Output</u>	<u>Phase Lead</u>	<u>D.F.*</u>
<u>f = 10 c/s</u>			
2.5 Volts	1.32 Volts	0 Deg.	0.52
3	1.36	4	0.45
3.5	1.38	4	0.39
4	1.40	6	0.35
4.6	1.40	15	0.30
4.8	1.40	41	0.29
<u>f = 20 c/s</u>			
0.1	0	52	0
0.2	0.62	48	0.1
0.4	0.125	20	0.31
0.6	0.29	8	0.49
0.8	0.44	5	0.55
1	0.61	3	0.61
1.5	1.01	2	0.672
2	1.42	1	0.71
2.5	1.85	0	0.74
3	2.23	0	0.745
3.5**	2.5	7	0.716
4	2.54	14	0.635
4.5	2.62	20	0.582
5	2.70	24	0.54
5.5	2.70	28	0.49
<u>f = 30 c/s</u>			
0.2	0.04	41	0.2
0.4	0.147	12	0.367
0.6	0.294	7	0.49
0.8	0.46	4	0.575
1	0.63	1½	0.63
2	1.45	0	0.725
2.5	1.87	0	0.75
3	2.25	0	0.75
3.5	2.68	0	0.765
4	3.1	0	0.77
4.5**	3.46	0	0.77
5	3.72	4	0.75
5.5	3.82	9	0.69
6	3.9	13	0.65
6.5	3.9	17	0.6
6.7	4	19	0.597

* = In order to obtain the describing function (D.F.), divide the 1st harmonic output by the input voltage.

** = Saturation.

Table B.5: (Continued)

<u>Input Voltage</u>	<u>1st Harmonic Output</u>	<u>Phase Lead</u>	<u>D.F.*</u>
<u>f = 50 c/s</u>			
0.2 Volts	0.042 Volts	49 Deg.	0.21
0.4	0.126	20	0.314
0.6	0.273	6	0.455
0.8	0.44	3	0.55
1	0.61	0	0.61
1.5	0.01	0	0.672
2	1.45	0	0.725
2.5	0.85	0	0.74
3	2.25	0	0.75
3.5	2.64	0	0.775
4	3.1	0	0.775
4.5	3.5	0	0.777
5	3.92	0	0.782
5.5	4.32	0	0.785
6	4.74	0	0.79
6.5	5.16	0	0.795
7	5.56	0	0.795
7.5**	5.56	0	0.785
8	6.12	0	0.765
9	6.42	6	0.715
9.8	6.55	10	0.667

* = In order to obtain the describing function (D.F.), divide the 1st harmonic output by the input voltage.

** = Saturation.